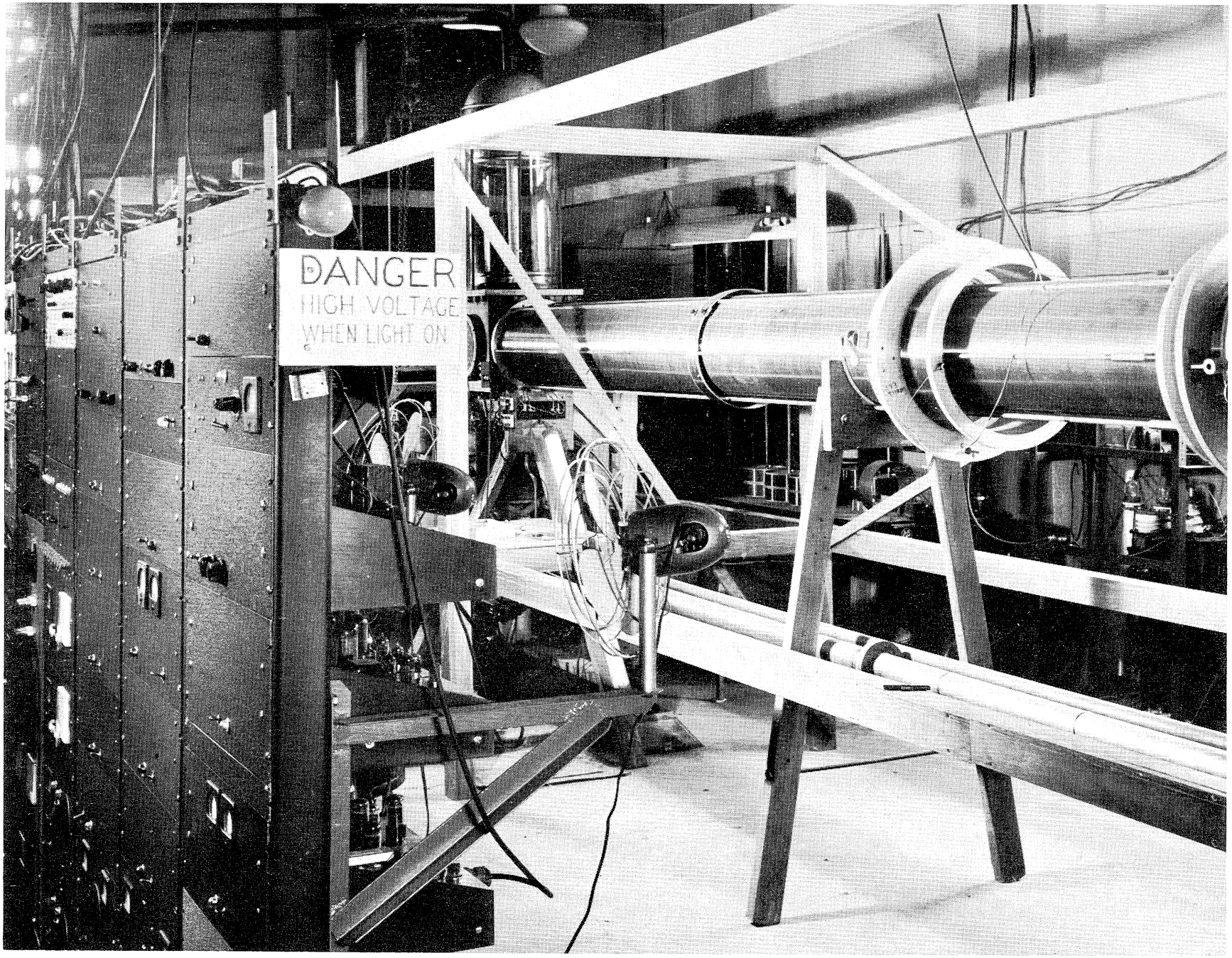
DANGER
HIGH VOLTAGE
WHEN LIGHT ON

THE UNIVERSITY OF MICHIGAN

INDUSTRY PROGRAM OF THE COLLEGE OF ENGINEERING

MEASUREMENT OF THE MOTT ASYMMETRY IN DOUBLE SCATTERING OF ELECTRONS

Donald F. Nelson

A dissertation submitted in partial fulfillment
of the requirements for the degree of
Doctor of Philosophy in the
University of Michigan
1958

August, 1958

IP-306

Doctoral Committee:

Associate Professor Robert W. Pidd, Chairman
Professor H. Richard Crane
Assistant Professor Noah Sherman
Professor George E. Uhlenbeck
Assistant Professor Joseph L. Ullman

ACKNOWLEDGMENTS

The author wishes to express his appreciation to the chairman of his committee, Dr. R. W. Pidd, for his guidance and encouragement throughout this work, to Dr. H. R. Crane for many helpful discussions about the experiment, to Dr. K. M. Case for several enlightening conversations on the theory of the experiment, and to Dr. N. Sherman for the special calculations of the Mott asymmetry factor that he carried out for this experiment.

The author also wishes to thank Mr. A. A. Schupp for his cooperation in alternating with the author in the use of the equipment and to Mr. H A. Westrick for his cooperation and skill in the construction of the apparatus. Last but not least, the author wishes to thank his wife for her patience and fine cooperation throughout the work.

The author wishes to express his appreciation to the United States Atomic Energy Commission for support of this work under Contract No. AT(11-1)-70, to the Industry Program of the College of Engineering for the typing, drafting of figures, and printing of the thesis, and to the Horace H. Rackham School of Graduate Studies for twice awarding the author the Engineering Research Institute Fellowship during the course of this work.

TABLE OF CONTENTS

TABLE OF CONTENTS (CONT'D)

LIST OF TABLES

LIST OF FIGURES

LIST OF FIGURES CONT'D

I. INTRODUCTION

Qualitative Discussion of Double Scattering of Electrons

Double scattering of electrons is an experiment in which (a) an unpolarized beam (a beam in which the spins are randomly oriented) of electrons is allowed to impinge upon a target called the "polarizer"; (b) a portion of the scattered wave from this target is allowed to impinge on a second target called the "analyser"; (c) the angular distribution of this second scattered wave is studied. The motivation for performing this type of experiment lies in the fact that in certain scattering processes a partially polarized beam (a beam in which there is a preferred direction for the spins) of scattered electrons may be produced from an incident, unpolarized beam. This polarized beam, when scattered by the analyser, will produce an angular distribution of scattered electrons that depends on the azimuthal angle ϕ (that angle measured around the direction of the incident beam). In contrast, the angular distribution from an unpolarized beam has no azimuthal dependence at all. A measurement of the azimuthal asymmetry after double scattering yields information about the polarization of the first scattered beam and thus about the spin-orbit interaction in the scattering process.

A study of double scattering is of interest for several reasons. (1) The theory of it developed by Mott[1] in 1929, has been only sketchily verified in the twenty-nine years since then. Quantitative agreement is almost totally absent and several qualitative effects are still unobserved. (2) It is one of a very few presently available methods of obtaining a polarized beam of electrons and of analysing the polarization. This fact has already been utilized in the first experiment[2,3] that measured the gyromagnetic ratio of the free electron. (3) Measurement of the azimuthal

asymmetry serves as a calibration for using single Mott scattering as a polarization analyser for beams of arbitrary polarization. This is currently in demand in connection with determining the polarization of β-rays. [Mott scattering, however, serves only as a detector for transverse polarization (preferential spin direction perpendicular to the momentum direction) while β-rays from unaligned nuclei possess purely longitudinal polarization (preferential spin direction parallel or antiparallel to the momentum direction). Thus the polarization direction of the β-rays must first be rotated so that at least a measureable component of the polarization is transverse to the beam.] (4) It is expected that when the present lack of agreement of theory and experiment is resolved either better experimental techniques will have been devised, or that information on the perturbing effects, such as atomic electron screening, will have been learned, or perhaps both. (5) Measurement of the Mott asymmetry is one of three measurements necessary to confirm the theory of Coulomb scattering which is assumed to be correct in high energy electron scattering where deviations are attributed to nuclear size effects.

That three independent measurements (for a given energy E, scattering angle θ, and atomic number Z) are needed can be seen as follows. For a spin 1/2 particle a two-component wave function is necessary. Two scattering amplitudes $f(\theta)$ and $g(\theta)$ result, each being a complex number. Thus, there are four real numbers needed for a given E,θ, and Z to describe the scattering. One of them, however, is a phase common to both $f(\theta)$ and $g(\theta)$ which will be unobservable in pure Coulomb scattering. The other three, the magnitudes of $f(\theta)$ and $g(\theta)$ and their relative phase, need

to be measured. Measurements of the single scattering cross section for an unpolarized beam, of the Mott asymmetry in double scattering (which measures essentially the polarization of the first scattered beam), and of the azimuthal asymmetry in triple scattering (which measures essentially the polarization of the second scattered beam) are sufficient. The phase common to both $f(\theta)$ and $g(\theta)$ will be observable only when there is an interference between the nuclear Coulomb scattering and another type of scattering such as electron-electron scattering. Measurement of this phase would thus be necessary for a complete experimental confirmation of Coulomb scattering.

The origin of the azimuthal asymmetry may be seen from a classical model.[2] Consider an unpolarized beam of negative point charges, which also possess magnetic dipole moments, incident on the Coulomb field of the nucleus. Borrowing from quantum mechanics[4], we will represent the unpolarized beam as consisting of equal numbers of electrons with spin up and with spin down. Consider first an electron incident on a nucleus with an impact parameter b_1, see Figure 1(A), such that by Rutherford scattering alone the electron would be scattered into an angle θ, path (a) in Figure 1(A), at which a detector is placed. It experiences an attractive Coulomb force $F_c \sim -1/b_1^2$ in the process. Since, however, the electron is endowed with a magnetic moment, it will experience a second force, the spin-orbit force. The magnetic moment of the electron will experience a torque, also, but a discussion of this torque is not necessary to obtain the qualitative conclusions desired. The spin-orbit force may be understood as follows: An electron moving through a static electric field sees a magnetic field in the coordinate system fixed in the electron by a Lorentz transformation of the electric field. If the electric

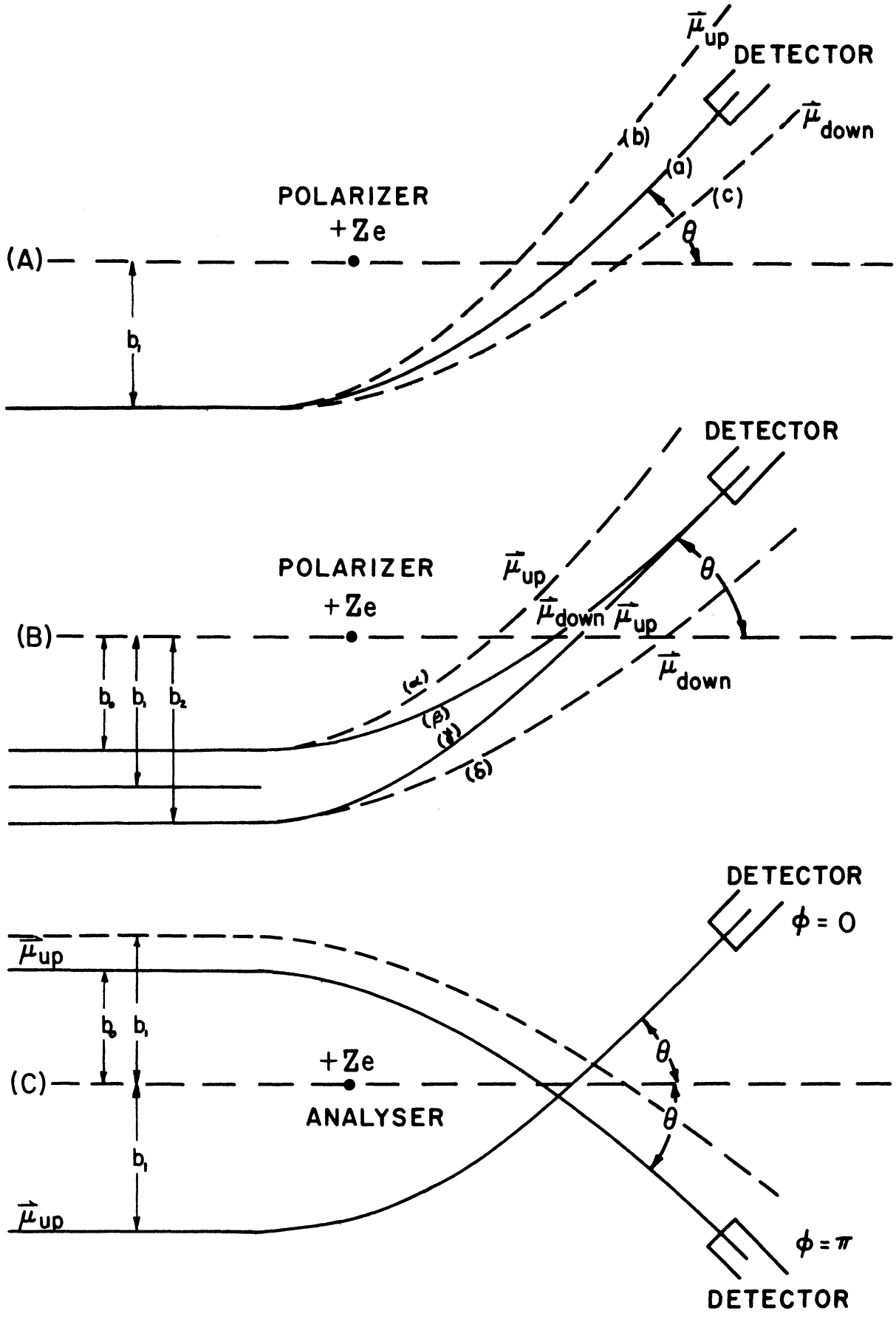

Figure 1. Azimuthal Asymmetry on Double Scattering

field is also inhomogeneous, as a Coulomb field is, a force on the magnetic dipole will result. This is the spin-orbit force. Since it is due to a gradient of the Coulomb field, it has the form $F_{s\text{-}o} \sim \mp 1/b_1^3$ where the minus [plus] sign depends on whether the magnetic moment is up [down]. Note that it depends on a Lorentz transformation. In the nonrelativistic limit $\left(\beta \equiv \frac{v}{c} \to 0\right)$ the spin-orbit force will thus become vanishingly small. Hence relativistic electrons ($\beta \sim 1$) must be considered. Now, for electrons with $\vec{\mu}$ pointing up [down], the spin-orbit force is attractive [repulsive] and causes the electron to follow path (b) [(c)] in Figure 1(A). In both these cases, the electron misses the detector. However, for electrons with impact parameter $b_0 < b_1$ [$b_2 > b_1$], see Figure 1(B), only those with $\vec{\mu}$ down [up] will enter the detector by path (β) [(γ)] while those with $\vec{\mu}$ up [down] will miss it by paths (α) [(δ)]. Since there are as many electrons with $\vec{\mu}$ up as with $\vec{\mu}$ down at any impact parameter for an unpolarized beam, the ratio of the numbers of electrons entering the detector with $\vec{\mu}$ up to those with $\vec{\mu}$ down will be equal to the ratio of the elements of area perpendicular to the beam at the impact parameters b_2 and b_0. This ratio becomes just b_2/b_0 which is greater than one. Hence, the beam entering the detector is partially polarized, the direction of polarization being up.

If now the partially polarized beam is allowed to impinge on a second target, an azimuthal asymmetry results. This is seen as follows: Only that number of electrons with $\vec{\mu}$ up in excess of the number of electrons with $\vec{\mu}$ down need be considered since the remainder will give rise to a scattered distribution which is symmetric in the azimuthal angle φ. Electrons with $\vec{\mu}$ up incident at the bottom of the nucleus with impact parameter b_1, see Figure 1(C), are scattered by the attractive Coulomb

force and attractive spin-orbit force into a detector located at a scattering angle θ in the $\varphi = 0$ direction. However, electrons with $\vec{\mu}$ up incident at the top of the nucleus with the same impact parameter b_1 are scattered by the attractive Coulomb force and the repulsive spin-orbit force and, thus, miss the detector located at a scattering angle θ in the direction $\varphi = \pi$. Nevertheless, electrons with $\vec{\mu}$ up incident on the left with an impact parameter $b_0 < b_1$ are scattered into this detector. Since the ratio of the elements of area, perpendicular to the incident beam, at b_1 to that at b_0 is $b_1/b_0 > 1$, more electrons are scattered in the $\varphi = 0$ direction than in the $\varphi = \pi$ direction. Thus, an azimuthal asymmetry after double scattering has been demonstrated by a classical model.

Certain qualitative features of the asymmetry factor δ, defined as one-half the difference in the counting rates at $\varphi = 0$ and $\varphi = \pi$, may be inferred from the classical model. The asymmetry factor is a function of θ_1, θ_2, Z_1, Z_2, and β (or the energy). It is expected that the dependence is symmetric in the polarizer and the analyser parameters. Hence, let θ refer to either θ_1 or θ_2 and Z refer to either Z_1 or Z_2 in the following discussion.

For a very small angle of scattering ($\theta \rightarrow 0$) the asymmetry factor vanishes. This is understood as follows: For small θ the impact parameter will be large. Since the spin-orbit force is a $1/b_1^3$ law and the Coulomb force is a $1/b_1^2$ law, an electron impinging on the nucleus with a large impact parameter will feel essentially no spin-orbit force compared with the Coulomb force. The spin states of electrons incident at this large impact parameter are thus only slightly separated. This is to say that for small θ the trajectories (b) and (c) in Figure 1(A)

are nearly coincident: Thus, referring now to Figure 1(B), the change in impact parameter from b_1 to b_2 and from b_1 to b_o necessary to bring into the detector the opposite spin states is very small and so $b_o \approx b_2$. The ratio of the number of electrons with $\vec{\mu}$ up to those with $\vec{\mu}$ down entering the detector (for $\theta \to 0$), which is proportional to b_2/b_o, is essentially unity. Thus, no significant polarization results on single scattering for small θ. The asymmetry factor will be small, if the second scattering angle is also small, because of the small polarization of the beam and also because of the action at the analyser. By the latter is meant that for small θ, the deflection due to the spin-orbit force is so small that, referring to Figure 1(C), b_o and b_1 are essentially equal. The asymmetry factor being proportional to b_1/b_o, as shown before, is thus small.

In the limit of very large scattering angles ($\theta \to \pi$) the asymmetry factor again vanishes. This may be understood as follows: For back angle scattering the impact parameters are small. The spin-orbit force then becomes dominant over the Coulomb force, causing wide separation of the spin states, see Figure 2(A). Thus, for only small changes in impact parameter, from b_1 to b_o and b_1 to b_2 in Figure 2(B), are needed to bring the different spin states into the detector. Thus, $b_o \approx b_2$ and so a small polarization results. If this beam is scattered by the analyser at a large angle ($\theta \to \pi$), the asymmetry will be vanishingly small. Again this is due to both the small polarization and the action at the analyser, see Figure 2(C). By arguments similar to those above, it is seen that $b_o \approx b_1$ in Figure 2(C) and hence the asymmetry is very small for extreme back angles.

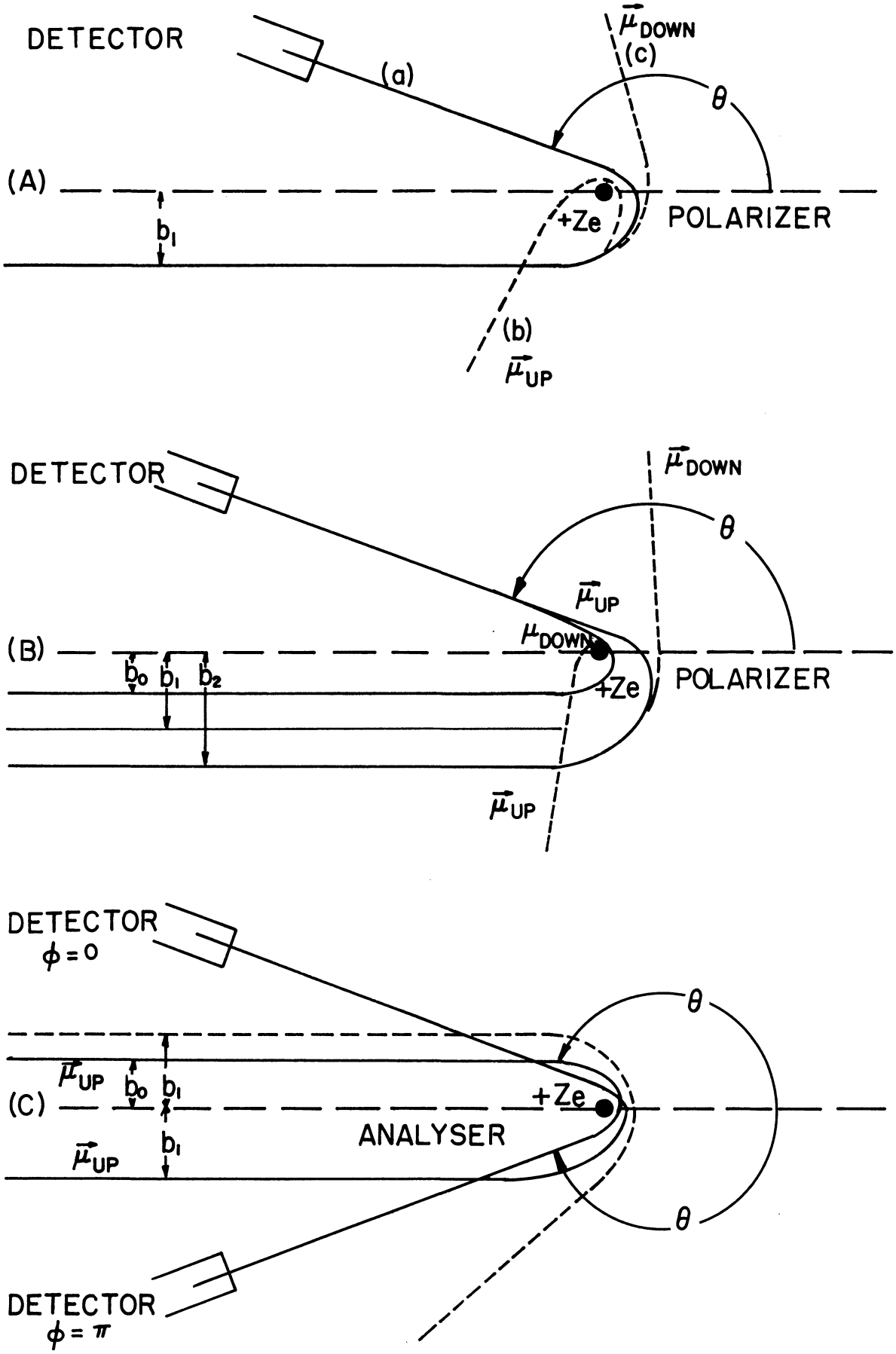

Figure 2. Azimuthal Asymmetry on Double Scattering ($\theta \sim \pi$)

The asymmetry factor increases with increasing atomic number Z. This is understood as follows: Consider an electron beam incident on a nucleus of charge $+Z_\alpha e$ with a given energy and at such an impact parameter b_1^α that it is scattered at an angle θ. Consider also an electron beam incident on a different nucleus of charge $+Z_\beta e \ (Z_\beta > Z_\alpha)$ with the same energy and at such an impact parameter b_1^β that it is scattered at the same angle θ. If these two electron beams feel only a Coulomb force, they will follow respectively paths (a_α) and (a_β) in Figure 3(A). If the electron beams also feel a spin-orbit force, the spin states will be separated in each case. Since the spin-orbit force is proportional to Z, the separation will be greater for larger Z, see Figure 3(A). Since the spin-orbit force is a $1/b_1^3$ law, a proportionately larger change in the impact parameter for case (β) than for case (α) is necessary in order to bring the different spin states into the detector, see Figure 3(B). The ratio of the numbers of electrons with $\vec{\mu}$ up to those with $\vec{\mu}$ down, which is proportional to b_2/b_1, is thus greater in case (β) than in case (α). Hence a larger polarization results in case (β). This tends to make the asymmetry factor larger in case (β). The action at the analyser also tends to make the asymmetry factor larger for case (β). As explained before, only the excess of $\vec{\mu}$ up states need be considered. The asymmetry factor is proportional to b_1/b_o. Hence, it is seen from Figure 3(C) that the action at the analyser also tends to make the asymmetry factor larger for case (β). Hence the asymmetry factor increases with increasing Z. Also it can be seen from the above reasoning, that the asymmetry factor tends to zero as Z tends to zero.

The energy dependence of the asymmetry factor is more easily seen. It has been noted previously that the spin-orbit force depends

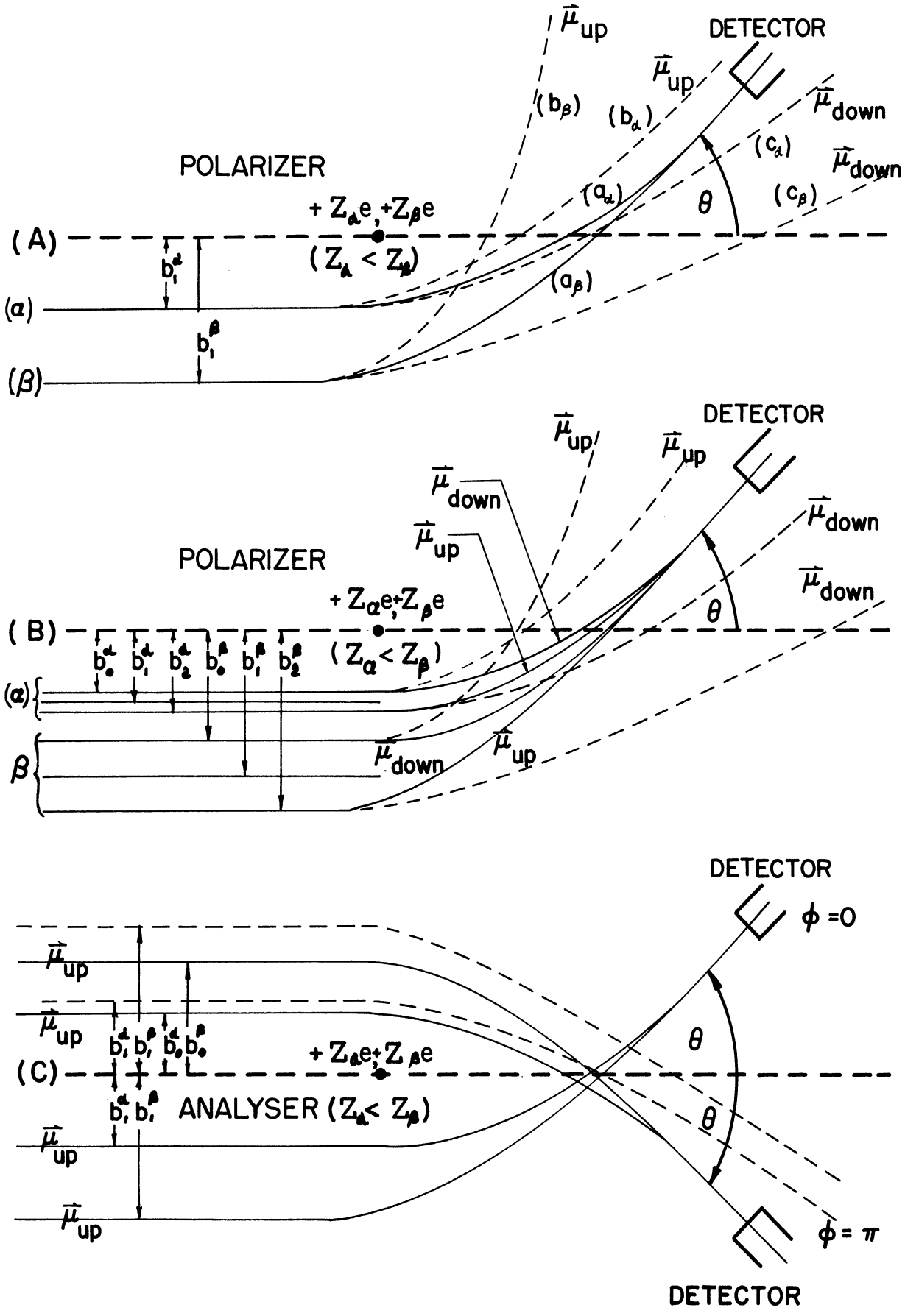

Figure 3. Atomic Number Dependence of Azimuthal Asymmetry

on a Lorentz transformation of the field and so tends to zero as the velocity of the electron tends to zero. Hence, $\delta \to 0$ as $\beta \to 0$. The high energy limit may be understood by remembering that the spin-orbit force is proportional to the magnetic moment of the electron and, hence, is inversely proportional to the relativistic mass of the electron. Hence, the spin-orbit force vanishes for high energies. Thus $\delta \to 0$ as $\beta \to 1$. The assumption of pure Dirac particles (no radiative corrections to the gyromagnetic ratio) has been made here. It is expected by this reasoning that δ would be a maximum for $\beta \sim 1/2$.

In spite of the success of the classical model, the scattering process cannot be considered a truly classical process since the de Broglie wavelength of the impinging electron is of the order of the impact parameter. For instance, for an electron of $\sim$100 kev of energy the de Broglie wavelength is $\sim 3 \times 10^{-10}$cm while for scattering at 90° its classical impact parameter is $\sim 10^{-11}$cm. The process is, therefore, essentially wave-mechanical. Hence, the classical model discussed above must be considered only as a heuristic mental picture.

From the viewpoint of wave-mechanics, the classical model violates the Heisenberg uncertainty principle in two ways. By simultaneously specifying the momentum and the position exactly, it violates the uncertainty principle in its most common form. Of more importance here, it violates the Bohr[5] form of the uncertainty principle by simultaneously specifying the magnetic moment direction and the trajectory. In the actual double scattering experiment, however, the magnetic moment is not resolved as a function of position. Only the asymmetry in scattered intensity is measured and this requires no knowledge of the orientation of the magnetic moment as a function of trajectory.

By avoiding any measurement of the trajectory, the spin effects can be measured precisely.

A resumé of the Mott theory[1] is given in Chapter II, but it is advantageous here to review the basic assumptions and the qualitative results of the Mott theory.

The assumptions are (1) the use of the Dirac relativistic wave equation to describe the electron, (2) the use of the ideal Coulomb field to describe the scattering field, (3) the use of positive energy wave functions only, (4) the initial beam being unpolarized, and (5) single, elastic scattering occuring in both the polarizer and analyser.

Based on these assumptions the theory is a mathematically exact (in the asymptotic region) partial wave analysis of the scattering process. The double scattering cross section that results has the form

$$\sigma(\theta_1,\theta_2,\phi_2) = \sigma(\theta_1)\sigma(\theta_2)\left[1 + \delta(\theta_1,\theta_2)\cos\phi_2\right] \tag{1.1}$$

where $\sigma(\theta)$ is the single scattering cross section for an unpolarized beam, $\delta(\theta_1,\theta_2)$ is the asymmetry factor and the subscripts 1 and 2 refer to the first and second scatterings.

The qualitative predictions of the Mott theory are (1) the double scattering cross section has an azimuthal asymmetry of the form given in Equation (1.1), (2) the asymmetry factor δ has its maximum value for $\beta \sim 1/2$, $\theta \sim 130°$, $Z\alpha \sim 1$ where $\alpha = e^2/\hbar c = 1/137$ (θ and Z refer to either scatterer), (3) $\delta \to 0$ as $\theta \to 0$ or 180°, (4) $\delta \to 0$ as $\beta \to 0$ or 1 and (5) $\delta \to 0$ as $Z \to 0$. Note that the classical model gives complete agreement with the quantum mechanical Mott theory in all the qualitative features.

Review of Previous Electron Double Scattering Experiments

Early attempts[6-14] to observe an azimuthal asymmetry after double scattering either found no asymmetry or one now believed to be of instrumental origin. The most significant of these experiments were those of Dymond[11], Thomson[12], Richter[13], and Kikuchi[14]. A brief discussion of the faults of these experiments is worthwhile.

The experiments of Dymond[11], Thomson[12], and Richter[13], observed no polarization asymmetry. Their failure to observe one is generally attributed to inadequate beam monitoring schemes that allowed the introduction of asymmetries caused by time varying beam energies and intensities and to their use of the "reflection side" of the scattering foils. The "reflection side" of a foil is that side on which the incident beam impinges [side (a) in Figure 4(A)]. Side (b) in Figure 4(A) is called the "transmission side." It was found by Chase and Cox[15] that the scattered intensity for a given scattering angle θ depended on which side of the foil the detector was located. They found that the detector on the reflection side received more electrons than the detector on the transmission side did, see Figure 4(B). This effect was attributed by Goertzel and Cox[16] to plural scattering, which is a combination of a small number of large angle scatterings. They obtained by an approximate theoretical treatment qualitative agreement with experiment. Their treatment has since been refined by Ryu[17] with correspondingly better agreement. Ryu, Hashimoto and Nonaka[18] have also studied the effect experimentally.

The so-called reflection-transmission asymmetry may be understood qualitatively from plural scattering by the following simplified picture. The most probable combination of scatterings for a very thin

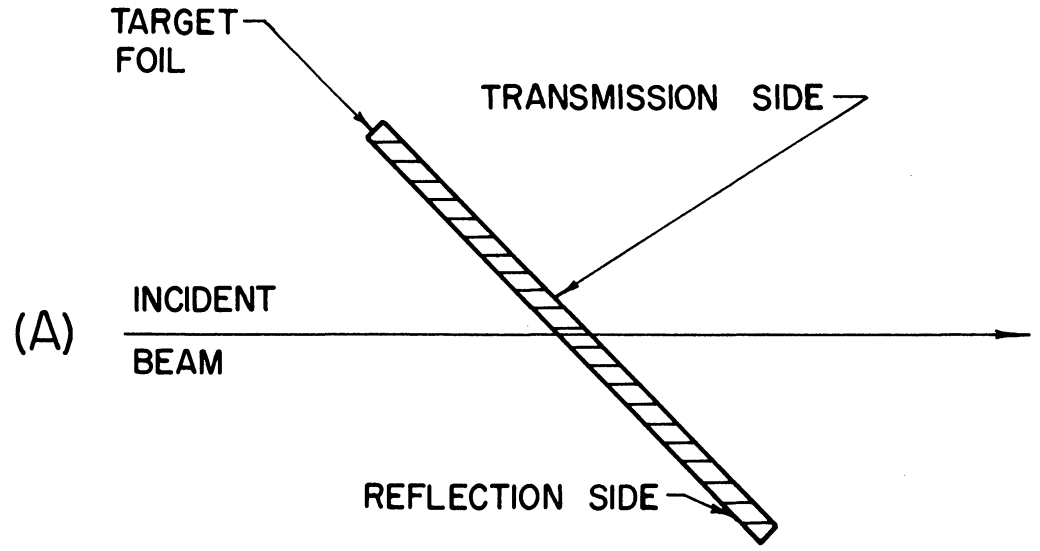

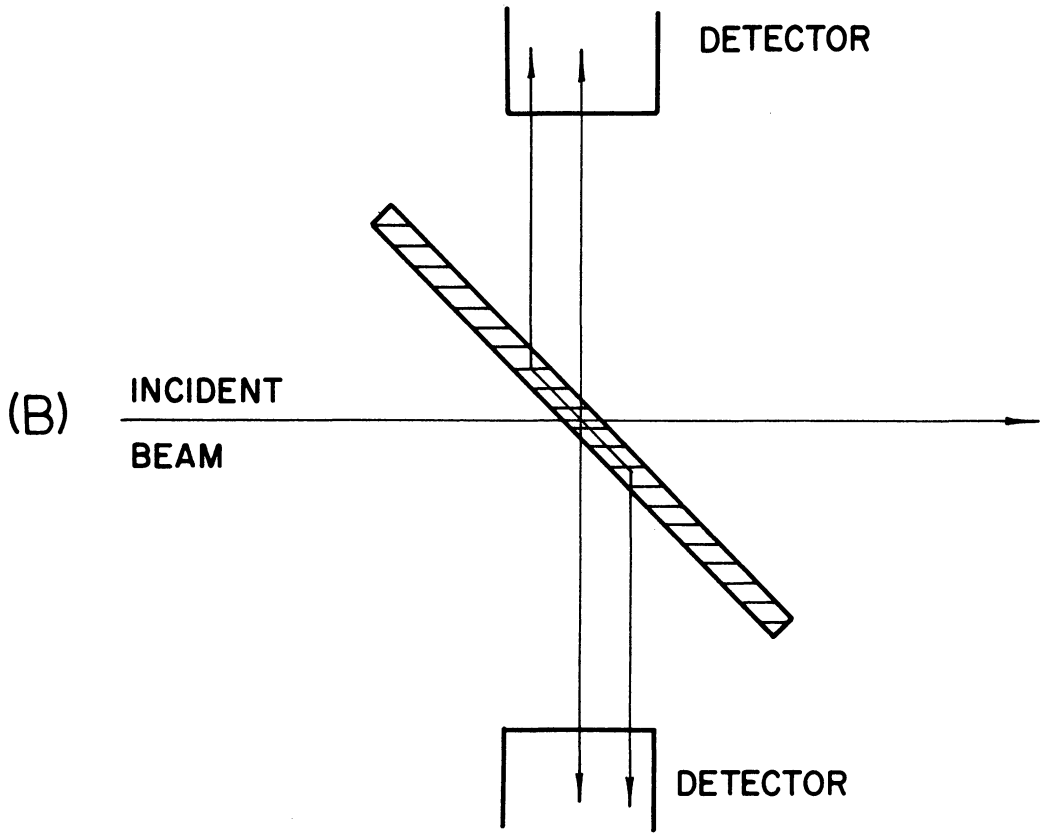

Figure 4. Reflection - Transmission Effect

foil consists of a first scattering in the plane of the foil and a second scattering out of the foil into the detector. The detector on the reflection side of the foil in Figure 4(B) thus receives electrons scattered through 90° and electrons twice scattered through 45°. The detector on the transmission side of the foil in Figure 4(B) receives electrons scattered through 90° and electrons scattered first at 135° and secondly at 45°. Since the cross section for scattering at 45° is much larger than at 135°, more electrons will enter the detector located on the reflection side of the foil. The point of most interest here is that, by using the reflection side of the foil, Dymond, Thomson, and Richter did not fulfill the single scattering assumption of the Mott theory.

The Kikuchi experiment did find asymmetries agreeing with the predictions of Mott over a range of energies from 39 kev to 86 kev. However, the reflection side of both the polarizer and analyser were used, thus allowing plurally scattered electrons to enter the detectors. The polarizer was a gold foil 10^{-3} cm thick. According to the calculations of Rose and Bethe[19,20] a depolarization of 40% would result from multiple scattering in a foil as thick as this. It is thus very doubtful that the asymmetry found by Kikuchi was the true Mott asymmetry. Though momentum analysis of the doubly scattered electrons was employed to eliminate inelastically scattered electrons from his data, the elastic peak must have contained many electrons either plurally or multiply scattered. Kikuchi's method of elimination of spurious instrumental asymmetries is open to question since his method requires the assumption that the spurious instrumental asymmetry is independent of the energy of the electrons. With the magnetic fields of the momentum analysers present this assumption seems doubtful. Also, because of the structure of the

apparatus Kikuchi was unable to demonstrate the cosine dependence in azimuth as predicted by Mott. Hence, it is now believed[21] that the asymmetry found by Kikuchi was of instrumental origin.

In 1942, Shull, Chase and Myers[22] detected an azimuthal asymmetry which agreed with the Mott value within experimental error. Thin foils were used to avoid depolarization by multiple scattering. The reflection-transmission asymmetry was eliminated from the data by taking suitable ratios. Spurious instrumental asymmetries were eliminated from the experimental asymmetry by dividing the asymmetry obtained with gold by that obtained with aluminum in the analyser. The asymmetry found in the latter case should be essentially the spurious instrumental asymmetry since the Mott asymmetry is very small for low Z elements. Unfortunately, they did not report any demonstration of the cosine dependence of the azimuthal asymmetry. Though successful, the experiment was very limited in scope. The asymmetry factor was found only for one set of the five parameters: $\theta_1 = \theta_2 = 90°$, $Z_1 = Z_2 = 79$(Au), E = 400 kev ($\beta = .83$). Trounson and Simpson[23] repeated this experiment with the same apparatus except for an improved detection system and obtained compatible results.

Shinohara and Ryu[24] attempted a study of the energy dependence of the Mott asymmetry. They used thin gold foils in transmission positions. The angles of scattering were $\theta_1 = 90°$ and $\theta_2 = 78°$. The energies studied were 45, 60, 70, 90, and 92 kev. Rough agreement with theory was obtained. Though care was taken in the construction of the apparatus to avoid instrumental asymmetries, they were not directly measured nor were they eliminated from the data. The asymmetries reported were not shown to have a cosine dependence in azimuth as the Mott asymmetry possesses.

Ryu[18,25] subsequently studied the Mott asymmetry for angles of scattering greater than 90° over a range of energy from 60 to 130 kev. Thin gold foils were used. The polarizer was in the transmission position but the analyser was used in the reflection position. The instrumental asymmetries were divided from the data. The resulting asymmetries were shown to have a cosine dependence in azimuth but only about one-half the predicted amplitude. Plural scattering was suspected as the cause of the discrepancy but was not evaluated experimentally. A theoretical estimate of plural scattering was unsuccessful in accounting for the difference. Indeed, arrangements more conducive to plural scattering gave consistently larger asymmetries.

The experiment of Louisell, Pidd and Crane[3] that measured the gyromagnetic ratio of the free electron utilized Mott double scattering. Thin gold foils in transmission positions were used. The scattering angles were $\theta_1 = 90°$ and $\theta_2 = 78°$. The energy of the electrons was 420 kev. The instrumental asymmetry was found using aluminum as the analyser and was divided from the data. The resulting asymmetry was shown to have a cosine dependence in azimuth and about the predicted amplitude. Actually, the exact amplitude was not of interest in this experiment, so long as it was detectable, since only the rotation of the plane of maximum asymmetry by a perturbing magnetic field needed to be measured.

Recently Pettus[26] has studied the Mott asymmetry using thin gold targets. Using scattering angles of 90° and 120° at the polarizer and analyser respectively, he measured the Mott asymmetry for eight energies between 80 kev and 200 kev. The measured values of δ are from 10% to 80% low compared to theory, the better agreement being obtained

at the higher energies. Spurious instrumental asymmetries were measured using an aluminum scatterer in the polarizer and were eliminated from the data. The cosine dependence of the asymmetry was not demonstrated however. The reflection side of the analyser foil was used by each counter. At 130 kev Pettus also measured the Mott asymmetry at second scattering angles of 60° and 90°, the first scattering angle being fixed at 90°. The point at 60° is in good agreement with theory. Since the reflection - transmission effect was not eliminated from the measurement at 90° this point is of doubtful validity.

To summarize, the Mott asymmetry has been observed by four groups of experimenters - Shull, Chase and Myers, Ryu and co-workers, Louisell, Pidd and Crane, and Pettus. Quantitative agreement with theory is almost entirely lacking. Also, several qualitative features of the Mott theory have not been satisfactorily demonstrated. Among these is the increase in the asymmetry factor with increasing energy in the low energy region (30 kev to 130 kev for gold at right angle scatterings). Both Ryu and Pettus obtained limited success in observing this effect. Ryu had even less success in demonstrating the increase in the asymmetry factor with increasing angle at angles of scattering somewhat greater than 90°. No attempt has been made to observe the decrease in the asymmetry at extreme back angles or at high energies. Essentially no study of the atomic number dependence of the asymmetry factor has been made. Only gold ($Z = 79$) and aluminum ($Z = 13$) have been studied except for the insertion of a silver ($Z = 47$) foil in the analyser in the Louisell, Pidd and Crane experiment to check whether the observed asymmetry had the expected property of smaller asymmetry for smaller Z. A summary of the experimental values of the asymmetry factor has been given by Tolhoek[21].

Present Experimental Proposal

It is readily seen from the last section that further experimental study of the Mott asymmetry is desirable. Thus, an experiment aimed at obtaining quantitative agreement with theory over a range of scattering angles was undertaken. The particular energy 121 kev was chosen for intensive study because the Mott asymmetry is near its maximum there and because corrections to the Mott theory due to atomic electron screening of the Coulomb field should be small. This is true since the bombarding energy 121 kev is larger than the binding energy of any of the atomic electrons (80.67 kev for the K electrons in gold). The element gold was chosen for intensive study since it is a high Z element ($Z = 79$) and self-supporting targets 10^{-6} cm thick can be made while gold leaf 9×10^{-6} cm thick is even commercially available. Due to this fact, most experiments in the past have used gold and many theoretical calculations have been done for it.

Since the asymmetry factor depends symmetrically upon the parameters of the polarizer and the analyser, it was decided, for experimental convenience, to fix the angle of scattering at the polarizer at 90° and to construct the analyser assembly so as to allow detection of scattered electrons at scattering angles between 65° and 165°. This range includes the increase of the asymmetry factor with increasing angle and its subsequent decrease with increasing angle at extreme back angles. The analyser assembly was also constructed so as to allow rotation about the direction of incidence to the second target and thus allow measurement of the cosine dependence of the asymmetry. Both the polarizer and the analyser were constructed so as to allow insertion of different target elements.

Three major experimental problems were anticipated in the construction of the apparatus: inclusion in the data of spurious instrumental asymmetries, poor signal to background ratio, and the possibility of non-single or non-elastic scattering in the target foils. Actually the three problems are not completely distinct, but are somewhat interrelated. The equipment was built so as to minimize if not eliminate these errors.

To avoid the inclusion of spurious instrumental asymmetries in the data, a two-pronged attack was undertaken. First the apparatus was built and adjusted to have as complete symmetry about the direction of incidence to the analyser as possible. To eliminate any residual spurious asymmetry from the gold data, the theoretical prediction that low Z elements should exhibit no appreciable Mott asymmetry was used. The asymmetry found after inserting aluminum targets in place of the gold targets was considered to be spurious and this asymmetry was then divided from the gold data.

The problem of obtaining a good signal to background ratio was believed to be a potentially difficult problem since for typical scattering angles, aperture, energy, and atomic number only one electron would be counted after double scattering for every 10^{12} electrons impinging on the first target. Lead shielding and collector cups to absorb the transmitted beam at each target were used. They were not expected to be adequate. Further reduction of background at the analyser may be obtained, using the inverse square law, by removing the analyser far from the polarizer. If the beam were allowed to also fall off by the inverse square law, nothing would be gained. If, however, the beam were magnetically focused from the polarizer to the analyser, as originally suggested

by Crane[27], the signal to background would be greatly improved. Magnetic, rather than electric, focusing was used since it preserves the relation between the spin angular momentum vector and the momentum vector.[28-31] A transversely polarized beam thus remains transversely polarized.

To insure single scattering at each target precautions must be taken to avoid the occurrence of both multiple scattering and plural scattering. Multiple scattering may be minimized by using thin target foils. The gold foils used, which were 9×10^{-6} cm thick, were thin enough to insure single scattering in the range of scattering angles 65° to 165° that was used. As pointed out previously, the occurrence of plural scattering in thin foils is markedly affected by the angles the target foil makes with both the direction of incidence and direction of scattering. For this reason, a mechanism for tilting the target foil independent of all other adjustments was built into the analyser head.

In most previous investigations of the Mott asymmetry, two counters separated in azimuth by 180° were used. It can be seen, however, that for scattering angles greater than 90° two such counters cannot both view the transmission side of the target. To avoid the use of the reflection side of the target, this symmetric arrangement of counters was abandoned and only one counter was used to actually observe the Mott asymmetry. A second counter was used to monitor the beam intensity. A monitor placed at a position where multiple or plural scattering is prevalent can give erroneous readings of the beam intensity if slight variations in the target orientation or the beam alignment occur. The effect might be magnified if there were local variations in the target thickness

in the region where the beam strikes the target. Thus, it seems that a beam monitor should be located so as to monitor the single-scattered beam intensity. To do this, it must be on the transmission side of the target, out of the way of the working counter, and away from the transmitted beam. For these reasons, the monitor was placed at a scattering angle of 45° on the transmission side of the target and in the azimuthal plane of the working counter.

Though there are some theoretical grounds to believe that inelastic scattering does not appreciably affect the measurement of the Mott asymmetry, it was felt worthwhile to investigate this experimentally. Since it was felt that only the inelastic tail on the energy distribution need be discriminated against, a low resolution electrostatic energy analyser was constructed. It was made interchangeable with the plain Geiger counter. Thus, a comparison between measurements of the Mott asymmetry with and without rough energy analysis was possible.

Results and Conclusions

The Mott asymmetry has been observed for 121 kev electrons scattering from thin gold targets at scattering angles of 90° at the polarizer and from 80° to 140° at the analyser using energy analysis. Good agreement between the measured asymmetry factors and the theoretical predictions for an unscreened Coulomb field was obtained for angles between 90° and 110°. The discrepancy between observed and predicted values from 120° to 140° is believed due to plural scattering. The measurement at 80° is enough higher than the unscreened field prediction to indicate, though perhaps not prove, the existence of screening effects on the asymmetry amplitude at this angle. For all measurements of the asymmetry amplitude, the cosine dependence on the azimuthal angle was observed.

It is believed that the success of the present experiment in comparison to previous attempts at observation of the Mott asymmetry in this energy region can be attributed in the most part to the following techniques: 1) the observation of the entire azimuthal dependence of the double scattering cross section rather than just at the points of expected maximum and minimum asymmetry, 2) the careful design and testing of the slit system and analyser assembly, 3) the great improvement in the ratio of scattered electron counting rate to the background counting rate through the use of a magnetic lens between the two scatterings, and 4) the use of energy selection after double scattering. On the basis of the present data, it cannot be concluded that energy selection is necessary in a double scattering experiment in which no magnetic lens between the two scatterings is used. Such a conclusion does, however, remain a possibility.

II. THEORY OF THE EXPERIMENT

The Mott Theory

In 1929 Mott[1] investigated theoretically the scattering of relativistic electrons by a central field. Specifically, he calculated by the Dirac relativistic wave equation the single and double scattering cross sections of a beam of electrons, described by positive energy wave functions and initially unpolarized, which undergo single, elastic scattering by an ideal atomic Coulomb field. Implicit in the Dirac equation is the fundamental property of spin possessed by the electron. It is the interaction of this spin with the scattering field that gives Mott double scattering its great importance.

Mott[1] found that the wavefunction in asymtotic form describing this scattering process could be expressed as

$$\psi_3 \sim A e^{ikz - i\gamma \ln k(r-z)} + \left[Af(\theta) - Bg(\theta)e^{-i\Phi}\right] \frac{e^{ikr + i\gamma \ln kr}}{r} \tag{2.1}$$

$$\psi_4 \sim B e^{ikz - i\gamma \ln k(r-z)} + \left[Bf(\theta) + Ag(\theta)e^{i\Phi}\right] \frac{e^{ikr + i\gamma \ln kr}}{r} \tag{2.2}$$

with

$$f(\theta) = \frac{1}{k}\left[-i\gamma' F(\theta) + G(\theta)\right] \tag{2.3}$$

$$g(\theta) = \frac{1}{k}\left[i\gamma' \cot\frac{\theta}{2} F(\theta) + \tan\frac{\theta}{2} G(\theta)\right] \tag{2.4}$$

$$F(\theta) = \frac{i}{2}\sum_{\ell=0}^{\infty} (-1)^{\ell}\left[\ell C_{\ell} + (\ell+1)C_{\ell+1}\right] P_{\ell}(\cos\theta) \tag{2.5}$$

$$G(\theta) = \frac{i}{2}\sum_{\ell=0}^{\infty} (-1)^{\ell}\left[\ell^2 C_{\ell} - (\ell+1)^2 C_{\ell+1}\right] P_{\ell}(\cos\theta) \tag{2.6}$$

$$C_\ell = -e^{-i\pi\ell}\,\Gamma(\rho_\ell - i\gamma)/\Gamma(\rho_\ell + 1 + i\gamma) \tag{2.7}$$

$$\rho_\ell = +\sqrt{\ell^2 - \alpha^2} \tag{2.8}$$

$$\alpha = \frac{Ze^2}{\hbar c} \tag{2.9}$$

$$\gamma = \frac{\alpha}{\beta} \tag{2.10}$$

$$\gamma' = \gamma\sqrt{1-\beta^2} \tag{2.11}$$

$$\beta = \frac{v}{c} \tag{2.12}$$

$$k = \frac{m_0 c}{\hbar}\,\frac{\beta}{\sqrt{1-\beta^2}} \tag{2.13}$$

Mott scattering may be characterized by a scattering matrix Ω which is the matrix that transforms the incident amplitudes in (2.1) and (2.2) into the scattered amplitudes, denoted by u_3 and u_4.

$$\begin{pmatrix} u_3 \\ u_4 \end{pmatrix} = \begin{pmatrix} f(\theta) & -g(\theta)e^{-i\phi} \\ g(\theta)e^{i\phi} & f(\theta) \end{pmatrix} \begin{pmatrix} A \\ B \end{pmatrix} \tag{2.14}$$

$$\Omega(\theta,\phi) = \begin{pmatrix} f(\theta) & -g(\theta)e^{-i\phi} \\ g(\theta)e^{i\phi} & f(\theta) \end{pmatrix} \tag{2.15}$$

Mott double scattering may conveniently be described by density matrix techniques.[32,33,21,29]. It is not a necessary formalism for the purposes of this section but it will be necessary for the calculations in a later section and so will be used here.

The double scattering experiment is schematically represented in Figure 5. The first incident beam, characterized by the density matrix ρ_{1i}, the first scattered beam, characterized by ρ_{1s}, the second incident beam, characterized by ρ_{2i}, the x_1 axis, the z_1 axis, the x_2 axis, and the Z_2 axis all lie in the plane of the paper of Figure 5. The y_1 axis and the y_2 axis are directed into the paper.

The beam incident on the first target is assumed unpolarized and of unit intensity. It may be characterized by the density matrix

$$\rho_{1i} = \frac{1}{2} 1 \tag{2.16}$$

where 1 is the 2 x 2 identity matrix. The first scattering matrix (2.15) may be expressed as

$$\Omega(\theta_1,\phi_1) = f(\theta_1) - i g(\theta_1) \vec{\sigma} \cdot \vec{n}_1 \tag{2.17}$$

The incident beam has been taken in the + Z_1 direction and σ_{Z_1} taken as diagonal, $\vec{\sigma}$ being the usual Pauli spin operator. $\vec{n}_1$ is a unit normal to the scattering plane defined by

$$\vec{n}_1 = \frac{\vec{k}_{1i} \times \vec{k}_{1s}}{|\vec{k}_{1i} \times \vec{k}_{1s}|} = (-\sin\phi_1, \cos\phi_1, 0) \tag{2.18}$$

where $\vec{k}_{1i}$ and $\vec{k}_{1s}$ are the wave vectors associated with the first incident and first scattered beams respectively.

The density matrix of the first scattered beam is given by

$$\rho_{1s} = \Omega(\theta_1,\phi_1)\, \rho_{1i}\, \Omega^{\dagger}(\theta_1,\phi_1) \tag{2.19}$$

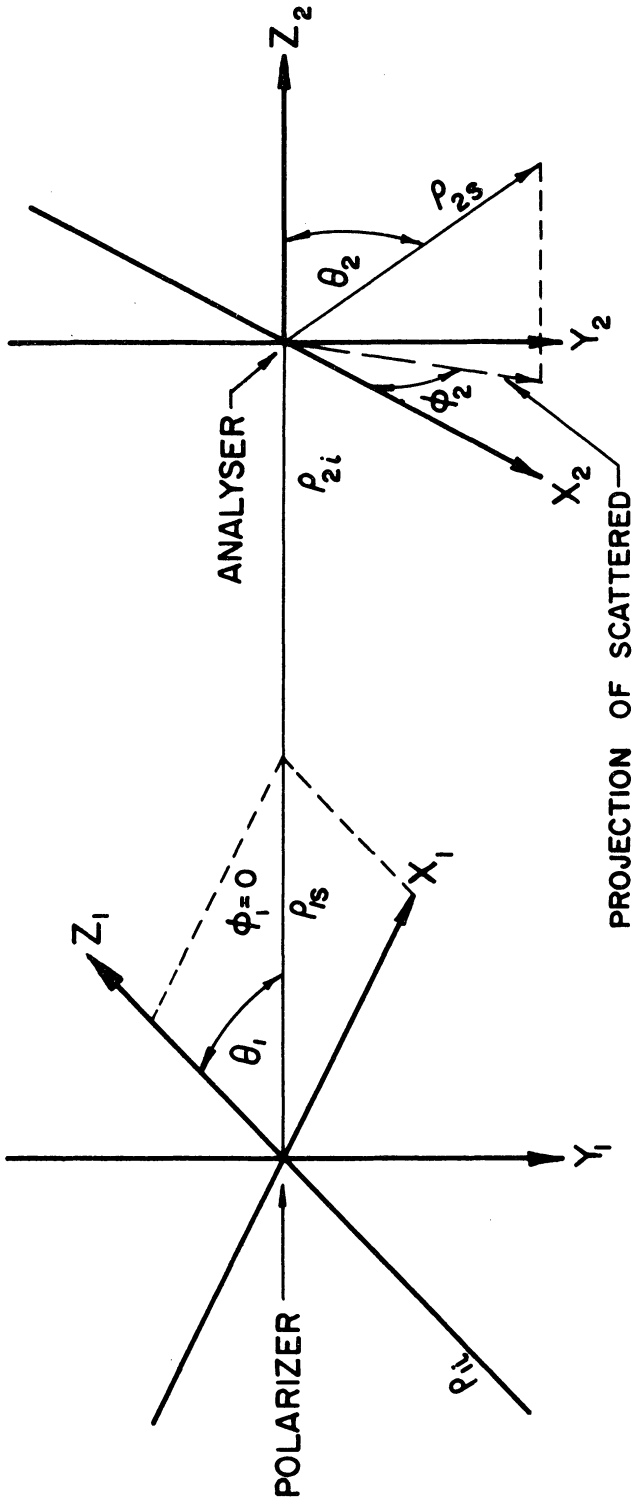

Figure 5. Coordinate System of Double Scattering Experiment

$$\therefore \rho_{1S} = \frac{1}{2}\left[|f(\theta_1)|^2 + |g(\theta_1)|^2\right] + \frac{i}{2}\left[f(\theta_1)g^*(\theta_1) - f^*(\theta_1)g(\theta_1)\right]\vec{\sigma}\cdot\vec{n}_1 \tag{2.20}$$

The first scattering cross section is given by

$$\sigma(\theta_1) = \frac{tr\ 1\rho_{1S}}{tr\ \rho_{1i}} \tag{2.21}$$

$$\therefore \sigma(\theta_1) = |f(\theta_1)|^2 + |g(\theta_1)|^2 \tag{2.22}$$

The polarization vector of the first scattered beam is given by

$$\vec{P}(\theta_1,\phi_1) = \frac{tr\ \vec{\sigma}\rho_{1S}}{tr\ \rho_{1S}} \tag{2.23}$$

$$\therefore \vec{P}(\theta_1,\phi_1) = P(\theta_1)\vec{n}_1 \tag{2.24}$$

where

$$P(\theta_1) = i\,\frac{f(\theta_1)g^*(\theta_1) - f^*(\theta_1)g(\theta_1)}{|f(\theta_1)|^2 + |g(\theta_1)|^2} \tag{2.25}$$

Thus the first scattered beam is partially polarized. Note that the polarization vector is normal to the scattering plane indicating that the polarization is entirely transverse. The degree of polarization is defined by the absolute value of $P(\theta_1)$. The density matrix of the first scattered beam may now be expressed as

$$\rho_{1S} = \frac{\sigma(\theta_1)}{2}\left[1 + P(\theta_1)\vec{n}_1\cdot\vec{\sigma}\right] \tag{2.26}$$

The second scattering matrix is given by

$$\Omega(\theta_2,\phi_2) = f(\theta_2) - i g(\theta_2)\vec{\sigma}\cdot\vec{n}_2 \tag{2.27}$$

where the second incident beam has been taken in the Z_2 direction and σ_{Z_2} taken as diagonal. $\vec{n}_2$ is the unit normal to the second scattering plane given by

$$\vec{n}_2 = \frac{\vec{k}_{2i}\times\vec{k}_{2s}}{|\vec{k}_{2i}\times\vec{k}_{2s}|} = (-\sin\phi_2, \cos\phi_2, 0) \tag{2.28}$$

where $\vec{k}_{2i}$ and $\vec{k}_{2s}$ are the wave vectors of the second incident and the second scattered beams respectively.

In order to properly represent the second incident beam the spin density matrix of the first scattered beam must be transformed from its representation having σ_{Z_1} diagonal to the representation having σ_{Z_2} diagonal. This is done by a rotation about the y axis through an angle θ_1.

$$\rho_{2i} = e^{\frac{i\theta_1\sigma_y}{2}}\rho_{1s}\,e^{-\frac{i\theta_1\sigma_y}{2}} \tag{2.29}$$

The direction of first scattering is taken as $\phi_1 = 0$ in accordance with the work of Mott.

$$\therefore \rho_{1s} = \frac{\sigma(\theta_1)}{2}\left[1 + P(\theta_1)\sigma_y\right] \tag{2.30}$$

$$\rho_{2i} = e^{\frac{i\theta_1\sigma_y}{2}}\frac{\sigma(\theta_1)}{2}\left[1+P(\theta_1)\sigma_y\right]e^{-\frac{i\theta_1\sigma_y}{2}} \tag{2.31}$$

$$\therefore \rho_{2i} = \frac{\sigma(\theta_1)}{2}\left[1 + P(\theta_1)\sigma_y\right] \tag{2.32}$$

Express this as

$$\rho_{2i} = \frac{\sigma(\theta_1)}{2}\left[1 + P(\theta_1)\vec{n}_1\cdot\vec{\sigma}\right] \tag{2.33}$$

remembering that $\vec{n}_1$ is now a unit vector in the y direction.

The second scattered beam is now given by

$$\rho_{2s} = \Omega(\theta_2,\phi_2)\,\rho_{2i}\,\Omega^{\dagger}(\theta_2,\phi_2)\,. \tag{2.34}$$

$$\therefore \rho_{2s} = \frac{\sigma(\theta_1)\sigma(\theta_2)}{2}\left[1 + P(\theta_1)P(\theta_2)\vec{n}_1\cdot\vec{n}_2 + P(\theta_1)\vec{n}_1\cdot\vec{\sigma} + P(\theta_2)\vec{n}_2\cdot\vec{\sigma}\right] + \frac{\sigma(\theta_1)P(\theta_1)}{2}\left[-Q(\theta_2)(\vec{n}_1\times\vec{n}_2)\cdot\vec{\sigma} + R(\theta_2)\left\{(\vec{n}_1\cdot\vec{n}_2)(\vec{n}_2\cdot\vec{\sigma}) - \vec{n}_1\cdot\vec{\sigma}\right\}\right] \tag{2.35}$$

where $$Q(\theta) = f(\theta)g^{*}(\theta) + f^{*}(\theta)g(\theta) \tag{2.36}$$

$$R(\theta) = 2|g(\theta)|^2 \tag{2.37}$$

The double scattering cross section is given by

$$\sigma(\theta_1,\theta_2,\phi_2) = \frac{tr\,1\rho_{2s}}{tr\;\rho_{1i}} \tag{2.38}$$

$$\therefore \sigma(\theta_1,\theta_2,\phi_2) = \sigma(\theta_1)\sigma(\theta_2)\left[1 + P(\theta_1)P(\theta_2)\vec{n}_1\cdot\vec{n}_2\right] \tag{2.39}$$

or

$$\sigma(\theta_1,\theta_2,\phi_2) = \sigma(\theta_1)\sigma(\theta_2)\left[1 + P(\theta_1)P(\theta_2)\cos\phi_2\right] \tag{2.40}$$

Thus the double scattering cross section has an azimuthal asymmetry.

The Mott asymmetry factor $\delta(\theta_1,\theta_2)$ is given by

$$\delta(\theta_1,\theta_2) = P(\theta_1)P(\theta_2) \tag{2.41}$$

The asymmetry factor is a function of the atomic numbers Z_1 and Z_2 of the two scatterers and the energy as well as the two scattering angles θ_1 and θ_2.

Numerical calculations of the single scattering cross section $\sigma(\theta)$ and the polarization $P(\theta)$ are very difficult owing to the slow convergence of the series for both $F(\theta)$ and $G(\theta)$ given in (2.5) and (2.6) respectively. Over the years a few calculations[1,34] of $P(\theta)$ have been made. Recently Sherman[35] has made an accurate and compreshensive tabulation of the polarization $P(\theta)$ and also the cross section $\sigma(\theta)$ with the aid of UNIVAC. His calculations cover the range of scattering angles from 15° to 165° in 15° intervals, the range of energies corresponding to $\beta = \frac{v}{c} = .2, .4, .5, .6, .7, .8, .9$, and atomic numbers 13, 48, and 80. Sherman[36] has also calculated $P(\theta)$ [and $\sigma(\theta)$] for gold ($Z = 79$) and aluminum ($Z = 13$) at 121 kev ($\beta = .59$) from 15° to 165°. These are given in Table I. His results for gold are plotted in Figure 6.

Mott Scattering in a Magnetic Field

Mott scattering in a magnetic field has been discussed by Louisell[2] and Mendlowitz[29,30]. Mendlowitz has shown that the effect of the magnetic field on the scattering process itself is negligible and only the space rotation and spin precession occurring between the two scatterings need be considered. For a magnetic field constant in space and time Mendlowitz showed that the effect of the field between the scatterers may be represented by an interaction operator

$$R = e^{i\xi} e^{-i(\vec{l}\cdot\vec{b})\omega t} e^{-\frac{i(\vec{\sigma}\cdot\vec{b})\omega t}{2}} \qquad (2.42)$$

TABLE I

MOTT POLARIZATION AND CROSS SECTION AS CALCULATED BY SHERMAN[36]

$\beta = .59$	GOLD (Z = 79)		ALUMINUM (Z = 13)	
θ	$P(\theta)$	$\sigma(\theta)$*	$P(\theta)$	$\sigma(\theta)$*
15°	.003347	2.349×10^{6}	-.0003192	6.318×10^{4}
30°	.01616	1.600×10^{5}	-.002338	4.086×10^{3}
45°	.001446	3.79×10^{4}	-.006359	8.414×10^{2}
60°	-.06133	1.494×10^{4}	-.01193	2.798×10^{2}
75°	-.1586	7.591×10^{3}	-.01823	1.217×10^{2}
90°	-.2666	4.482×10^{3}	-.02422	6.327×10^{1}
105°	-.3601	2.936×10^{3}	-.02869	3.753×10^{1}
120°	-.4136	2.093×10^{3}	-.03046	2.480×10^{1}
135°	-.4058	1.612×10^{3}	-.02851	1.804×10^{1}
150°	-.3264	1.336×10^{3}	-.02225	1.438×10^{1}
165°	-.1824	1.194×10^{3}	-.01229	1.254×10^{1}

* $\sigma(\theta)$ in Barns Per Steradian

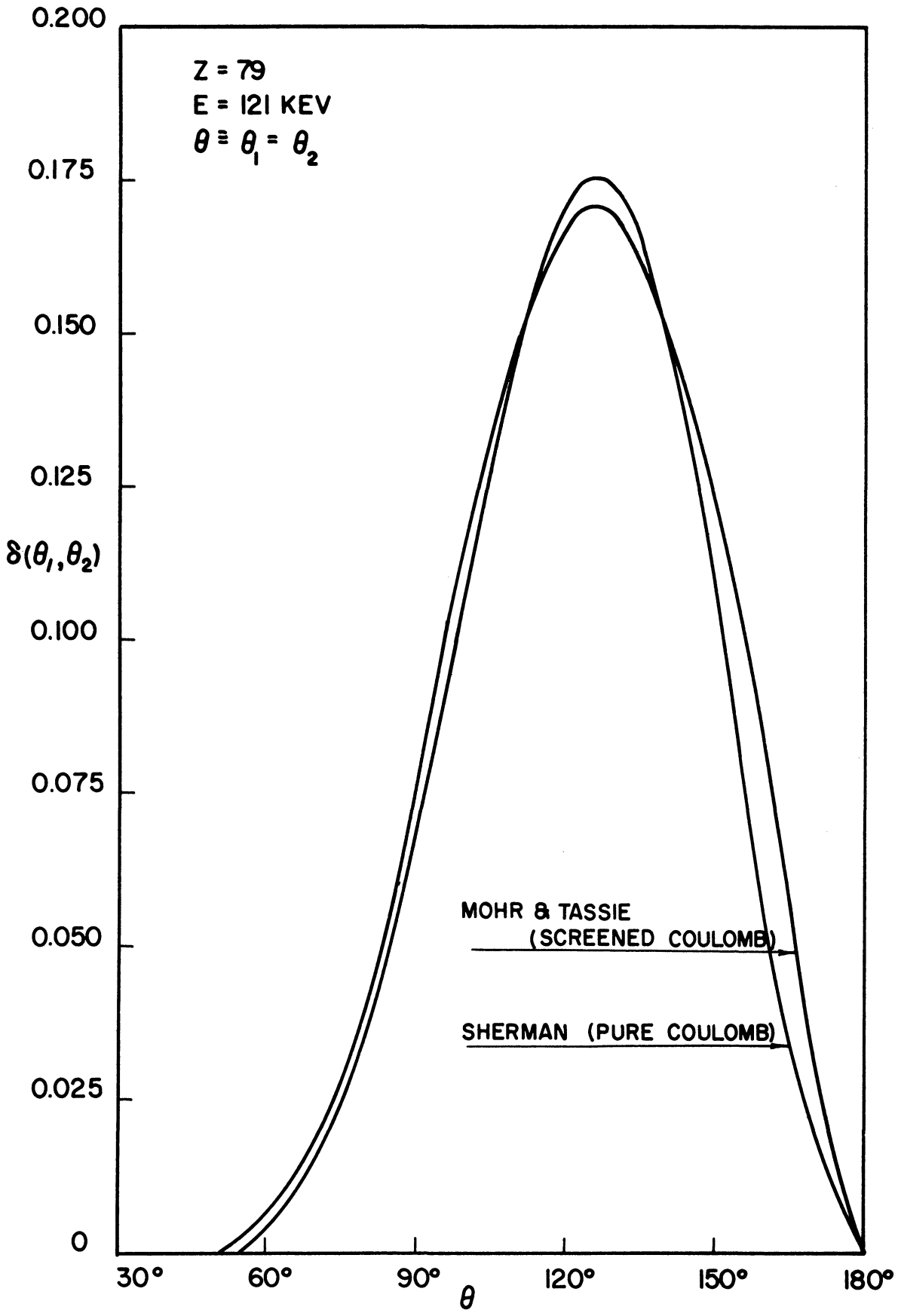

Figure 6. Mott Asymmetry Factor Vs. θ

where $\vec{\ell}$ is the orbital angular momentum in units of $\hbar$, $\vec{\sigma}$ is the Pauli spin vector, $\vec{b}$ is a unit vector in the direction of the magnetic field, ξ is just a phase for present purposes and

$$\omega = \frac{|e|B}{m} = \frac{|e|B\sqrt{1-\beta^2}}{m_0} \tag{2.43}$$

where B is the magnitude of the field.

The density matrix of the second incident beam is now given by

$$\rho_{2i}^{rot} = R\,\rho_{2i}R^{\dagger} \tag{2.44}$$

where ρ_{2i} is given by (2.33). This yields directly

$$\rho_{2i}^{rot} = \frac{\sigma(\theta_1)}{2}\Big[1+P(\theta_1)\vec{\sigma}\cdot\{\vec{n}_1\cos\omega t - \vec{n}_1\times\vec{b}\sin\omega t + (1-\cos\omega t)(\vec{n}_1\cdot\vec{b})\vec{b}\}\Big] \tag{2.45}$$

The polarization of this beam is

$$\vec{P}_{2i}^{rot}(\theta_1,\phi_1=0) = \frac{tr\ \rho_{2i}^{rot}\vec{\sigma}}{tr\ \rho_{2i}^{rot}} \tag{2.46}$$

$$\therefore \vec{P}_{2i}^{rot}(\theta_1,\phi_1=0) = P(\theta_1)\Big[\vec{n}_1\cos\omega t - \vec{n}_1\times\vec{b}\sin\omega t + (1-\cos\omega t)(\vec{n}_1\cdot\vec{b})\vec{b}\Big] \tag{2.47}$$

or

$$\vec{P}_{2i}^{rot}(\theta_1,\phi_1=0) = P(\theta_1)\,\vec{n}_1^{rot} \tag{2.48}$$

where

$$\vec{n}_1^{rot} = \vec{n}_1\cos\omega t - \vec{n}_1\times\vec{b}\sin\omega t + (1-\cos\omega t)(\vec{n}_1\cdot\vec{b})\vec{b} \tag{2.49}$$

This states that the polarization vector has precessed about the field direction through an angle ωt. It is just the classically expected result. Using the definition of $\vec{n}_1^{rot}$ the density matrix of the second incident beam is

$$\rho_{2i}^{rot} = \frac{\sigma(\theta_1)}{2}\left[1 + P(\theta_1)\vec{n}_1^{rot}\cdot\vec{\sigma}\right] \tag{2.50}$$

The second scattered beam is now characterized by

$$\rho_{2s}^{rot} = \Omega(\theta_2,\phi_2)\,\rho_{2i}^{rot}\,\Omega^{\dagger}(\theta_2,\phi_2) \tag{2.51}$$

where $\Omega(\theta_2,\varphi_2)$ is given by (2.27) as before. Substitution into (2.51) yields

$$\begin{aligned}\rho_{2S}^{rot} = \frac{\sigma(\theta_1)\sigma(\theta_2)}{2}\Big[1 + P(\theta_1)P(\theta_2)\vec{n}_1^{rot}\cdot\vec{n}_2 + P(\theta_1)\vec{n}_1^{rot}\cdot\vec{\sigma} \\ + P(\theta_2)\vec{n}_2\cdot\vec{\sigma}\Big] + \frac{\sigma(\theta_1)P(\theta_1)}{2}\Big[-Q(\theta_2)(\vec{n}_1^{rot}\times\vec{n}_2)\cdot\vec{\sigma} \\ + R(\theta_2)\{(\vec{n}_1^{rot}\cdot\vec{n}_2)(\vec{n}_2\cdot\vec{\sigma}) - (\vec{n}_1^{rot}\cdot\vec{\sigma})\}\Big]\end{aligned} \tag{2.52}$$

The double scattering cross section is given by

$$\sigma^{rot}(\theta_1,\theta_2,\phi_2) = \frac{tr\,1\,\rho_{2S}^{rot}}{tr\;\rho_{1i}} \tag{2.53}$$

$$\therefore \sigma^{rot}(\theta_1,\theta_2,\phi_2) = \sigma(\theta_1)\sigma(\theta_2)\left[1 + P(\theta_1)P(\theta_2)\vec{n}_1^{rot}\cdot\vec{n}_2\right] \tag{2.54}$$

If the magnetic field is assumed in the direction of the second incident beam, then

$$\sigma^{rot}(\theta_1,\theta_2,\phi_2) = \sigma(\theta_1)\sigma(\theta_2)\left[1 + P(\theta_1)P(\theta_2)\cos(\phi_2 - \omega t)\right] \quad (2.55)$$

It is seen from (2.54) and (2.55) that the precession of the polarization vector through an angle ωt has caused the azimuthal asymmetry in the double scattering cross section to rotate through an angle ωt as compared with (2.40). Note that the amplitude of the asymmetry is unchanged from the no-field case.

For an inhomogeneous static magnetic field an operator analogous to R is not easily obtainable. This difficulty stems from the inability to separate the spin and space dependences of the wave function as Mendlowitz did for the constant magnetic field. However, for the case of an axially symmetric, static magnetic field centered about the direction of second incidence it is apparent that the angle of precession of the polarization vector is

$$\alpha = \frac{e}{mv}\int_{z_P}^{z_A} B_{z_2}\, dz_2 \quad (2.56)$$

where B_{z_2} is the field along the z_2 axis. In this case the angle α would replace the angle ωt in (2.55).

Atomic Electron Screening Corrections

The Mott theory, as has been pointed out previously, deals with scattering of electrons from an ideal Coulomb field. The nuclear Coulomb field of an atom, however, is screened by the atomic electron cloud. By this is meant that at distances from the nucleus comparable to or greater

than the radii of the electron orbits the nuclear field becomes distorted from an ideal Coulomb field. Care must thus be taken experimentally to avoid appreciable scattering from the screened portion of the nuclear field.

At least three approaches to this problem are open. One approach would be to scatter electrons from completely ionized atoms. This, however, would be fruitless since only low Z elements can be completely ionized under reasonable conditions and the Mott asymmetry is predicted to be so small for low Z elements as to be unobservable. A second approach to the problem is to scatter electrons from un-ionized atoms at high enough energies so that screening corrections to the Mott asymmetry are negligibly small. For this to be true the bombarding energy should be greater than the binding energy of any of the atomic electrons.[37] This corresponds classically to the Rutherford impact parameter b being less than the radius a of the first Bohr orbit. This is easily shown. The Rutherford impact parameter relation is

$$b = \frac{Ze^2}{2E} \cot \frac{\theta}{2} \tag{2.57}$$

For $90° \leq \theta < 180°$, $\cot \frac{\theta}{2} \leq 1$ and so

$$b \leq \frac{Ze^2}{2E} \tag{2.58}$$

The binding energy of the first Bohr orbit is

$$E_B = -\frac{Ze^2}{2a} \tag{2.59}$$

where a is the radius of the first Bohr orbit. Hence, if $E = |E_B|$, then

$b \leq a$ and if $E > |E_B|$, then $b \ll a$. Two of the experiments[22,3] that have succeeded in observing the Mott asymmetry have worked at energies easily satisfying $E > |E_B|$. A third approach to the problem of screening is to calculate the atomic electron screening corrections for low bombarding energies and then check these predictions experimentally. Several numerical calculations of the screening corrections have been published.[38-41]

The present experiment lies in the border region between the second and third approaches. As was pointed out previously, the bombarding energy in this experiment (121 kev) is somewhat larger than the binding energy of the K electrons in the gold scatterer (80.67 kev). The screening corrections are thus small. They have, however, been calculated for this energy and scatterer as a function of scattering angle by Mohr[40] and later more accurately by Mohr and Tassie[41]. Their procedure was to replace the atomic number Z of gold with an effective atomic number Z_{eff} given by

$$Z_{eff} = 79 e^{-\frac{3r}{a_0}} \tag{2.60}$$

where

$$a_0 = \frac{\hbar^2}{m_0 e^2} \tag{2.61}$$

The replacement was made in the potential terms of the radial equation which determines the phase shifts which in turn determine the scattering amplitudes $f(\theta)$ and $g(\theta)$. The results of their calculations are shown in Figure 6.

The effect of the screening corrections is to slightly broaden and lower the peak in the Mott asymmetry as a function of scattering angle.

The differences between the curves of Sherman and of Mohr and Tassie could possibly be due to calculational errors or approximations in the work of Mohr and Tassie. The latter used hand calculator techniques while Sherman employed the UNIVAC. Sherman has pointed out that 2% errors in the values of $F(\theta)$ and $G(\theta)$ propagate into 15% errors in δ. Supporting this point of view is the fact that the curves differ the most at large scattering angles ($\delta_{M-T} \approx 1.6\ \delta_{SH}$ at $\theta = 162°$) where, due to the small impact parameters, screening effects would be expected to be smallest.

Depolarization

Any depolarizing event occuring between or in the polarizer and the analyser will lessen the magnitude of the asymmetry after double scattering and cause apparent disagreement with the Mott theory. Such events must be avoided. They fall into three broad categories: (1) interaction with the magnetic focusing field, (2) non-single scattering in the target foils, and (3) non-Coulomb scattering. Each of these are of two or more types. Depolarization due to the magnetic field may arise from the finite angular aperture of the beam or from the finite width in energy of the first scattered beam. Depolarization due to non-single scattering may arise from either multiple or plural scattering. Depolarization due to non-Coulomb scattering may arise from inelastic collisions with the atomic electrons, exchange scattering with the atomic electrons or from radiative scattering. (The effect of atomic electron screening on the asymmetry has already been discussed.) These will be discussed in the order mentioned.

A constant magnetic field will cause a Larmor precession of the spin of an electron and hence of the polarization vector of a beam of electrons about the direction of the field. If the beam were of finite aperture the focus of a point source would be of finite length. The spins of all electrons reaching the focus would have undergone the same precession (2π radians). However, the electrons reaching a plane perpendicular to the focus line would not have all undergone the same precession. Thus a finite aperture beam in a constant magnetic field can be depolarized. It would be a small effect for any reasonable aperture in this experiment.

In an inhomogeneous magnetic field a beam of vanishingly small aperture would experience only a precession of the polarization vector without any depolarization. If the beam were of finite aperture a more serious depolarization would result than for the constant field case since electrons in different portions of the beam aperture would pass through differing magnetic fields and thus experience different precessions. However, for a beam originating at a point on the axis of an axially symmetric field and which does not proceed very far off axis, as in this experiment, the depolarization from this cause is negligible. This is easily seen. The focusing properties of such a beam are described by the paraxial ray equation.[42] In the development of this equation it is shown that the rotation of the beam about the field axis is given by

$$\dot{\phi} = \frac{e B_z(0,z)}{2m} \qquad (2.62)$$

Here $B_z(o,z)$ is the field on the axis. The factor of two comes from the fact that the electron starts from the axis about which the angle is measured. The criterion of validity of this equation is that the electrons remain close enough to the axis throughout their trajectory that the field they see may be expressed only in terms of the field on the axis and its first derivative. It is a consequence of (2.62) that the spins of the electrons traversing the trajectories described will all precess the same amount. Thus no depolarization of any significance results from this mechanism.

The finite energy width of the first scattered beam in conjunction with the magnetic focusing field can also cause a depolarization. The mechanism is simply that lower energy electrons spend a longer time in the magnetic field than higher energy electrons while traveling between the polarizer and analyser targets. Their spins then precess more than those of the more energetic electrons. The net effect is to reduce the magnitude of the polarization vector. The amount of depolarization from this cause may be calculated by the following method.(43)

Consider a transversely polarized beam of electrons having a distribution in energy moving close to the axis of an axially symmetric, time independent magnetic field. For macroscopically varying magnetic fields the force on the electron through its magnetic moment caused by the inhomogeneity of the magnetic field is negligibly small compared to the Lorentz force. The effect on the spacial motion by the spin of the electron is thus negligibly small for such fields. The rotation of the spin will be that due to the magnetic field $\vec{B}$ along the trajectory. The wave equation for the spin function χ is thus, to a good approximation,

$$i\hbar \frac{\partial \chi}{\partial t} = +\mu \vec{\sigma} \cdot \vec{B} \chi \tag{2.63}$$

where

$$\mu = \frac{|e|\hbar}{2m} = \frac{|e|\hbar}{2m_o}\sqrt{1-\beta^2} \tag{2.64}$$

For convenience consider the trajectory that follows the axis (the z axis) of the magnetic field exactly. Any other trajectory close to the axis would give the same result but would be much harder to calculate.

$$z = vt - d \tag{2.65}$$

$$\therefore i\hbar \frac{\partial \chi}{\partial t} = \mu \sigma_z B_z(vt-d)\chi \tag{2.66}$$

$$\therefore \chi(t) = e^{-\frac{i\mu\sigma_z}{\hbar}\int_o^t B_z(vt'-d)dt'} \chi(0) \tag{2.67}$$

or $$\chi(t) = U(t)\chi(0) \tag{2.68}$$

where $$U(t) = e^{-\frac{i\sigma_z \alpha}{2}} \tag{2.69}$$

and $$\alpha = \frac{2\mu}{\hbar}\int_o^t B_z(vt'-d)dt' \tag{2.70}$$

The spin density matrix of an electron beam of unit intensity and polarization $\vec{P}(0)$ at t = o is

$$\rho(0) = \frac{1}{2}\left(1 + \vec{P}(0)\cdot\vec{\sigma}\right) \tag{2.71}$$

At time t,

$$\rho(t) = U(t)\,\rho(0)\,U^{\dagger}(t) \tag{2.72}$$

$\vec{P}(o)$ represents the polarization due to Mott scattering. Thus, it is in the y direction.

$$\vec{P}(0) = (0, P(0), 0) \tag{2.73}$$

Putting (2.69), (2.71) and (2.73) into (2.72) yields

$$\rho(t) = \frac{1}{2}\left[1 - \sigma_x P(0)\sin\alpha + \sigma_y P(0)\cos\alpha\right] \tag{2.74}$$

The density matrix must now be averaged over the energy distribution of the beam. Denote such an average by $\langle\ \rangle$.

$$\langle\rho(t)\rangle = \frac{\int_{T_0-\frac{\Delta T}{2}}^{T_0+\frac{\Delta T}{2}} \rho(t)\, d(T)\, dT}{\int_{T_0-\frac{\Delta T}{2}}^{T_0+\frac{\Delta T}{2}} d(T)\, dT} \tag{2.75}$$

$d(T)$ is the number of electrons per unit of kinetic energy, ΔT is the kinetic energy interval accepted by the detector, and T_0 is the mean kinetic energy of the electrons accepted by the detector. Assume that the initial polarization $P(0)$ is independent of T.

$$\therefore \langle\rho(t)\rangle = \frac{1}{2}\left(1 - \sigma_x P(0)\langle\sin\alpha\rangle + \sigma_y P(0)\langle\cos\alpha\rangle\right) \tag{2.76}$$

This is of the form

$$\langle\rho(t)\rangle = \frac{1}{2}\left(1 + \langle\vec{P}(t)\rangle\cdot\vec{\sigma}\right) \tag{2.77}$$

from which it follows that the degree of polarization is

$$\langle P(t)\rangle = \sqrt{2\,\mathrm{tr}\langle\rho(t)\rangle^2 - 1} \tag{2.78}$$

Substituting (2.76) into (2.78) yields

$$\langle P(t)\rangle = P(0)\sqrt{\langle\sin\alpha\rangle^2 + \langle\cos\alpha\rangle^2} \tag{2.79}$$

The amount of depolarization is defined by

$$D(t) = \frac{P(0) - \langle P(t) \rangle}{P(0)} \tag{2.80}$$

$$\therefore D(t) = 1 - \sqrt{\langle \sin\alpha \rangle^2 + \langle \cos\alpha \rangle^2} \tag{2.81}$$

In order to calculate $< \sin \alpha >$ and $< \cos \alpha >$ the magnetic field along the axis and the energy distribution of the beam must be known. Assume the energy distribution to be of the form

$$d(T) = \frac{1}{\Delta T} \qquad \left(T_0 - \frac{\Delta T}{2} \le T \le T_0 + \frac{\Delta T}{2}\right) \tag{2.82}$$

$$\therefore \left\langle \begin{matrix} \sin \\ \cos \end{matrix} \alpha \right\rangle = \frac{1}{\Delta T} \int_{T_0 - \frac{\Delta T}{2}}^{T_0 + \frac{\Delta T}{2}} \begin{matrix} \sin \\ \cos \end{matrix} \alpha \, dT \tag{2.83}$$

For a solenoid field

$$B_z^{\text{axis}}(z) = \frac{nI\mu_0}{2}\left[\frac{z+\ell}{\sqrt{(z+\ell)^2+a^2}} - \frac{z-\ell}{\sqrt{(z-\ell)^2+a^2}}\right] \tag{2.84}$$

where n is the turns per meter, I the current in amperes, l the half length of the solenoid in meters, a the radius in meters, z the coordinate in meters measured from the center of the solenoid, and $\mu_0 = 4\pi \times 10^{-7}$.

From (2.70)

$$\alpha = \frac{\mu n I \mu_0}{\hbar} \int_0^t \left[\frac{vt'-d+\ell}{\sqrt{(vt'-d+\ell)^2+a^2}} - \frac{vt'-d-\ell}{\sqrt{(vt'-d-\ell)^2+a^2}}\right] dt' \tag{2.85}$$

Use (2.65) to change the integration variable.

$$\alpha = \frac{\mu n I \mu_0}{\hbar v} \int_{-\ell}^{vt-d} \left[\frac{z'+\ell}{\sqrt{(z'+\ell)^2+a^2}} - \frac{z'-\ell}{\sqrt{(z'-\ell)^2+a^2}}\right] dz' \tag{2.86}$$

This integral must be evaluated at vt - d = +d, the analyser position, since the depolarization of the beam at a particular point in space is wanted irrespective of the time it takes different electrons to arrive there.

$$\alpha = \frac{K}{\beta}\sqrt{1-\beta^2} \tag{2.87}$$

where

$$K = \frac{|e|nI\mu_o}{m_o c}\left[\sqrt{(d+\ell)^2+a^2} - \sqrt{(d-\ell)^2+a^2}\right] \tag{2.88}$$

Relativistically the kinetic energy is

$$T = mc^2 - m_o c^2 \tag{2.89}$$

From this it follows that

$$\frac{1}{\beta}\sqrt{1-\beta^2} = \frac{1}{\sqrt{\left[1+\frac{T}{m_o c^2}\right]^2-1}} \tag{2.90}$$

$$\therefore \left\langle \begin{matrix}\sin\\ \cos\end{matrix}\alpha\right\rangle = \frac{1}{\Delta T}\int_{T_o-\frac{\Delta T}{2}}^{T_o+\frac{\Delta T}{2}} \begin{matrix}\sin\\ \cos\end{matrix}\left(\frac{K}{\sqrt{\left[1+\frac{T}{m_o c^2}\right]^2-1}}\right)dT \tag{2.91}$$

Taking T_o = 121 kev, ΔT = 6 kev, I = 1.325 amp, n = 745 m^{-1}, l = 2.9m, d = .28m, and a = .17m, (2.91) may be evaluated by Simpson's rule to give

$$\langle \sin\alpha \rangle = -.62492 \tag{2.92}$$

$$\langle \cos\alpha \rangle = +.77935 \tag{2.93}$$

$$\therefore \sqrt{\langle \sin\alpha \rangle^2 + \langle \cos\alpha \rangle^2} = .9989 \tag{2.94}$$

$$\therefore D(t) = .001 \tag{2.95}$$

Thus the depolarization arising from the energy spread of the beam is only .1% for an energy spread of 6 kev, which is believed to be an ample estimate.

A further mechanism of depolarization in the magnetic field is that of radiative spin flip transitions. Mendlowitz[29] has shown that the probability of such transitions is of the order of 10^{-12} for the parameters of this experiment.

Multiple scattering in the target foils can randomize the spin orientations and thus cause a depolarization. Rose and Bethe[19] have calculated the effect on the azimuthal asymmetry of multiple elastic scattering on a screened Coulomb field occuring between the large angle scattering in the polarizer foil and the large angle scattering in the analyser foil. They find that the asymmetry factor will be given by

$$\delta = \left(\frac{1-e^{-\gamma d}}{\gamma d}\right)\delta_{MOTT} \qquad (2.96)$$

where $\gamma = 890\ cm^{-1}$ for gold scatterers, electron energy of 100 kev, and a foil orientation of 45° with respect to the beam. They find γ to be insensitive to energy and screening length. For a foil of thickness $d = 9 \times 10^{-6}$cm, $\gamma d = 8.0 \times 10^{-3}$, and so $\delta = .992\ \delta_{MOTT}$

Plural scattering as a perturbing effect on double scattering was discussed in the Introduction. Ryu[17] has obtained an expression for the ratio of plurally scattered electrons to singly scattered electrons for 90° scattering on the transmission side of a foil oriented at 45° to both the incident and scattered beams.

It is given by

$$\frac{I_{p\text{-}T}}{I_s} = \frac{NdZ^2e^4}{2m_o^2c^4}\,\frac{1-\beta^2}{\beta^4}\,\frac{106-106\beta^2+58\beta Z\alpha+7(\pi\alpha\beta Z)^2-34\pi\beta^3Z+18\beta^4}{4-2\beta^2+\sqrt{2}\,\pi\beta\alpha Z} \qquad (2.97)$$

Here N = atoms per unit volume and $\alpha = \frac{e^2}{\hbar c} = \frac{1}{137}$. For a gold target ($Z = 79$) with a thickness $d = 9 \times 10^{-6}$cm and for an energy of 121 kev ($\beta = .59$) this yields $I_{p\text{-}T}/I_s = .019$. Since these plurally scattered electrons increase the number of scattered electrons somewhat equally at all azimuth angles (if the target foil is rotated with the detector) without changing the number of electrons scattered asymmetrically in azimuth, the amplitude of the azimuthal asymmetry is effectively reduced by 2%. Also, a further reduction of 2% in the asymmetry could result from plural scattering in the polarizer. Though this perhaps cannot properly be called a depolarization, its effect is nevertheless the same. Ryu's formula for the plural scattering contribution cannot be applied to other scattering angles or target angles. However, he states the contribution probably remains small if thin targets ($\sim 5 \times 10^{-6}$cm) are used in the transmission position.

Depolarization from inelastic scattering in which spin flip occurs has been calculated by Rose and Bethe.[19] Their treatment considers the excitation of any of the atomic electrons consistent with the condition that the energy loss of the incident electron is much less than its initial energy. Their expression for the azimuthal asymmetry has the same form as (2.96). For E = 100 kev and Z = 79 they obtain $\gamma = 5.0\text{cm}^{-1}$.

For $d = 9 \times 10^{-6}$cm, $\gamma d = 4.5 \times 10^{-5}$ and so $\delta = .999955\ \delta_{MOTT}$. Thus inelastic scattering is a negligible source of depolarization for electrons in the elastic peak of the energy distribution.

Rose and Bethe[19] also considered the depolarization from exchange scattering in which the outgoing electron has the opposite spin orientation to the incident electron. An equation of the form (2.96) results with $\gamma = 10^{-7}\text{cm}^{-1}$ for E = 100 kev and Z = 79. For $d = 9 \times 10^{-6}$cm, $\gamma d = 9 \times 10^{-13}$ and so $\delta = \delta_{MOTT}$.

A theoretical treatment of the depolarization from radiative scattering does not seem to be available. However, the probability of the emission of a photon of energy comparable to the average energy loss due to atomic excitations is very small at 100 kev. The interaction thus seems to be too weak to cause any appreciable depolarization.

III. APPARATUS

General Experimental Layout

In broad outline an electron double scattering experiment consists of four main elements: 1) a source of electrons, 2) the polarizer target, 3) the analyser target, and 4) an electron detector. In this experiment, two other components were added: 1) a weak magnetic lens between the polarizer and the analyser, and 2) a removable electrostatic energy selector following the analyser target. The mechanical and electrical construction of each of these will be described in the succeeding articles of this chapter. In Chapter IV, the tests to which the apparatus was subjected will be described. The general layout of the apparatus is shown in a photograph reproduced in the Frontispiece.

High Voltage Supply

For accelerating the electrons to a chosen energy prior to scattering, a simple voltage doubler type circuit is used. The high voltage supply is capable of producing any voltage form zero to 140 kilovolts. To regulate the high voltage, an error signal is taken from the voltmeter bleeder, converted to an A.C. signal, amplified, and reconverted to a D.C. signal. This signal is used then to control the primary voltage on the high voltage transformer. This regulator is capable, after a suitable warm-up, to maintain a given D.C. voltage to at least $\pm$ .25%. The regulator is not capable of eliminating the ripple of line frequency nor the sporadic hash due to corona. These, however, represent only an overall $\pm$ 2% ripple. Since the Mott asymmetry varies only of the order of .1% per kilo-electron-volt of energy in this energy region, this regulation is sufficient for this experiment.

The Electron Gun

Beam intensity for double scattering of electrons in the 100 kev region is not a major problem even for reasonably small apertures. For 90° - 90° scattering in gold (Z = 79) at 121 kev with total apertures of 3° at each scattering, 12,000 electrons per minute are expected in the detector for each microampere incident on the polarizer. Electron guns giving many times this current can be easily made. Thus, electron gun design is not a major problem for this experiment.

The structure of the gun used is shown in Figure 7. The cathode and anode structures are spherical in shape. The actual filament is made of tungsten ribbon with a .050-inch by .050-inch emitting surface. The filament is heated by a 0 - 25 amp. A.C. supply and is at a negative D.C. bias with respect to the anode. This bias can be varied from -300 v to -900 v. The anode and gun casing are at -121 kv with respect to ground. The emitted current is adjusted by changing either this bias or the filament current. Currents of up to 100 microamperes are obtained on the polarizer target as measured by the collector cup shown in Figure 7.

Polarizer Assembly

The polarizer assembly consists of a double slit leading to the polarizer target, a target wheel with positions for four targets, a collector cup to monitor the beam incident on the target, and an exit slit for the scattered beam. The essential features of the polarizer assembly are shown in Figure 7.

Since the Mott theory predicts that the azimuthal asymmetry in the double scattering cross section depends symmetrically on the parameters of the first and second scatterings, it was decided for

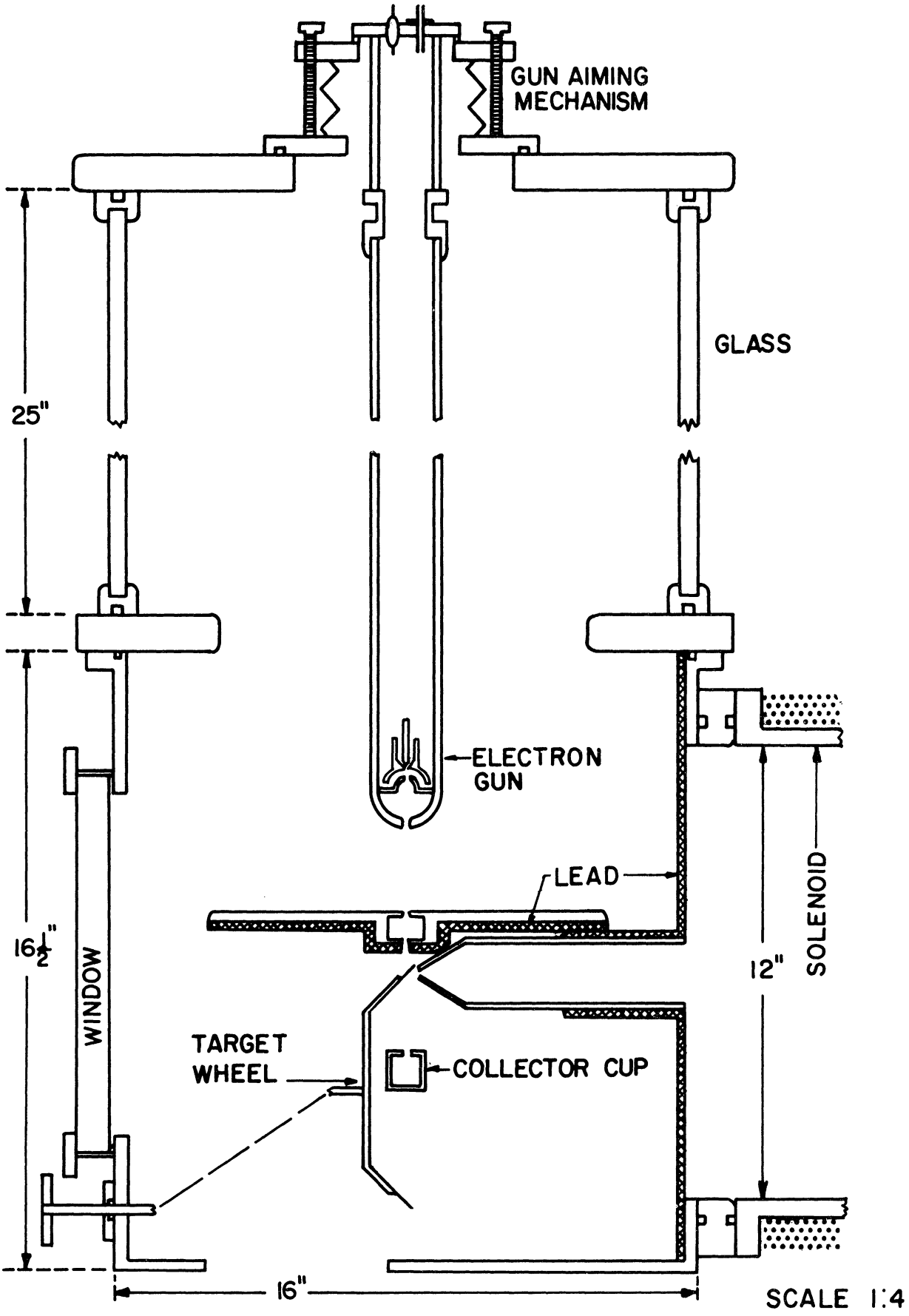

Figure 7. Cross Section of Polarizer Assembly

experimental convenience to vary the scattering angle of the second scattering only. The angle of first scattering was fixed at 90°. This is large enough to give an appreciable polarization (26.7% expected for gold at 121 kev). The target wheel is of aluminum construction and made so that the target foils bisect the supplement to the scattering angle, see Figure 7. Any of the four targets can be rotated into position by a knob external to the vacuum system. The target holders allow one-half inch diameter targets.

The collector cup was not designed to give an accurate reading of the absolute beam intensity. Its only use is to help locate the beam and give an approximate reading of its intensity to help in tuning up the apparatus. For these purposes, a relative reading of the beam intensity is sufficient.

Solenoid

The reason for using a weak magnetic focusing magnet between the two scatterers was discussed in the Introduction. It is, in a word, a device to improve the signal-to-noise ratio. The design parameters of such a focusing device are not critical to this experiment since presumably the measured values of the azimuthal asymmetry are independent of them. The design parameters were, therefore, chosen to meet the needs of another experiment that used concurrently a large part of the equipment of this experiment.

The focusing device is an air core solenoid consisting of four layers of 2160 turns each of #10 Heavy Formvar copper wire wound on an aluminum pipe, 19.2 feet long by 12.75 inches in outside diameter. For this experiment, the four windings were put in a series-parallel arrangement.

Both the polarizer and analyser are located in the end fields of the solenoid. The solenoid thus acts as a magnetic lens giving both z-focusing and radial focusing. So that the fields in the target regions would be as small as possible, the solenoid is operated at a current to put the first focus on the analyser target. This corresponds to a field of about 12.5 gauss in the center of the solenoid, and of about 1 gauss at the target positions.

A block diagram of the solenoid current supply is shown in Figure 8. The current is supplied by a 300-volt D.C. generator. The pass tubes are a bank of 6AS7 tubes in parallel. The error signal is obtained from a 2B23 tube, a magnetic field sensitive diode, in a coil in series with the solenoid. The error signal is fed into a D.C. amplifier which controls the pass tube grids. The regulator eliminates ripple to better than a part in a thousand, and after a suitable warm-up period D.C. drift is only one part in a thousand per hour.

Correction Coils

The entire path of the electrons is encompassed by two correction coils, one for lateral corrections in the beam position and one for vertical corrections. Each of these consists of two coils separated by 5 feet. Each coil contains 30 turns of #14 Formvar copper wire wound on a wooden frame 5 feet by 28.25 feet. These correction coils produce a nearly uniform magnetic field of .16 gauss/amp over the region of the electron trajectories. As far as possible, iron was excluded from this region. Under typical operation about 3 amperes are put through the vertical correction coil and .3 ampere through the lateral correction coil. These currents correspond to fields roughly in magnitude and opposite in direction to the components of the magnetic field of the earth in the

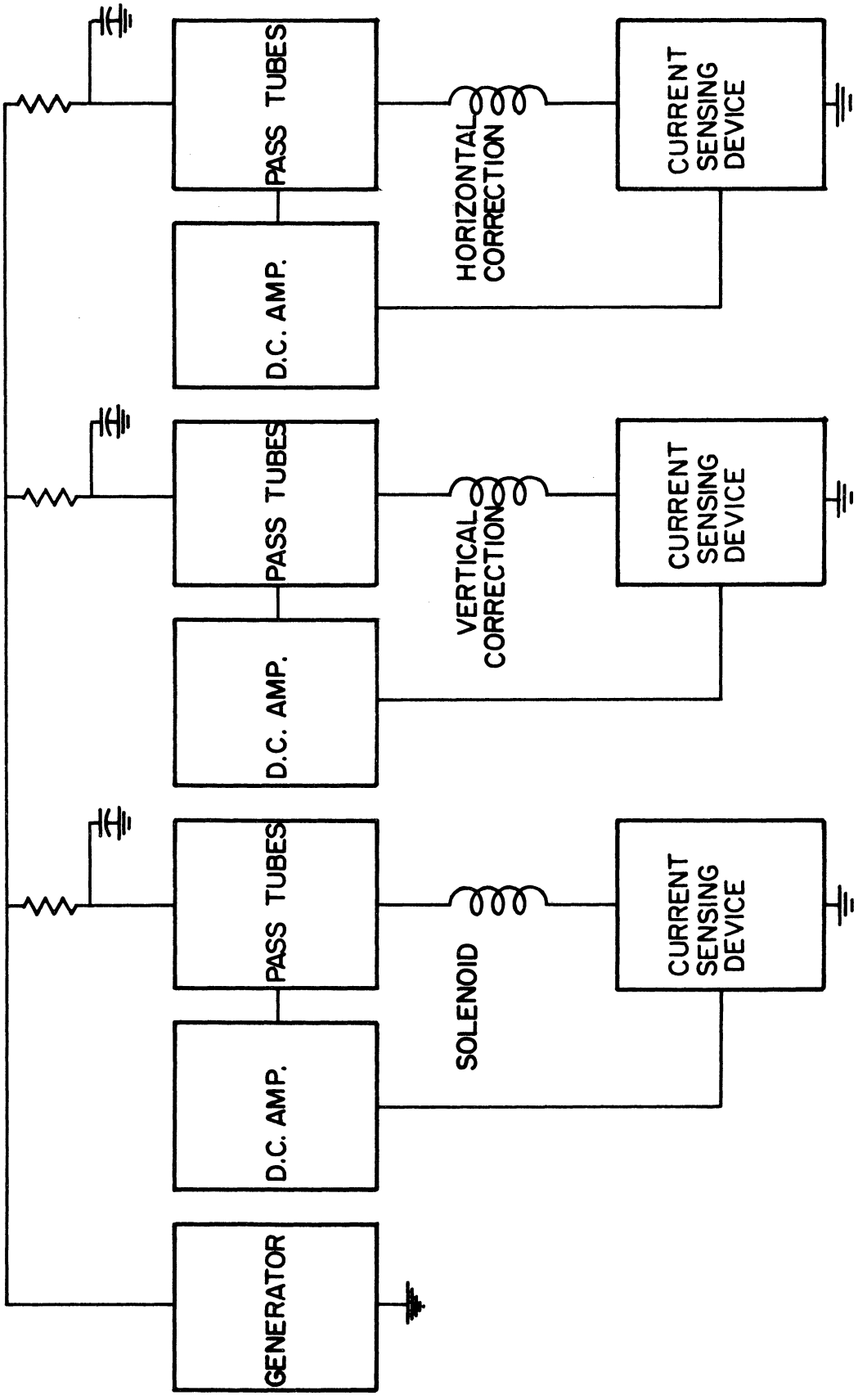

Figure 8. Regulated Current Supplies

laboratory. The correction coils are used not only to cancel the field of the earth, but to compensate for slight misalignments of the solenoid field with respect to the slit system. The mode of regulation of these currents is identical to that for the solenoid, see Figure 8.

Slit System

The slit system is shown schematically in Figure 9. All slits are made of aluminum to reduce slit edge scattering and prevent creation of hard x-rays from impinging electrons. All slits have lead backing to stop transmission of x-rays. All slits have a slight taper (10°) to reduce slit edge scattering. The double slit leading to the polarizer target is for the purpose of limiting the beam to the central portion of the target so as to avoid scattering from the target holder. The purpose of the slit after the polarizer is to mask the target holder, that is, to prevent any electrons that might strike the target holder from entering the solenoid. Its purpose is not to give aperture definition. This function is furnished by the slit in the center of the solenoid. It limits the aperture to $\pm$ 1°. The center of the slit is blocked to prevent passage of electrons which lose an appreciable energy in the first scattering. It also stops any x-rays from traversing the slit system. The double slit located just before the analyser was designed to hug the beam cone and thus remove extraneous electrons as well as to prevent movement of the beam spot on the target. After second scattering the beam aperture is defined at the counter face. A nozzle extending from the counter face toward the target is for the purpose of preventing entry into the counter of spuriously scattered electrons. The aperture of the monitor counter was reduced at the counter face, in comparison to the movable counter, so that more intense beams could be used

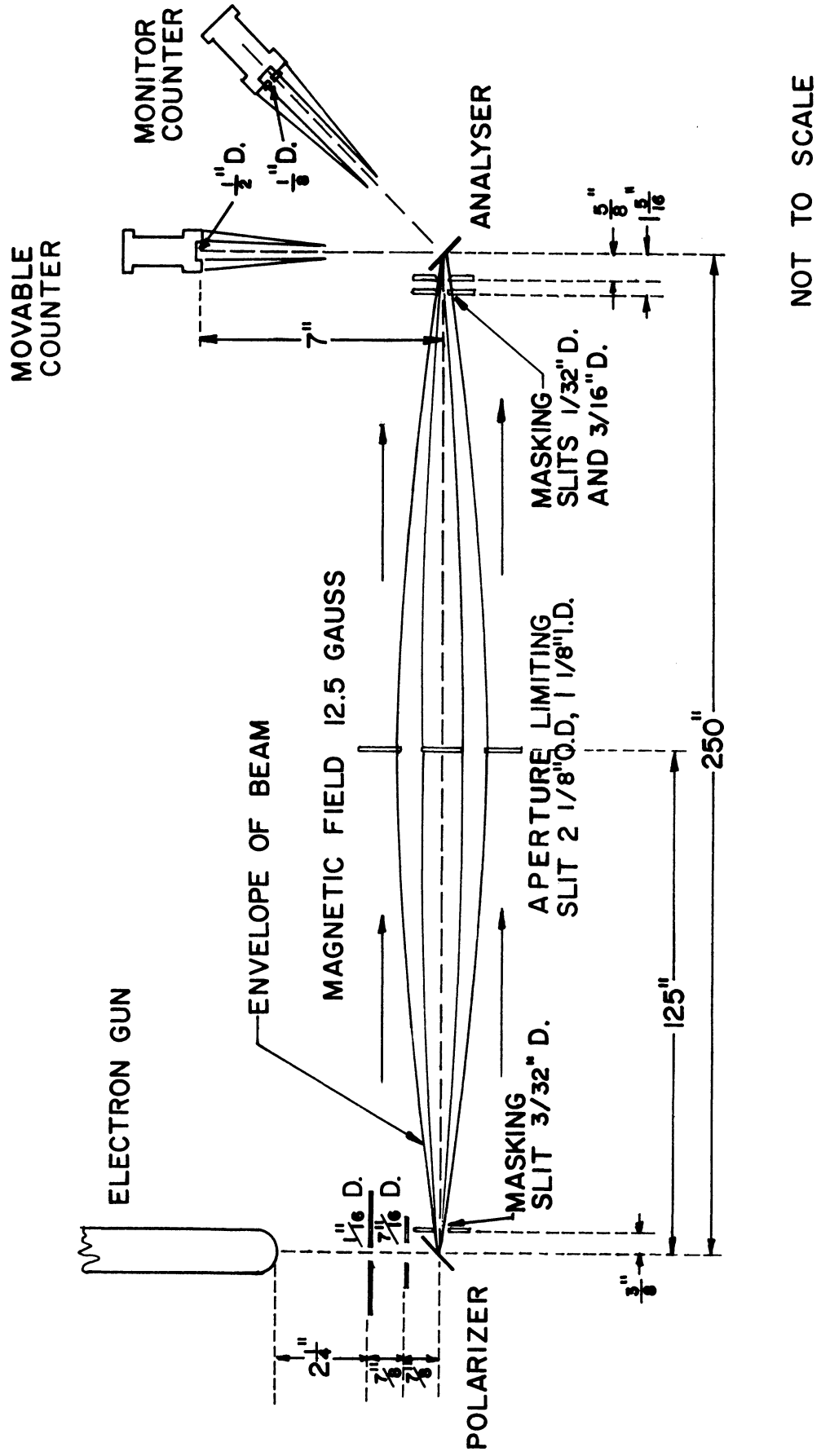

Figure 9. Slit System

without saturating the monitor. The electrostatic energy analyser has slits at each end of the deflecting plates in order to improve energy resolution. They are 1/4" in diameter.

Analyser Assembly

The analyser assembly consists of (a) a slit leading to the analyser target, (b) a four-position target wheel, (c) a mechanism to change the target angle, (d) a movable Geiger counter, (e) a movable electrostatic energy analyser with attached Geiger counter [this unit being interchangeable with the movable Geiger counter], (f) a fixed Geiger counter for monitoring beam intensity, and (g) a mechanism to rotate the entire assembly about the incident beam direction. A schematic view of the analyser assembly is shown in Figure 10, and a photograph is reproduced in Figure 11.

The target wheel is of aluminum construction. It has four target holders, one-inch inside diameter. The target wheel can be rotated to any of its four positions by a control external to the vacuum system. The target wheel is oriented so that any spurious electrons striking it could not enter the movable counter.

A target-tipping device was installed so that the target plane could be put at any angle to the incident beam from 90° to 180°. The control for this device is external to the vacuum system. A locking mechanism on the target-tipping device prevents slippage. The purpose of the target-tipping mechanism is to allow the counter to always look at the transmission side of the target foil so as to reduce the possibility of plural scattering.

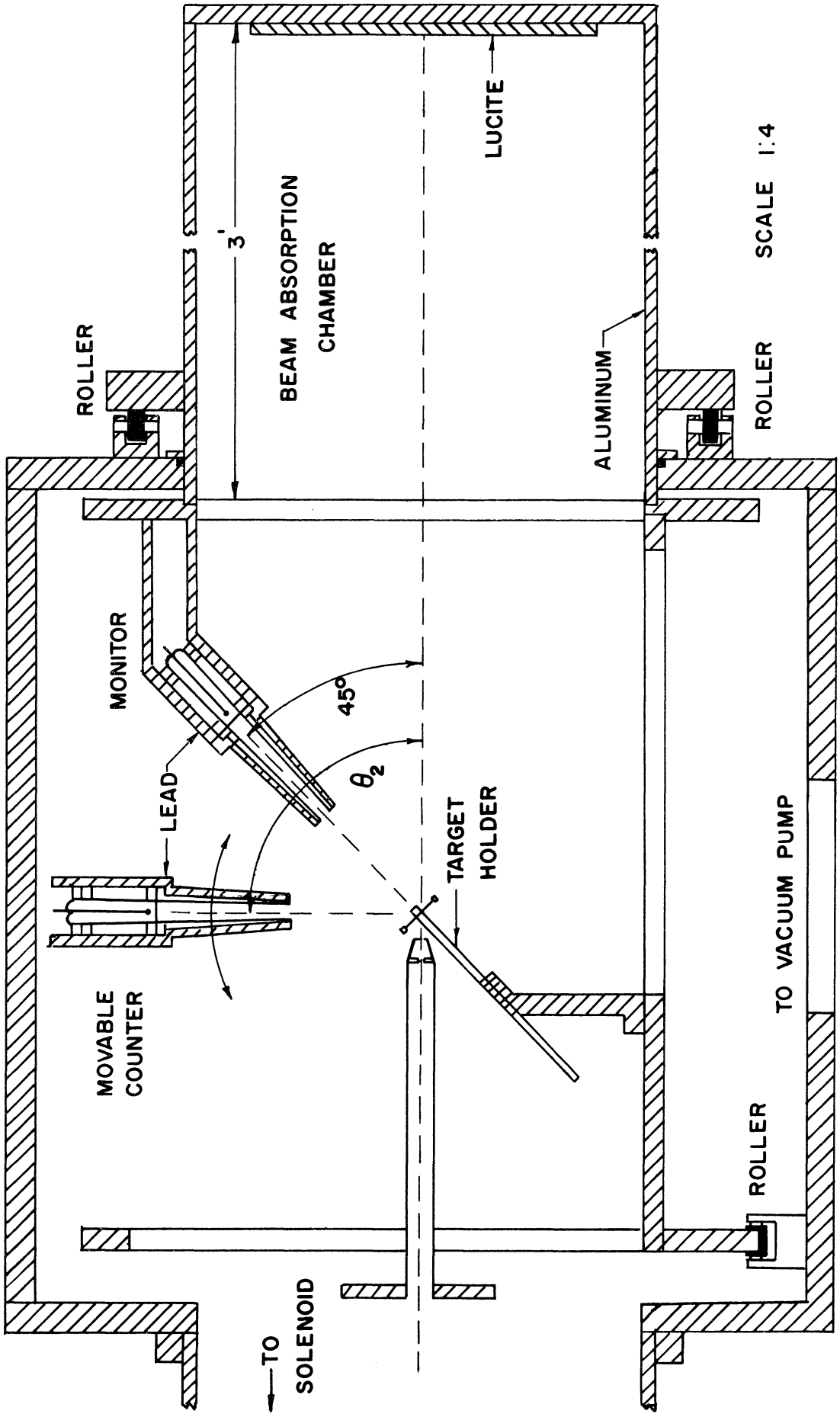

Figure 10. Cross Section of Analyser Assembly

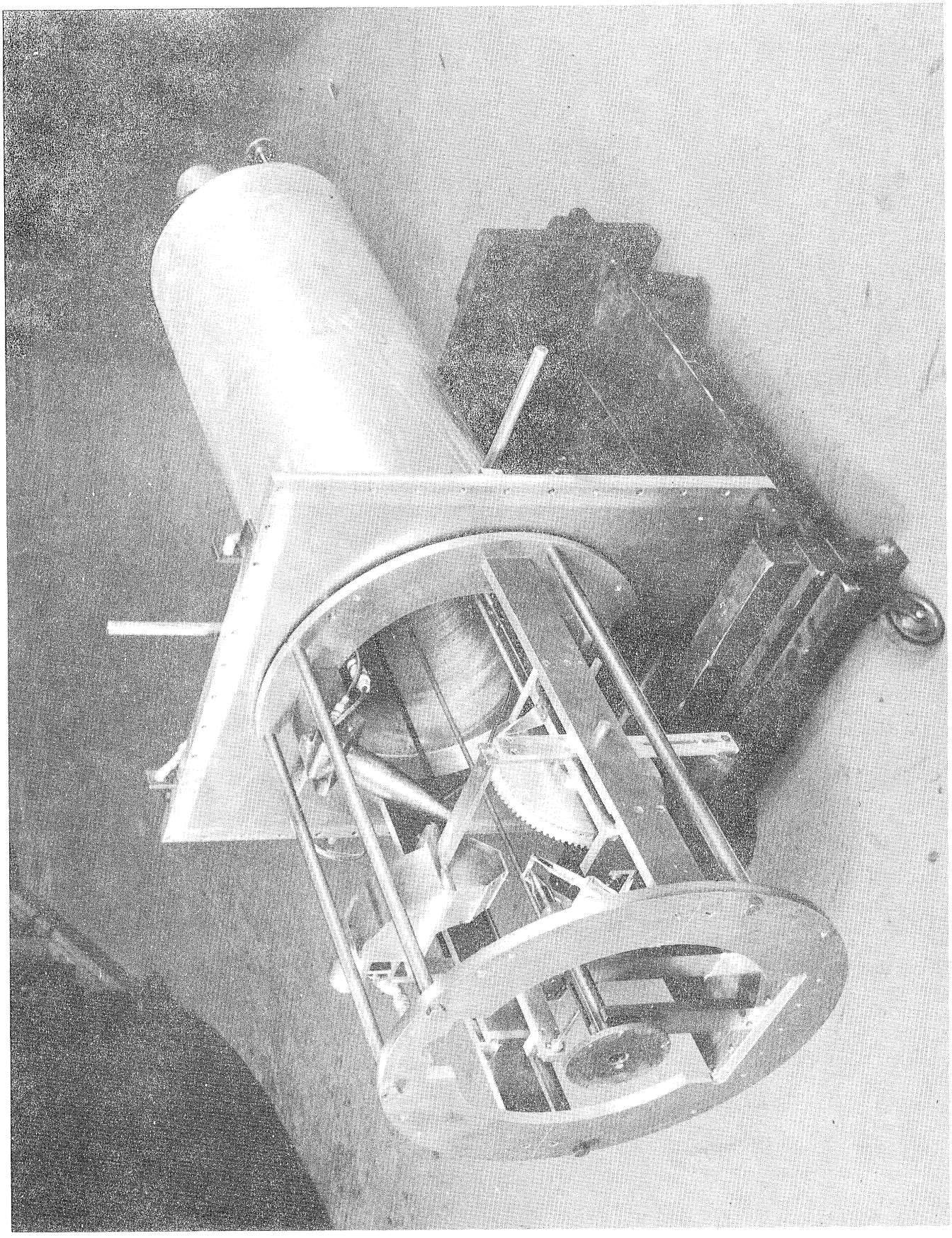

Figure 11. Photograph of Analyser Assembly

The movable Geiger counter is the counter that observes the azimuthal asymmetry. It can be set at scattering angles from 65° to 165° in 5° intervals.

An electrostatic energy analyser with attached Geiger counter can be inserted in place of the movable counter. Since this unit is more bulky than the movable counter, the range of scattering angles that it can cover is from 80° to 140°. The purpose of this unit is to study the effect of inelastically scattered electrons on the measurement of the Mott asymmetry. When set to accept the elastic peak in the energy profile it guarantees the condition of elastic scattering in observing the Mott asymmetry.

A Geiger counter fixed at a scattering angle of 45° and in the same azimuthal plane as the movable counter is used to monitor beam intensity. It views the transmission side of the target. This position was chosen, as discussed in Chapter I, because it best insures the monitoring of the single scattering counting rate, and because at 45° the Mott asymmetry is vanishingly small for gold and aluminum. It is also out of the way of the movable counter.

The entire analyser assembly was built in a cylindrical cage which could be rotated about the incident beam direction so that the azimuthal asymmetry can be studied. This rotation can be performed by a control external to the vacuum system.

An important feature of the design of the analyser assembly is the openness around the target and especially in the direction of the transmitted beam. In this direction, the beam is unobstructed for about 3 feet in length and 12 inches in diameter. The end of this chamber is lined with lucite to help in beam absorption. The entire assembly is of aluminum construction.

Geiger Counters

The three Geiger counters used are of identical construction. Each has a thin end window of aluminized 1/4-mil mylar (total thickness: $1.9 \pm .3$ mg/cm^2) 1/2-inch in diameter. The counter wall is a brass tube 2 inches long. The central wire is a 6-mil tungsten wire supported at one end and beaded at the other end. The counter is filled to a pressure of 10 cm of Hg with a 9:1 mixture of argon to alcohol, premixed before entering the counter. The counters can be filled without opening the vacuum system. An arrangement of pipes makes it possible to equalize pressure on both sides of the counter windows while pumping down the vacuum system in order to avoid undue stress on the windows.

These counters have plateaus 150 volts long with a slope of 7% per 100 volts. They are operated about 50 volts above threshold. The voltage supply used is regulated to better than .1%. The Geiger tube pulses are put through a cathode follower into a coaxial cable and then into an Atomic linear amplifier (model 204-B) which feeds them into an Atomic scalar (model 1090). A Tracerlab ratemeter is also put in parallel with the scalar for the monitor counter to aid in beam alignment.

Electrostatic Energy Analyser

The electrostatic energy analyser is a plug-in unit that can replace the movable counter in order to study the energy spectrum of the doubly-scattered electrons. The dimensions of the deflecting plates can be seen in Figure 12. The deflecting plates are completely encased to avoid any effect on the electron trajectories near the target by stray electric fields. A voltage of 23.25 kv on the deflecting plates is sufficient to bend 121 kev electrons on a 10 cm radius through the slits

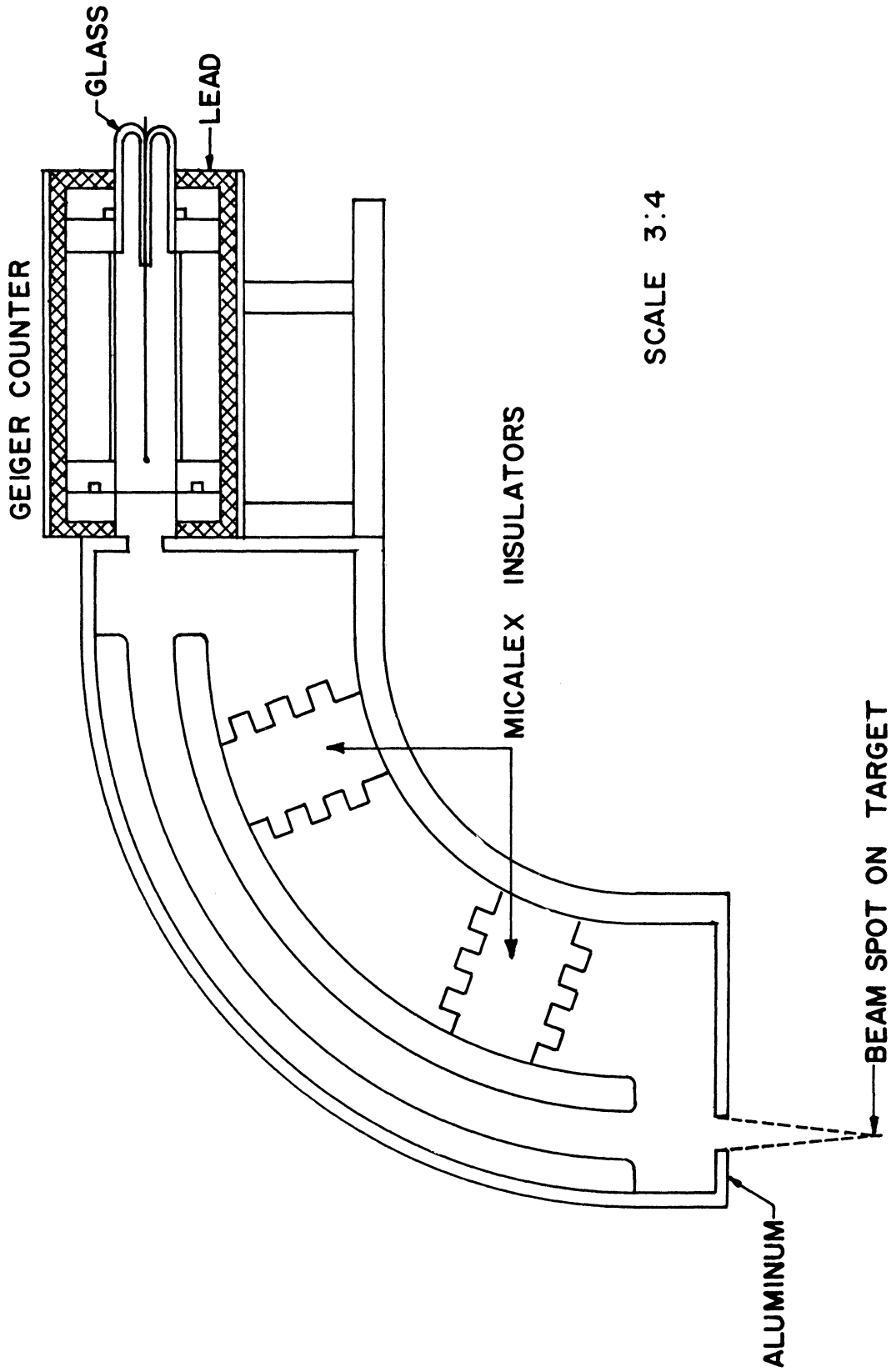

Figure 12. Cross Section of Electrostatic Energy Analyser

at each end of the deflecting plates and into the Geiger counter. The voltage supply for the deflection plates is a regulated rf type supply made by Dumont (model RA119).

IV. APPARATUS STUDIES

Beam Alignment

The alignment of the beam was done in several steps. First, a fluorescent material was placed around the slit leading to the polarizer target to facilitate aiming the gun at the slit. A fluorescent target in the polarizer target wheel served to check that the beam was striking the target properly. A collector cup beyond the target also aided in this respect besides yielding a rough measurement of the beam intensity. The alignment of the slit leading from the polarizer was checked with a beam of light. The alignment of the slits at the analyser was checked every 30° of rotation of the analyser assembly using a telescope with cross hairs. The alignment of the counters with the target was checked with light beams. The electrostatic energy analyser could not be aligned with light beams and so accurate machining and positioning had to be depended on.

To locate the beam at the analyser, a large fluorescent plate was originally used. Later a fluorescent target was placed in the target wheel for this use. It was found that a visual judgement of the proper centering of the beam using the fluorescent target coincided with a maximizing of the counting rate in either of the Geiger counters as measured by a ratemeter. The latter method was used thereafter. The centering was accomplished by peaking the counting rate successively with respect to the solenoid current, the vertical correction current, and the horizontal correction current. This centering procedure was found to be independent of the scatterer (Au or Al), of whether the movable counter or monitor was used, and of the azimuth angle.

Spurious Asymmetries Study

Spurious instrumental asymmetries arise from misalignments in the slits, target holders, and counters, from wobble in the rotation in azimuth of the analyser assembly, from asymmetric magnetic fields present, and from the use of finite apertures. The elimination of misalignments was discussed in the previous section.

The elimination of wobble in the rotation of the analyser assembly was very important in reducing spurious asymmetries. This was accomplished by centering the slit leading to the analyser target with respect to the outer circular ring of the analyser assembly. This ring was then made to roll on positioning rollers in the analyser chamber. The accuracy of this procedure was then checked with a cross hair telescope as was described in the previous section.

It was found early in the work that deviations from axial symmetry of the magnetic focusing field, caused apparently by iron equipment in the room and in the structure of the building, could lead to a spurious asymmetry large compared with the Mott asymmetry. The focusing field at that time was around 100 gauss. To minimize the effect, the focusing field was reduced to about 12.5 gauss at the center of the solenoid. This field corresponded to the first focus of the beam falling on the analyser target. With this field and the slit system employed in the final measurements, the spurious instrumental asymmetry was about 5% (one-half of peak-to-peak value) when the electrostatic energy analyser was used and about 2% when just the movable Geiger counter was used. These values are smaller than the Mott asymmetry factors measured. Instrumental asymmetries typical of these two situations are shown in Figure 13.

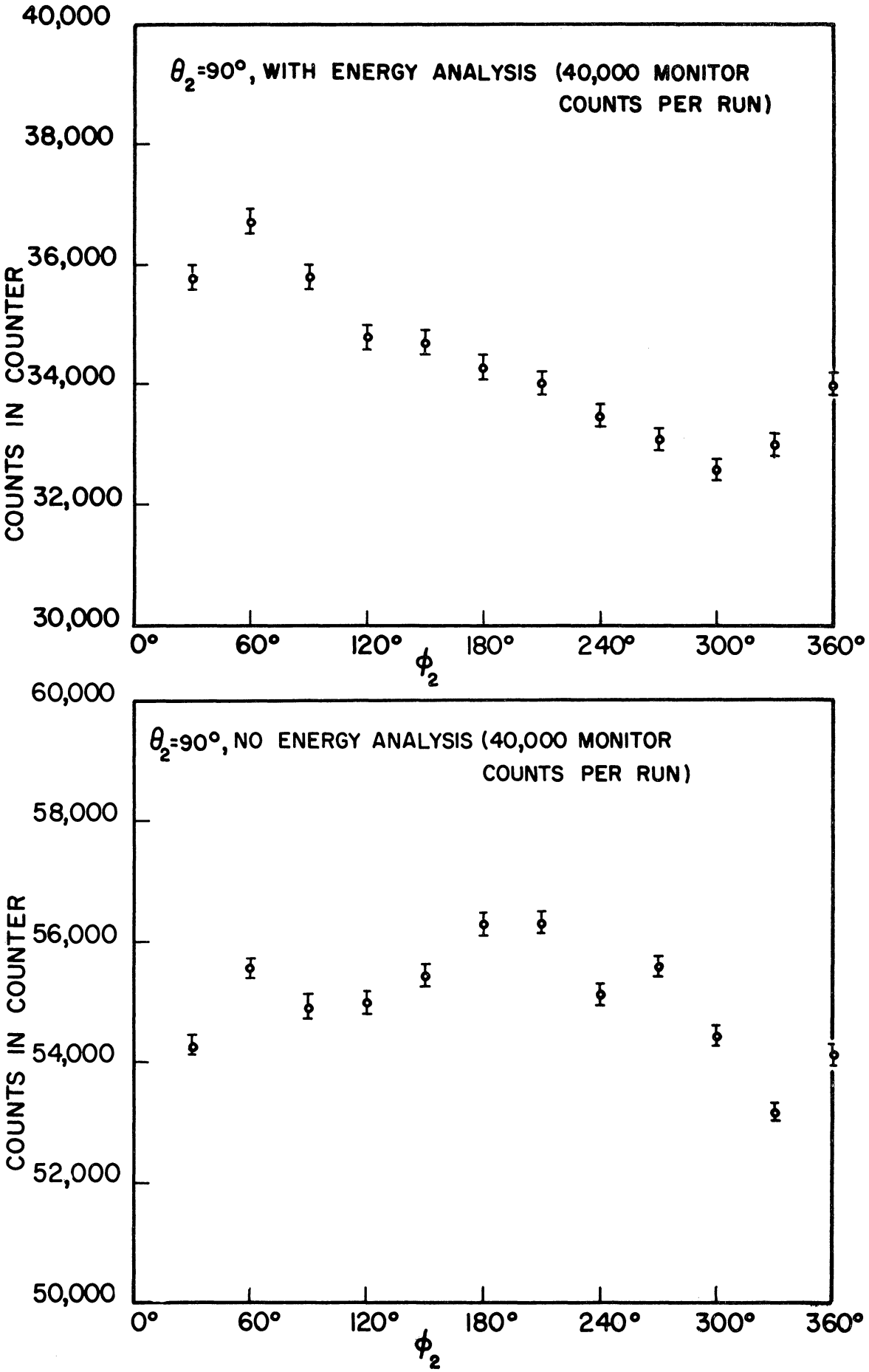

Figure 13. Spurious Instrumental Asymmetries

As was pointed out in Chapter I, the spurious instrumental asymmetry was measured by inserting an aluminum target in the polarizer, the analyser, or both, using the fact that the Mott asymmetry for low Z elements is very small. This asymmetry could then be eliminated from the experimental asymmetry found with gold targets in order to obtain the Mott asymmetry.

An aluminum target with a thickness such as to give the same scattering power as the gold foil was used. For this thickness of aluminum the average energy loss, due mainly to ionization collisions, is greater than for the gold foil used. If the gold polarizer were replaced by an aluminum target, the focusing field would thus bring the beams from the two targets to focus at slightly different points. The evaluation of the instrumental asymmetry under such a circumstance would be imperfect. Thus the spurious instrumental asymmetry was measured by replacing the gold foil by an aluminum foil at the analyser.

The spurious asymmetries discussed in the previous paragraphs may be described as static ones since they do not vary in time. Another type of spurious asymmetry is that which varies in time. This type is potentially more serious since it is much more difficult to measure. Such an asymmetry could arise from time variations in the solenoid focusing field, the vertical and horizontal correction fields, the accelerating voltage, and the deflecting voltage of the electrostatic energy analyser.

To avoid these spurious effects a two pronged approach was used. First the slit system was built so that detuning these parameters made as small a change as practical in the ratio of counting rates which was used

for the measurement of the Mott asymmetry. Secondly, each of the five parameters mentioned was electronically regulated. Figures 14, 15, and 16 show the change in the ratio of the counter-to-monitor counting rate ratio for gold to that for aluminum for changes in the five parameters. These changes extend from the setting for the beam focus lying on the target to settings where the counting rate has dropped to roughly half value as compared with the focus. The regulation range indicated is the maximum drift per hour observed. From these graphs it can be seen that detuning errors in the three magnetic fields are negligible. Drifts in the accelerating voltage and the deflecting voltage can be more serious. Under the worst conditions either could cause a change in the ratio of 3%.

Since the measurement of the Mott asymmetry must be independent of the magnetic focusing field, it must be guaranteed that this field introduces no spurious effects. The detuning test shown in Figure 15 shows that small changes in this field do not affect the measurements appreciably. It must also be shown that large changes in this field do not introduce systematic errors in the measurement of the Mott asymmetry. To show this, successive runs were made to measure δ_{MOTT} with the solenoidal focusing field in the two opposite polarities. The values of δ_{MOTT} (90°, 120°) obtained, .074 $\pm$ .006 and .073 $\pm$ .006, agreed within statistical error.

Another type of spurious asymmetry arises from the use of a finite aperture at the polarizer target and from the fact that the cross section varies as a function of the scattering angle. It does not arise from misalignments of slits, from the presence of magnetic fields, nor

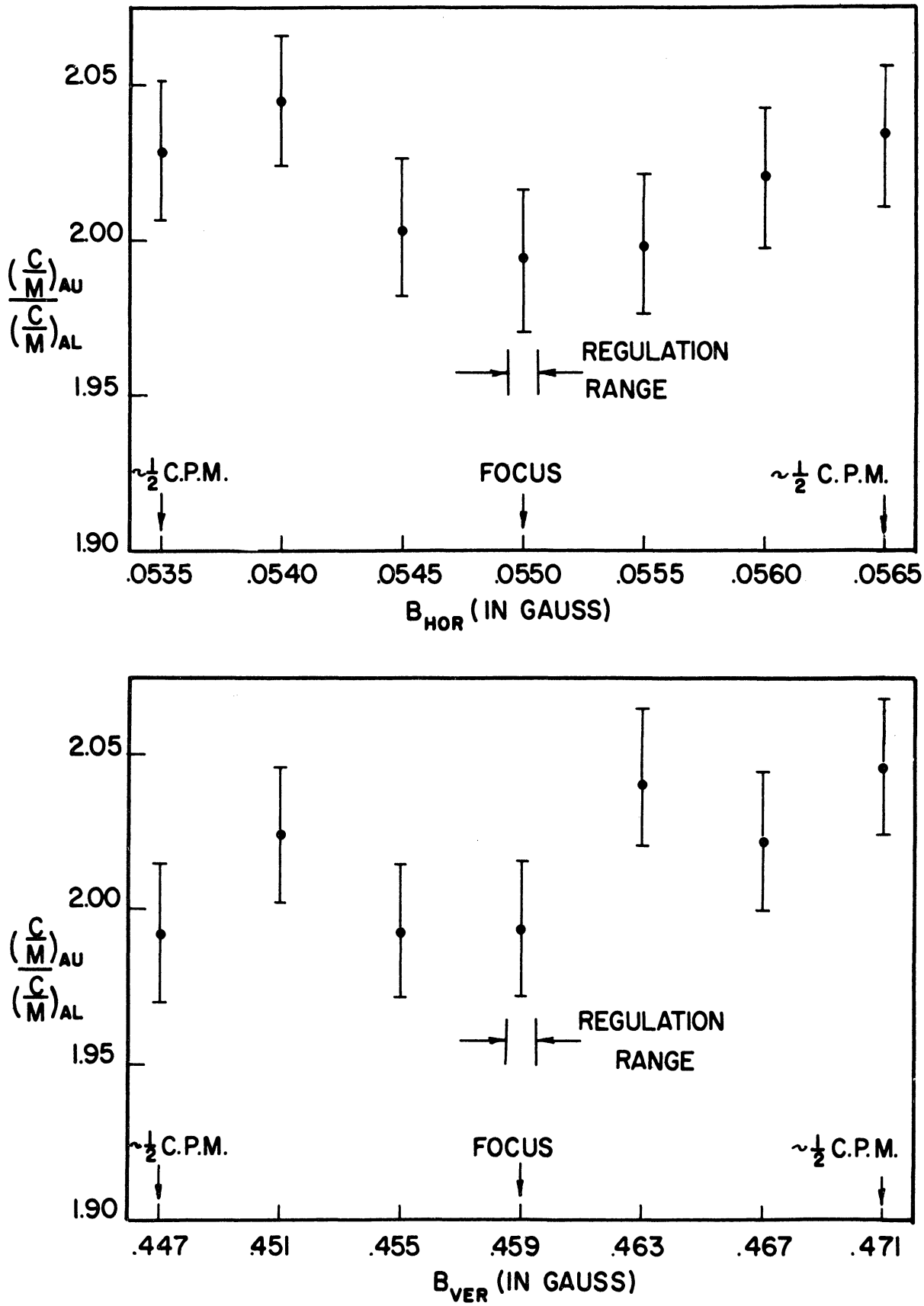

Figure 14. B_{hor} and B_{ver} Detuning Studies

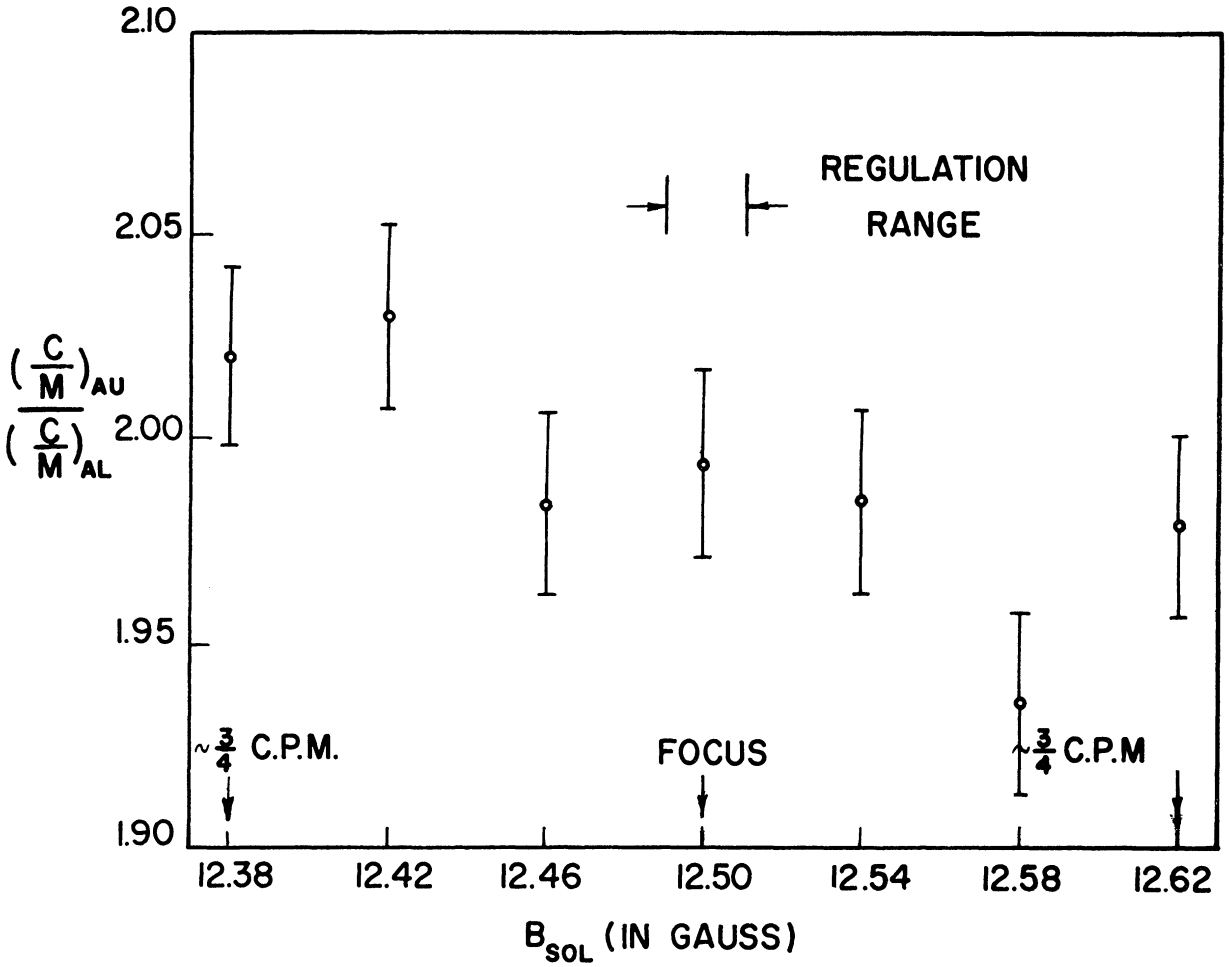

Figure 15. B_{sol} Detuning Study

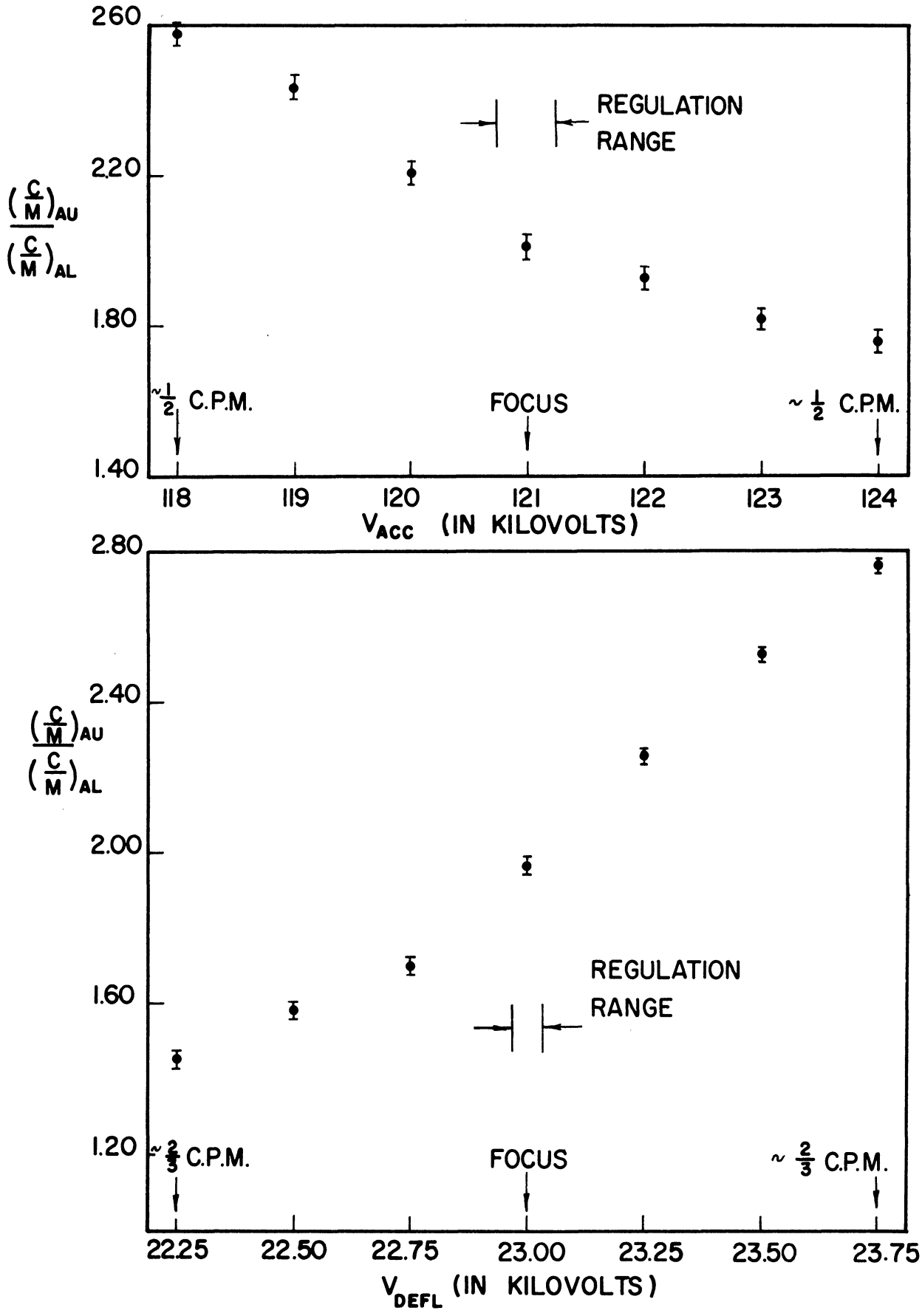

Figure 16. V_{acc} and V_{defl} Detuning Studies

from the spin of the electron. It can be understood qualitatively with the use of Figure 17. Consider a beam scattered at an angle θ_1 from a point on the polarizer target with a total aperture angle of 2α. If a constant magnetic field in the direction shown in Figure 17 is present, this beam will be brought to a focus at a point on the analyser target where it is scattered at some angle θ_2. The inclusion of the magnetic field in no way affects the calculation to follow and is included only to emphasize that this effect does not depend on a finite sized collision area of the beam on the analyser target. It also emphasizes the applicability of the calculation to the present experimental geometry. The solid line portions of the electron trajectories in Figure 17 lie in the plane of the paper while the dashed line portions are projections of the trajectories on the plane of the paper. The effect may be described by this essentially two dimensional picture.

Consider first the electrons following trajectory (a) in Figure 17. They must be scattered through a angle $\theta_2 + \alpha$ in order to proceed in the $\varphi_2 = \pi$ direction or through an angle $\theta_2 - \alpha$ in order to proceed in the $\varphi_2 = 0$ direction. Assuming a cross section which decreases monotonically with increasing scattering angle, more of these electrons will be scattered into the $\varphi_2 = 0$ direction. Reasoning similarly for electrons following trajectory (b), it can be seen that more of these are scattered in the $\varphi_2 = \pi$ direction than in the $\varphi_2 = 0$ direction. If the same number of electrons followed each of these two trajectories, no difference in the numbers of electrons scattered into directions $\varphi_2 = 0$ and $\varphi_2 = \pi$ would result. However, if the same type of cross section that holds for the analyser is assumed to hold for the polarizer, then there are more electrons

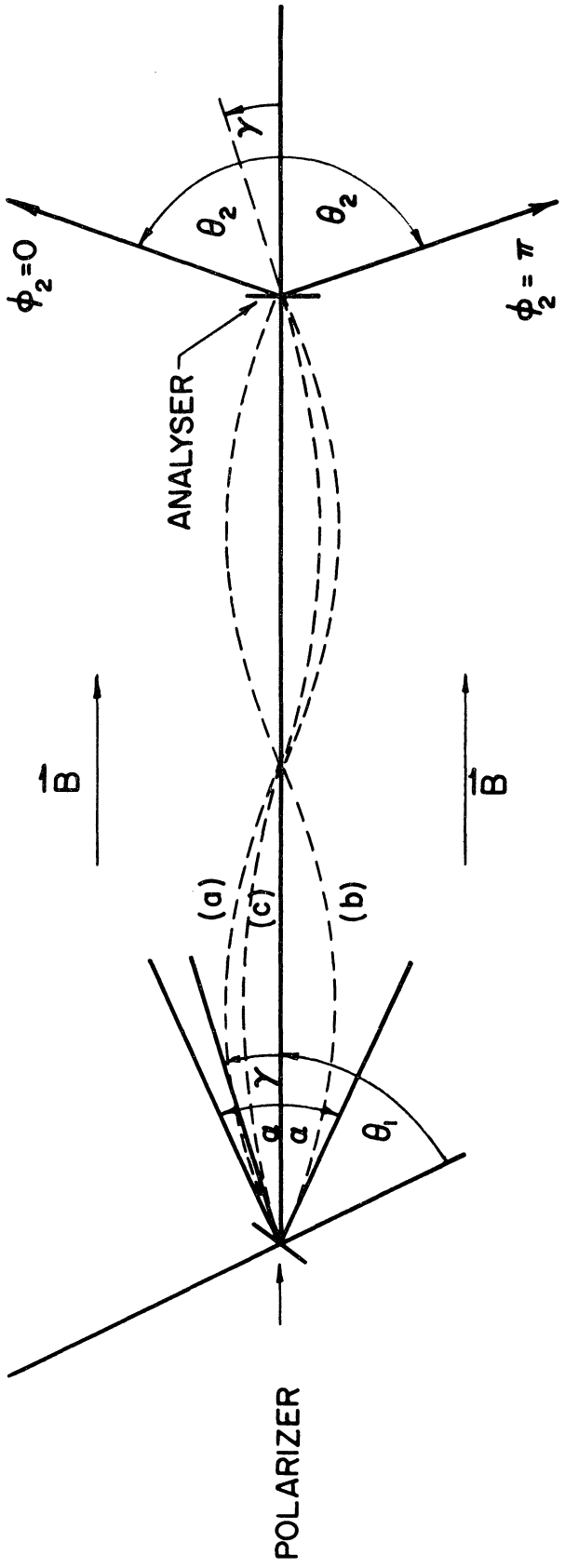

Figure 17. Finite Aperture Assymmetry

scattered along trajectory (b) than along (a). A predominance of electrons scattered in the $\varphi_2 = \pi$ direction over those scattered in the $\varphi_2 = 0$ direction results. This is the finite aperture asymmetry.

Louisell[2,3] first discussed this effect. He calculated the expected asymmetry for 90° scattering at both targets. His estimate of the effect agrees with the more general treatment below. Since his treatment contains several serious errors, the agreement must be regarded as coincidental.

Consider the trajectory (c) in Figure 17. The intensity of the beam scattered in direction $\varphi_2 = \pi$ at the analyser from a solid angle $d\Omega_1$ at the polarizer is

$$I_\pi d\Omega_1 = I_i N_1 N_2 t_1 t_2 \sigma_1 \sigma_2 \Delta\Omega_2 d\Omega_1 \tag{4.1}$$

Here I_i is the beam intensity before the first scattering, N the density of atoms in the target, t the effective target thickness, σ the differential cross section, and $\Delta\Omega_2$ the solid angle accepted by the detector. The subscripts 1 and 2 refer to the first and second scatterings respectively. Let us assume the Rutherford scattering law to hold.

$$I_\pi d\Omega_1 = I_i N_1 N_2 t_1 t_2 \Delta\Omega_2 \left(\frac{Z_1 e^2}{2mv^2}\right)^2 \left(\frac{Z_2 e^2}{2mv^2}\right)^2 \frac{\sin\theta_1^{(\pi)} d\theta_1^{(\pi)} d\varphi_1^{(\pi)}}{\sin^4\frac{\theta_1^{(\pi)}}{2} \sin^4\frac{\theta_2^{(\pi)}}{2}} \tag{4.2}$$

The scattering angles $\theta_1^{(\pi)}$ and $\theta_2^{(\pi)}$ for this beam may be expressed in terms of the aperture angle γ by

$$\theta_1^{(\pi)} = \theta_1 + \gamma \tag{4.3}$$

and

$$\theta_2^{(\pi)} = \theta_2 + \gamma \tag{4.4}$$

The effective target thickness t_2 is given in terms of the perpendicular target thickness d by

$$t_2 = d \sec\gamma \tag{4.5}$$

Let

$$K = I_\lambda N_1 N_2 t_1 d \left(\frac{Z_1 e^2}{2mv^2}\right)^2 \left(\frac{Z_1 e^2}{2mv^2}\right)^2 2\sin\theta_1 \sin\alpha \, \Delta\Omega_2 \tag{4.6}$$

$$\therefore I_\pi \sin\theta_1^{(\pi)} d\theta_1^{(\pi)} = \frac{K}{2\sin\theta_1 \sin\alpha} \frac{\sec\gamma \sin(\theta_1+\gamma)\, d\gamma}{\sin^4\left(\frac{\theta_1}{2}+\frac{\gamma}{2}\right)\sin^4\left(\frac{\theta_2}{2}+\frac{\gamma}{2}\right)} \tag{4.7}$$

The average of I_π over the aperture at the polarizer is

$$\bar{I}_\pi = \int_{\theta_1-\alpha}^{\theta_1+\alpha} I_\pi \sin\theta_1^{(\pi)} d\theta_1^{(\pi)} . \tag{4.8}$$

$$\therefore \bar{I}_\pi = \frac{K}{2\sin\theta_1 \sin\alpha} \int_{-\alpha}^{+\alpha} \frac{\sec\gamma \sin(\theta_1+\gamma)\, d\gamma}{\sin^4\left(\frac{\theta_1}{2}+\frac{\gamma}{2}\right)\sin^4\left(\frac{\theta_2}{2}+\frac{\gamma}{2}\right)} \tag{4.9}$$

$$\bar{I}_\pi = \frac{K}{2\sin^4\frac{\theta_1}{2}\sin^4\frac{\theta_2}{2}\sin\alpha} \int_{-\alpha}^{+\alpha} \frac{(1+\cot\theta_1 \tan\gamma)\, d\gamma}{\left(\cos\frac{\gamma}{2}+\cot\frac{\theta_1}{2}\sin\frac{\gamma}{2}\right)^4\left(\cos\frac{\gamma}{2}+\cot\frac{\theta_2}{2}\sin\frac{\gamma}{2}\right)^4} \tag{4.10}$$

Assuming α small ($\sim 1°$), the integrand may be expanded for small γ provided θ_1 and θ_2 are large enough so that both $\cot\frac{\theta_1}{2}$ and $\cot\frac{\theta_2}{2}$ are less than, say, ten.

$$\bar{I}_\pi = \frac{K}{\sin^4\frac{\theta_1}{2}\sin^4\frac{\theta_2}{2}} \frac{1}{2\alpha} \int_{-\alpha}^{+\alpha} \Big[1+\gamma\left(\cot\theta_1 - 2\cot\frac{\theta_1}{2}+2\cot\frac{\theta_2}{2}\right)+\gamma^2\Big(4 + 4\cot\frac{\theta_1}{2}\cot\frac{\theta_2}{2}+\frac{3}{2}\cot^2\frac{\theta_1}{2}-2\cot\frac{\theta_1}{2}\cot\theta_1+\frac{3}{2}\cot^2\frac{\theta_2}{2}-2\cot\frac{\theta_2}{2}\cot\theta_1\Big)\Big] d\gamma \tag{4.11}$$

Integrating, this becomes

$$\bar{I}_{\pi} = \frac{K}{\sin^4\frac{\theta_1}{2}\sin^4\frac{\theta_2}{2}} R(\theta_1,\theta_2,\phi_2=\pi,\alpha) \tag{4.12}$$

where

$$R(\theta_1,\theta_2,\phi_2=\pi,\alpha) = 1+\frac{\alpha^2}{3}\left(4+4\cot\frac{\theta_1}{2}\cot\frac{\theta_2}{2}+\frac{3}{2}\cot^2\frac{\theta_1}{2}\right.$$
$$\left.+\frac{3}{2}\cot^2\frac{\theta_2}{2}-2\cot\frac{\theta_1}{2}\cot\theta_1-2\cot\frac{\theta_2}{2}\cot\theta_1\right) \tag{4.13}$$

The beam intensity scattered in the direction $\varphi_2 = 0$ can be calculated in a similar manner, the only change being that $\theta_2^{(0)} = \theta_2 \ominus \gamma$. The result is

$$\bar{I}_0 = \frac{K}{\sin^4\frac{\theta_1}{2}\sin^4\frac{\theta_2}{2}} R(\theta_1,\theta_2,\phi_2=0,\alpha) \tag{4.14}$$

where

$$R(\theta_1,\theta_2,\phi_2=0,\alpha) = 1+\frac{\alpha^2}{3}\left(4-4\cot\frac{\theta_1}{2}\cot\frac{\theta_2}{2}+\frac{3}{2}\cot^2\frac{\theta_1}{2}\right.$$
$$\left.+\frac{3}{2}\cot^2\frac{\theta_2}{2}-2\cot\frac{\theta_1}{2}\cot\theta_1+2\cot\frac{\theta_2}{2}\cot\theta_1\right) \tag{4.15}$$

$$\therefore \frac{\bar{I}_0}{\bar{I}_{\pi}} = \frac{R(\theta_1,\theta_2,\phi_2=0,\alpha)}{R(\theta_1,\theta_2,\phi_2=\pi,\alpha)} = 1-\frac{4\alpha^2}{3}\left(2\cot\frac{\theta_1}{2}-\cot\theta_1\right)\cot\frac{\theta_2}{2} \tag{4.16}$$

The ratio of beam intensity in the $\varphi_2 = 0$ direction to that in the $\varphi_2 = \pi$ direction due to this effect is therefore less than one since both $(2\cot\frac{\theta_1}{2} - \cot\theta_1)$ and $\cot\frac{\theta_2}{2}$ are positive for θ_1 and θ_2 between 0 and π. Hence the

finite aperture asymmetry opposes the Mott asymmetry and tends to reduce the measured value of it.

This can be a large effect. If $\theta_1 = \theta_2 = 60°$ and $\alpha = 3°$ then the difference of the ratio (4.16) from unity is .018 which is large compared with $2\delta_{MOTT}$ (60°,60°) = .008 for gold targets at 121 kev. The finite aperture asymmetry decreases with increasing scattering angles θ_1 and θ_2 and with a decreasing aperture angle α. For this experiment $\alpha = 1°$ and $\theta_1 = 90°$ and so

$$\frac{I_o}{I_\pi} = 1 - .000406 \cot\frac{\theta_2}{2} \qquad (4.17)$$

The biggest effect in this experiment will be on the monitor at $\theta_2 = 45°$. For this angle the ratio differs from unity by less than a part in a thousand (.00098).

Since the finite aperture asymmetry, as calculated above from the Rutherford cross section, is independent of the atomic number of the scatterer, even this small effect would be divided out of the data by the procedure of taking a ratio of counting rates for gold to that for aluminum. However, the scattering of spin 1/2 particles of relativistic energies is not accurately described by the Rutherford cross section. The Mott theory must be used. In the Mott cross section formula the Z and θ dependences are not multiplicative. However, the Mott cross section formula may be written as the product of the Rutherford cross section multiplied by a function of Z and θ. This function has at most a value of about two for Z = 79, E = 121 kev and any θ.[41] Thus, by taking a ratio of the counting rate for gold to that for aluminum, at least half of the already small finite aperture asymmetry will be

eliminated from the data. It is concluded that the finite aperture asymmetry causes no significant error in the present experiment.

Background Studies

Use of the magnetic focusing field between the polarizer and analyser allowed the analyser to be far enough from the polarizer so that background from the very intense source of x-rays at the polarizer was negligible. Lead shielding aided in this job. This source of background was evaluated by measuring the counting rates with the beam on and off when no polarizer foil was present.

With the polarizer foil in position and an empty target holder in the analyser position, the counting rate dropped to cosmic ray level for all scattering angles studied. This was true for both the movable counter, the monitor, and the counter attached to the energy analyser.. This was taken as an indication that no significant source of background arose from the transmitted beam colliding with the end of the analyser chamber. It must be called an indication rather than a proof since the geometry of the beam is different with target in and out. Since the number of electrons scattered at large angles is relatively small compared to the number in the transmitted beam, the main difference is that, with the target in, the transmitted beam is contained roughly in a cone with an apex angle equal to the root-mean-square angle of multiple scattering rather than in a fine line as when the target is out. However, care was taken in the construction of the analyser chamber to allow this cone of beam to proceed about three feet before encountering the chamber wall. For this reason target-out background and target-in background were believed identical.

Thus the only background was that of cosmic rays. For the counters used the counting rate from this cause was about ten counts per minute. Since the lowest beam counting rate used was about 10,000 counts per minute, the background represented a correction of only .1%. Since this error is a factor of ten below the statistical error quoted for each of the twelve points used to measure the cosine asymmetry, it was not subtracted from the observed counting rates. It might be added, however, that even this negligible source of error was partially eliminated by the procedure of ratio taking.

Energy Analysis and Calibration

The energy analyser was built to determine whether inelastic scattering could affect the measurement of the Mott asymmetry. The work of Rose and Bethe[19], discussed in Chapter II, indicates that no significant depolarization results from inelastic processes in which only a small fraction of the electron's energy is lost. Their treatment therefore does not apply to those electrons in the low energy tail of the energy profile of the doubly-scattered beam. Even if these electrons retained the same polarization as those in the elastic peak, it would be necessary to discriminate against them in the present experimental arrangement since their spins would have precessed more due to their slower speed in the magnetic focusing field than the spins of the electrons in the elastic peak. This leads to a depolarization as discussed in Chapter II. From these considerations it is seen that only a low resolution analyser is needed since only the tail of the profile need be excluded.

Energy profiles of the doubly-scattered beam for a gold analyser and for an aluminum analyser are shown in Figure 18. In each case a gold polarizer of thickness 9×10^{-6} cm was used. Since one kilovolt change on the deflecting plates corresponds to six kilovolts change in the accepted beam energy, the full width of the elastic peak at half maximum for a gold analyser is about 12 kilovolts. For the aluminum it is about 14.5 kilovolts. The deflector voltage used in measuring δ_{MOTT} is indicated in Figure 18. Its position between the elastic peaks for the gold and aluminum was chosen so that running time would be a minimum.

The energy analyser in conjunction with a radioactive source was used to calibrate the beam accelerating voltage. A weak ($\sim$ 7000 disintegrations per second) Eu^{152} - Eu^{154} source was mounted on a thin film in the analyser target holder. The K conversion line at 73 kev and the L conversion lines (a close doublet) at 115 kev from a 122 kev γ-ray were observed. The deflector voltage corresponding to 121 kev electrons was then found by extrapolation. The high voltage meter was then calibrated by determining the setting for which the elastic peak of the doubly scattered beam corresponded to the deflector voltage for 121 kev electrons. The error in this calibration was estimated to be 3%. From the width of the conversion lines the resolution of the energy analyser was estimated to be 8%.

Target Thickness and Orientation

The gold targets used were commercially available gold leaf. By weighing, the thickness was found to vary from .18 to .19 mg/cm^2. This corresponds to about 9×10^{-6} cm. The main requirement on the gold

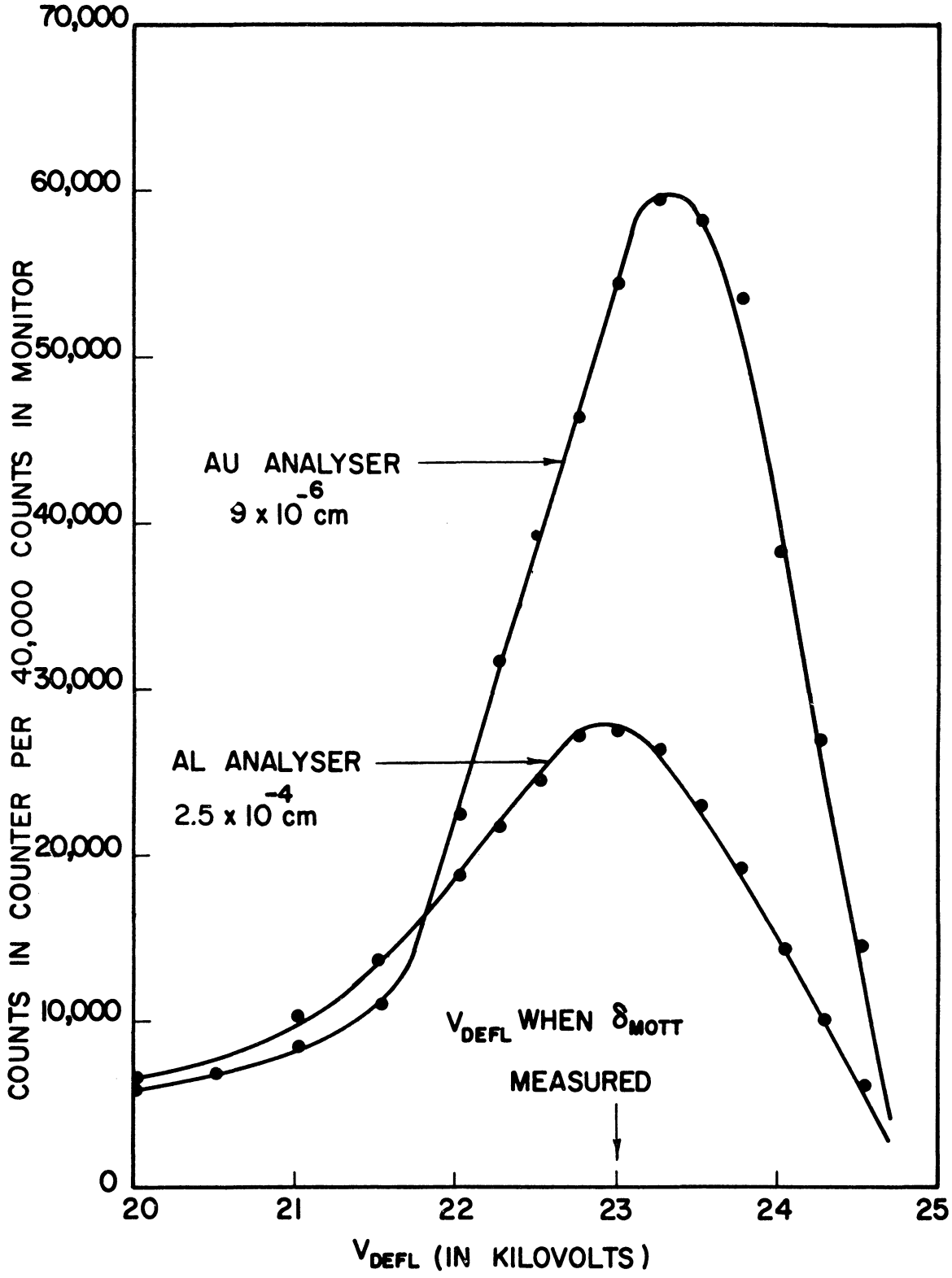

Figure 18. Energy Profiles

target is that it be thin enough to insure single scattering, or at least, to avoid multiple scattering. Mohr and Tassie[44] have studied the multiple scattering of electrons in gold foils at the energy 121 kev. They state that the Williams[45] formula for the root-mean-square angle

$$\sqrt{\overline{\theta^2}} = \sqrt{\frac{8\pi N d Z^2 e^4 (1-\beta^2)}{m_0^2 c^4 \beta^4} \ln\left(\frac{231 (Nd)^{1/2} Z^{2/3} e^2}{m_0 c^2 \beta}\right)} \quad (4.1)$$

gives the best fit to their exact numerical treatment. For gold (N = 5.91×10^{22} atoms per cm^3), an energy of 121 kev ($\beta = .59$), and a target thickness of 9×10^{-6} sec 40° cm (the effective thickness of the target for the orientation used for measurements at an 80° scattering angle), this root-mean-square angle of multiple scattering is 9°. However, Mohr and Tassie[44] state that values of this angle below 30° for this energy and element are rather meaningless since they correspond to target thicknesses so thin that an insufficient number of collisions occur to allow the application of multiple scattering theory. The average number of collisions n is given by the William's treatment to be

$$n = 5.36 \times 10^4 \frac{N d Z^{4/3} e^4}{m_0^2 c^4 \beta^2} \quad (4.2)$$

For the parameters given above, $n \approx 3$. This bears out the statement of Mohr and Tassie. Thus multiple scattering is negligible for the gold targets used.

The aluminum target used had a thickness of .67 mg/cm^2 corresponding to 2.5×10^{-4} cm. The multiple scattering is small since the root-mean-square angle ($\sim 11°$) and the average number of collisions ($n \approx 3$) are close to those discussed for the gold foil. The main criterion in choosing a foil thickness for the aluminum was to match the counting rate

for the gold target for a scattering angle of about 90°. In doing this an energy analyser setting corresponding roughly to acceptance of the elastic peak from the gold target was used.

At the lowest angle of scattering studied ($\theta_2 = 80°$) the effect of target thickness on the measurement of the Mott asymmetry was studied experimentally. A gold foil of thickness 1.8×10^{-5}cm was used as the analysing foil. The δ_{MOTT} measured for this foil ($.053 \pm .003$) agreed within statistical error with δ_{MOTT} measured with a foil $.9 \times 10^{-5}$cm ($.056 \pm .003$). At larger scattering angles the effect of target thickness would be expected to be less important. Hence, it was concluded that targets thin enough to insure single scattering were used.

The calculations of Ryu on plural scattering, discussed in Chapter II, indicate that the transmission side of the foil should face the detector if single scattering is to be insured. For this reason the plane of the target was placed so as to bisect the supplement to the scattering angle. The plane of the target was also perpendicular to the plane determined by the trajectories of the electrons scattered into the counter and monitor. For this target orientation grazing of the target by both the incident and scattered beams is minimized consistent with using the transmission side of the foil. For large scattering angles the angle of scattering approaches the target plane with this scheme. Thus plural scattering contributions may thus increase with scattering angle even while using the transmission side of the foil. Unfortunately no calculations are available to estimate the amount.

Unpolarized Nature of Initial Beam

An electron beam obtained from a hot filament has always been considered to be unpolarized. The reasons for this belief have been theoretical rather than experimental. Since it is easy to check this assumption of the Mott theory experimentally with this apparatus, it was felt worthwhile to do so.

From symmetry considerations it can be seen that the beam leaving the electron gun, if polarized, must be longitudinally polarized. This is apparent since the only preferred directions are the momentum and the accelerating electric field which are in the same direction. Hence, any polarization must be parallel or anti-parallel to the momentum.

A method of detecting this longitudinal polarization with the present apparatus is to use an aluminum target at the polarizer position and a gold analyser target. The aluminum target will not produce any appreciable Mott polarization but will rotate the longitudinal polarization vector into a predominantly transverse orientation[28] since the angle of scattering at the first target is 90°. Therefore, since Mott scattering on the gold second target acts as an analyser for transverse polarization, an azimuthal asymmetry should result if the first incident beam were longitudinally polarized. A run of this type was made. The results are shown in Figure 19. A Fourier analysis of the experimental points yielded an asymmetry amplitude of .007 $\pm$ .006. This amplitude of the cosine asymmetry agrees well with δ_{MOTT} (Al,90°; Au,90°) = .0065 calculated by Sherman[36] (see Table I). Of equal importance is the fact that the phase of the cosine agreed with that expected of a Mott asymmetry considering the precession of the polarization vector in the

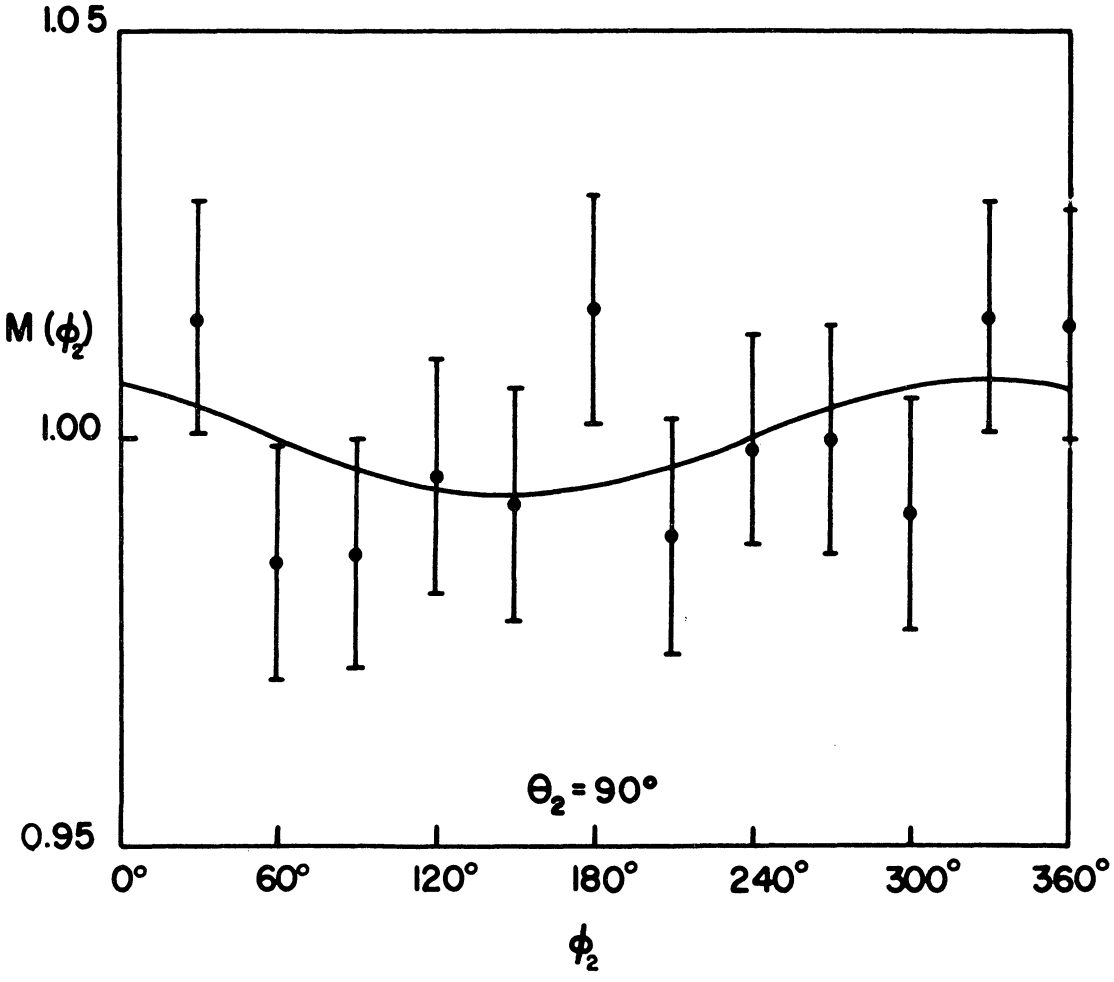

Figure 19. Mott Asymmetry for Al-Au Scattering

magnetic focusing field. Any asymmetry resulting from longitudinal polarization of the first incident beam should differ in phase from the Mott asymmetry by 90°. It is concluded that the first incident beam is unpolarized.

V. EXPERIMENTAL RESULTS AND ANALYSIS

Procedure for Measuring the Asymmetry Factor

For a measurement of the Mott asymmetry factor to be reliable it is necessary that the cosinusoidal dependence on the azimuthal angle φ of the double scattering cross section be demonstrated experimentally. For this reason measurements of the counting rate were made at twelve equally spaced points in azimuth. Runs were made at each azimuth alternately with a gold polarizer and a gold analyser and with a gold polarizer and an aluminum analyser, the latter being done to evaluate the spurious instrumental asymmetry. The electrostatic energy analyser was used for some runs; the plain Geiger counter for others. For each run counts were recorded from the counter stationed at some scattering angle θ and from the monitor fixed at a scattering angle of $45°$, the purpose of the latter being to monitor the beam intensity so as not to allow the introduction of a spurious asymmetry due to time variations in the beam intensity. The scalars were set so that they both turned off when a predetermined number of counts had been recorded in the monitor scalar. This number was chosen to be 40,000 for the gold analyser and 100,000 for the aluminum analyser. Runs varied in length from two to ten minutes depending on the target element and the target orientation.

With this procedure four experimental numbers were obtained for each azimuthal angle studied. Denote any one of these numbers by $n_{Z_1 Z_2}(\theta_2, \varphi_2)$ where Z_1 and Z_2 refer to the elements of first and second scattering respectively and θ_2, φ_2 are the angles of second scattering. Any one of these four may be expressed as

$$n_{Z_1Z_2}(\theta_2,\phi_2) = I(t)\left(N_{Z_1} d_{Z_1} \sec\frac{\pi}{4}\Delta\Omega_1\right)\left(N_{Z_2} d_{Z_2} \sec\frac{\theta_2}{2}\Delta\Omega_2\right)\epsilon\,\sigma_{Z_1}\left(\frac{\pi}{2}\right) \times \sigma_{Z_2}(\theta_2)\left[1+\delta\left(Z_1,\frac{\pi}{2};Z_2,\theta_2\right)\cos(\phi_2-\alpha)\right]R_{Z_1Z_2}(\theta_2,\phi_2)A(\theta_2,\phi_2) \tag{5.1}$$

Here I(t) is the beam intensity, which may depend on time, striking the first scatterer, N_Z is the density of atoms in the target, d is the perpendicular target thickness, $\Delta\,\Omega$ is the solid angle, ϵ is the counting system efficiency, $\sigma(\theta)$ is the single scattering cross section for an unpolarized beam, the angle α is given by equation (2.56), $\delta(Z_1,\theta_1;\ Z_2,\theta_2)$ is the Mott asymmetry factor, $R_{Z_1Z_2}(\theta_2,\varphi_2)$ is the finite aperture asymmetry given by (4.13) and (4.15), and $A(\theta_2,\varphi_2)$ is the spurious instrumental asymmetry. The factor $\sec\frac{\theta_2}{2}$ is present to give the effective target thickness for either counter when the target plane bisects the supplement to the scattering angle. As was discussed in Chapter IV the finite aperture asymmetry for this experiment is negligibly small. If the following ratio of the four experimental numbers is taken, the beam intensity I(t) incident on the first target and the spurious instrumental asymmetry $A(\theta_2,\ \varphi_2)$ are divided out:

$$\frac{n_{79\text{-}79}(\theta_2,\phi_2)\,n_{79\text{-}13}(\frac{\pi}{4},\phi_2)}{n_{79\text{-}79}(\frac{\pi}{4},\phi_2)\,n_{79\text{-}13}(\theta_2,\phi_2)} = C\,\frac{\left[1+\delta(79,\frac{\pi}{2};79,\theta_2)\cos(\phi_2-\alpha)\right]}{\left[1+\delta(79,\frac{\pi}{2};79,\frac{\pi}{4})\cos(\phi_2-\alpha)\right]} \times \frac{\left[1+\delta(79,\frac{\pi}{2};13,\frac{\pi}{4})\cos(\phi_2-\alpha)\right]}{\left[1+\delta(79,\frac{\pi}{2};13,\theta_2)\cos(\phi_2-\alpha)\right]} \tag{5.2}$$

The factor C is a constant with respect to the azimuth angle and the time t. This follows from the above discussion and the following assumptions

implicit in equation (5.1): The spurious instrumental asymmetry is assumed independent of the analyser target element (or, at worst, its dependence on Z_2 is through a multiplicative function independent of φ_2) and independent of time. The time variation of the beam intensity is assumed small enough so that the variation in the counting efficiencies from counting losses is negligible. The beam energy is assumed sufficiently constant in time so that no time dependence is introduced into (5.2) through the dependence of $\sigma(\theta)$ on the energy.

Equation (5.2) has the experimentally measured quantities on the left side and the theoretically predicted quantities on the right side. Using the theoretical predictions that each of the two factors in the denominator differ only slightly from unity, the right side may be simplified by expanding to first order. Denote the left side of (5.2) by $CM(\varphi_2)$.

$$M(\phi_2) = \frac{1}{C} \frac{n_{79\text{-}79}(\theta_2,\phi_2)\, n_{79\text{-}13}(\frac{\pi}{4},\phi_2)}{n_{79\text{-}79}(\frac{\pi}{4},\phi_2)\, n_{79\text{-}13}(\theta_2,\phi_2)} \tag{5.3}$$

$$M(\phi_2) = 1 + [\delta(79,\tfrac{\pi}{2};79,\theta_2) + \delta(79,\tfrac{\pi}{2};13,\tfrac{\pi}{4}) - \delta(79,\tfrac{\pi}{2};79,\tfrac{\pi}{4}) - \delta(79,\tfrac{\pi}{2};13,\theta_2)]\cos(\phi_2-\alpha) \tag{5.4}$$

Referring to Table I it can be seen that δ (79, $\frac{\pi}{2}$; 13, $\frac{\pi}{4}$) and δ (79, $\frac{\pi}{2}$; 79, $\frac{\pi}{4}$) are entirely negligible compared to δ (79, $\frac{\pi}{2}$; 79, θ_2) and that δ (79, $\frac{\pi}{2}$; 13, θ_2) is less than 10% of δ (79, $\frac{\pi}{4}$; 79, θ_2). Since the experimental error in the measured values of the asymmetry factor in this experiment are about 5%, it is seen that the actual quantity measured is δ (79, $\frac{\pi}{2}$; 79, θ_2) - δ (79, $\frac{\pi}{2}$; 13, θ_2).

$$\therefore M(\phi_2) = 1 + \left[\delta(79, \tfrac{\pi}{2}; 79, \theta_2) - \delta(79, \tfrac{\pi}{2}; 13, \theta_2)\right]\cos(\phi_2 - \alpha) \quad (5.5)$$

The amplitude of $\cos(\varphi_2 - \alpha)$ in (5.5) was found by a Fourier analysis of the twelve such ratios as on the left side of (5.2), each of which corresponds to one of the twelve equally spaced values of φ_2. The twelve ordinate method of calculation as given by Whittaker and Robinson[46] was used. This gives the best fit to the data in the least squares sense. A three term Fourier series of the form

$$a_0 + a_1 \cos\phi_2 + b_1 \sin\phi_2 \quad (5.6)$$

was sufficient to represent the experimental points. The asymmetry amplitude $[\delta(79, \frac{\pi}{2}; 79, \theta_2) - \delta(79, \frac{\pi}{2}; 13, \theta_2)]$ and the angle of spin precession in the magnetic focusing field are given by

$$\delta(79, \tfrac{\pi}{2}; 79, \theta_2) - \delta(79, \tfrac{\pi}{2}; 13, \theta_2) = \frac{1}{a_0}\sqrt{a_1^2 + b_1^2} \quad (5.7)$$

and

$$\alpha = + \arctan \frac{b_1}{a_1} \quad (5.8)$$

Measured Values of the Asymmetry Factor

Using the procedure outlined in the previous section the azimuthal asymmetry in the double scattering cross section was measured in seventeen separate runs for scattering angles between 80° and 140° using the electrostatic energy analyser. Six runs were also made without the energy analyser at scattering angles between 90° and 130°. The raw data from these runs are tabulated in the Appendix. All the runs for a given

scattering angle using the energy analyser have been combined and the resulting $M(\varphi_2)$ plotted against φ_2 in Figures 20, 21, 22, and 23. A similar procedure was used for the runs not using the energy analyser. The results of them are shown in Figures 24 and 25.

The asymmetry factors obtained by a Fourier analysis of these curves are given in Table II along with the theorectical asymmetry factors calculated for the pure Coulomb field by Sherman[36] and for the screened Coulomb field by Mohr and Tassie.[41] They are also shown in Figure 26. Since Mohr and Tassie did not calculate the asymmetry factor for the screened field of aluminum, the Sherman calculation of this for the unscreened field has been used for both theoretical curves. This is justified since the beam energy of 121 kev is so much larger than the binding energy of the K electrons in aluminum (1.56 kev), that screening effects should be completely negligible.

The data obtained with the energy analyser is replotted in terms of the polarization function $P(Z,\theta)$ for gold in Figure 27. To do this a theoretical correction has been applied to the data to compensate for the decrease in the measured asymmetry amplitude caused by the use of aluminum to evaluate the spurious instrumental asymmetry. A corrected asymmetry factor is obtained as follows:

$$\delta(79,\tfrac{\pi}{2};79,\theta_2)^{CORR} = \left[\delta(79,\tfrac{\pi}{2};79,\theta_2) - \delta(79,\tfrac{\pi}{2};13,\theta_2)\right]^{EXP} + \delta(79,\tfrac{\pi}{2};13,\theta_2)^{THEO} \qquad (5.9)$$

This correction amounts to less than 10%. The absolute value of the polarization function is then obtained using (2.41).

$$|P(79,\theta_2)|^{CORR} = \frac{\delta(79,\tfrac{\pi}{2};79,\theta_2)^{CORR}}{\sqrt{\delta(79,\tfrac{\pi}{2};79,\tfrac{\pi}{2})^{CORR}}} \qquad (5.10)$$

TABLE II

ASYMMETRY FACTORS AND POLARIZATIONS-EXPERIMENTAL AND THEORETICAL

	θ_2	$[\delta(79,90^\circ;79,\theta_2) - \delta(79,90^\circ;13,\theta_2)]^{EXP}$	α^{EXP}	$[\delta(79,90^\circ;79,\theta_2) - \delta(79,90^\circ;13,\theta_2)]^{THEO}$ Sh.	M.&T.	$\delta(79,90^\circ;13,\theta_2)^{THEO}$	$\delta(79,90^\circ;79,\theta_2)^{CORR}$	$\lvert P(79,\theta_2)\rvert^{CORR}$	$\lvert P(79,\theta)\rvert^{THED}$ Sh.	M.&T.
WITH ENERGY ANALYSIS	80°	.055 ± .002	302° ± 3°	.0467	.0510	.0054	.060 ± .002	.219 ± .008	.195	.204
	90°	.068 ± .002	302° ± 2°	.0647	.0703	.0065	.075 ± .002	.274 ± .008	.267	.277
	100°	.077 ± .002	314° ± 2°	.0809	.0873	.0073	.084 ± .002	.307 ± .008	.330	.342
	110°	.096 ± .003	307° ± 2°	.0945	.0988	.0079	.104 ± .003	.378 ± .012	.384	.386
	120°	.086 ± .004	316° ± 2°	.1023	.1045	.0081	.094 ± .004	.344 ± .015	.414	.409
	130°	.089 ± .004	301° ± 3°	.1033	.1058	.0079	.097 ± .004	.354 ± .015	.417	.411
	140°	.079 ± .005	303° ± 3°	.0956	.1006	.0071	.086 ± .005	.314 ± .019	.385	.389
NO ENERGY ANALYSIS	90°	.042 ± .002	327° ± 3°	.0647	.0703					
	110°	.067 ± .004	339° ± 4°	.0945	.0988					
	120°	.060 ± .004	335° ± 4°	.1023	.1045					
	130°	.056 ± .004	329° ± 5°	.1033	.1058					

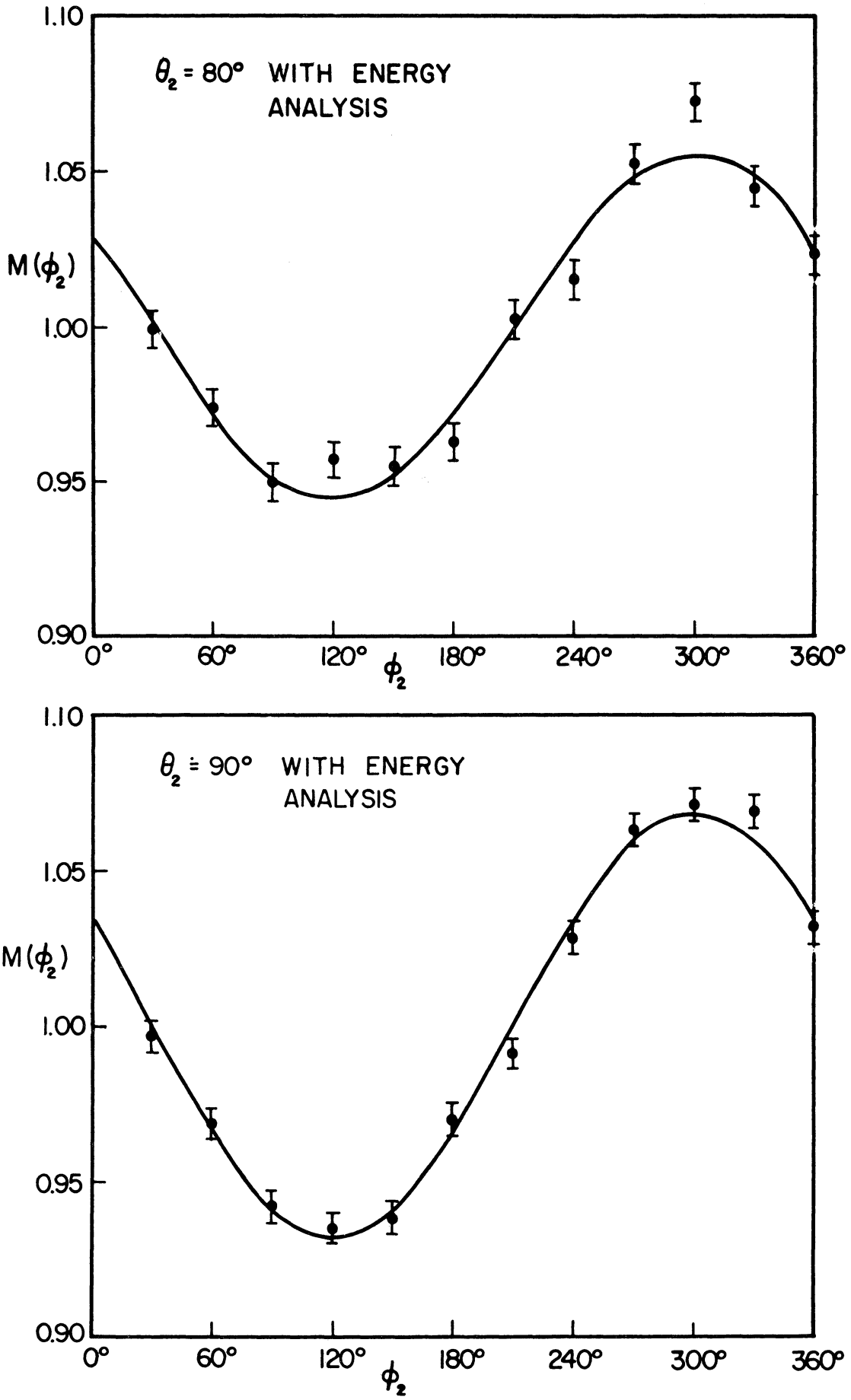

Figure 20. Mott Asymmetry with Energy Analysis (θ_2 = 80°, 90°)

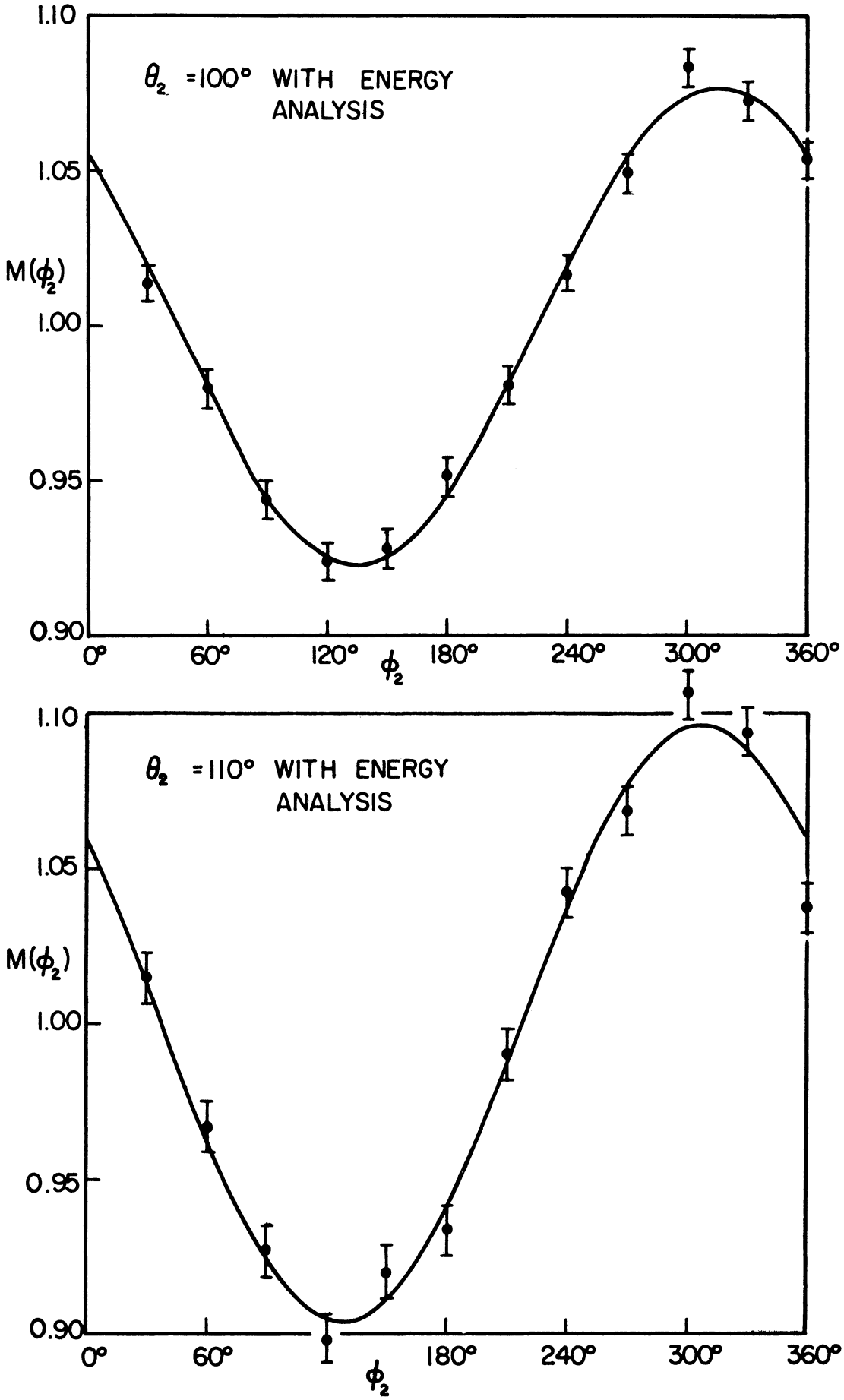

Figure 21. Mott Asymmetry with Energy Analysis (θ_2 = 100°, 110°)

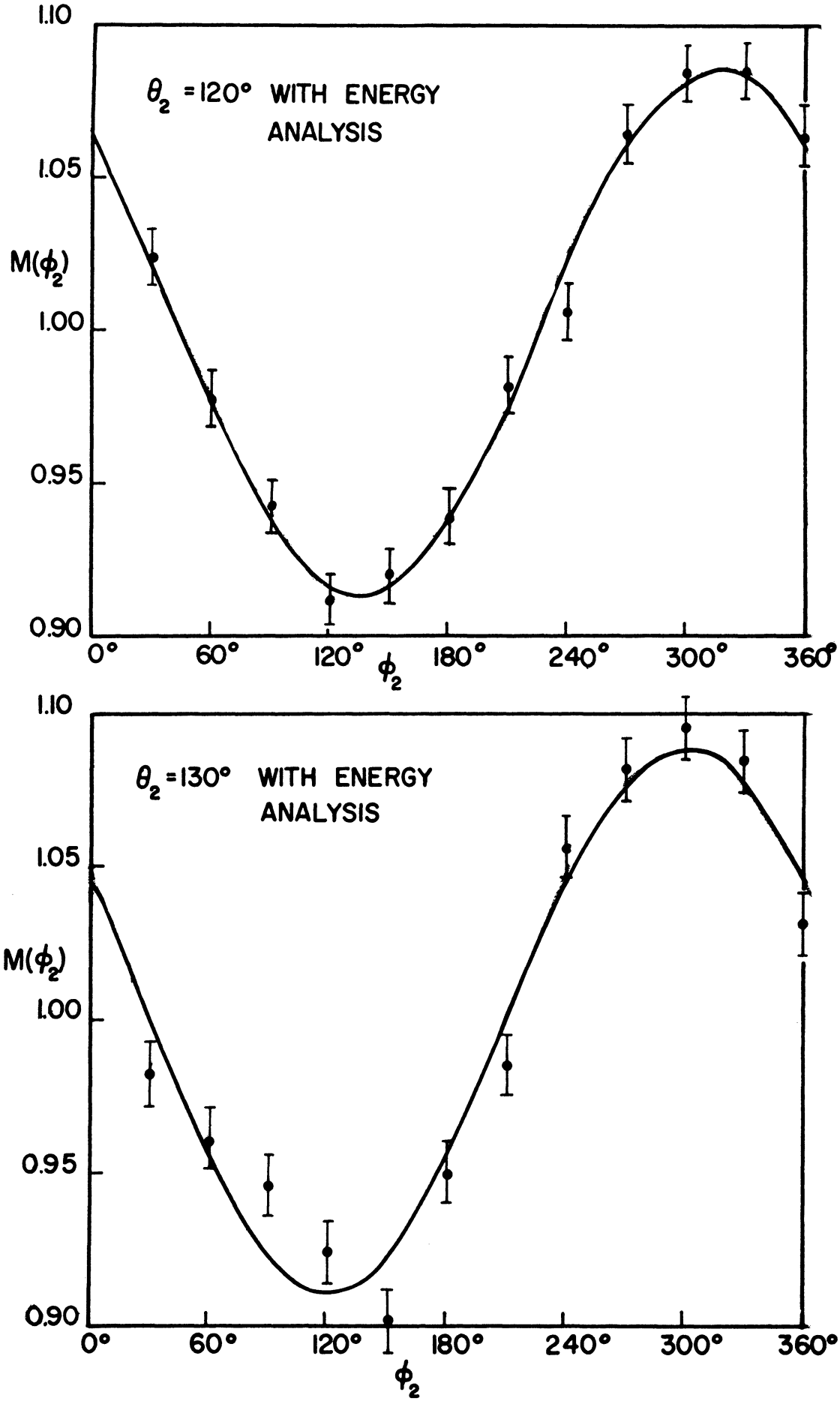

Figure 22. Mott Asymmetry with Energy Analysis (θ_2 = 120°, 130°)

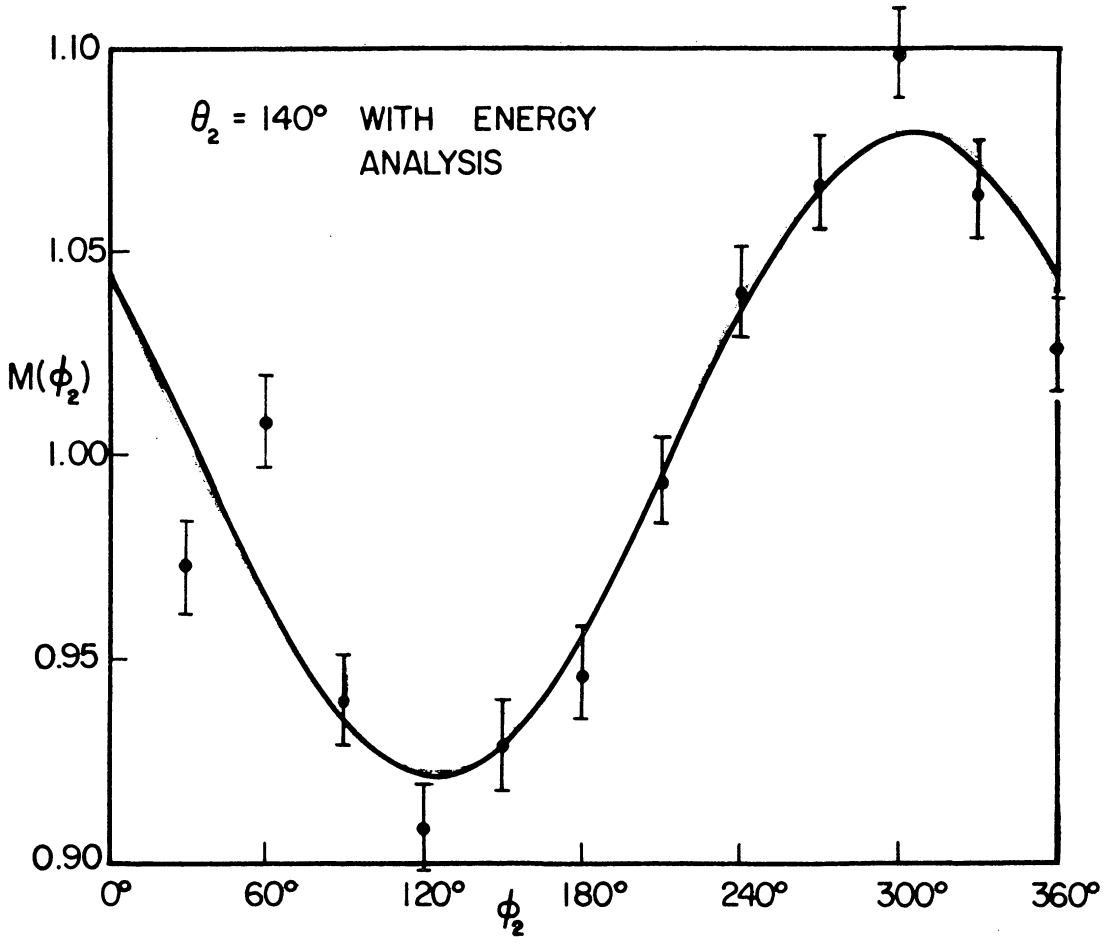

Figure 23. Mott Asymmetry with Energy Analysis ($\theta_2 = 140°$)

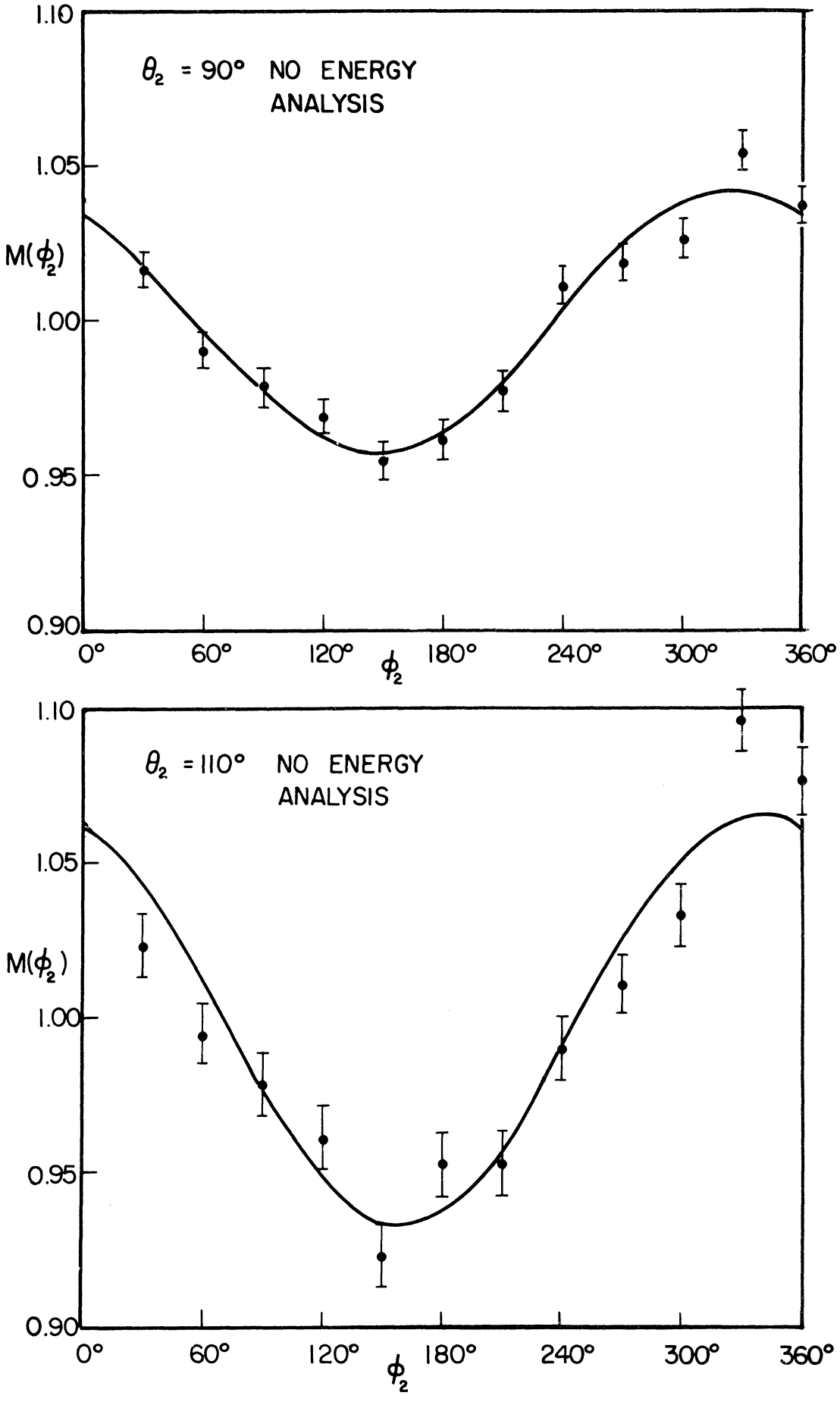

Figure 24. Mott Asymmetry - No Energy Analysis (θ_2 = 90°, 110°)

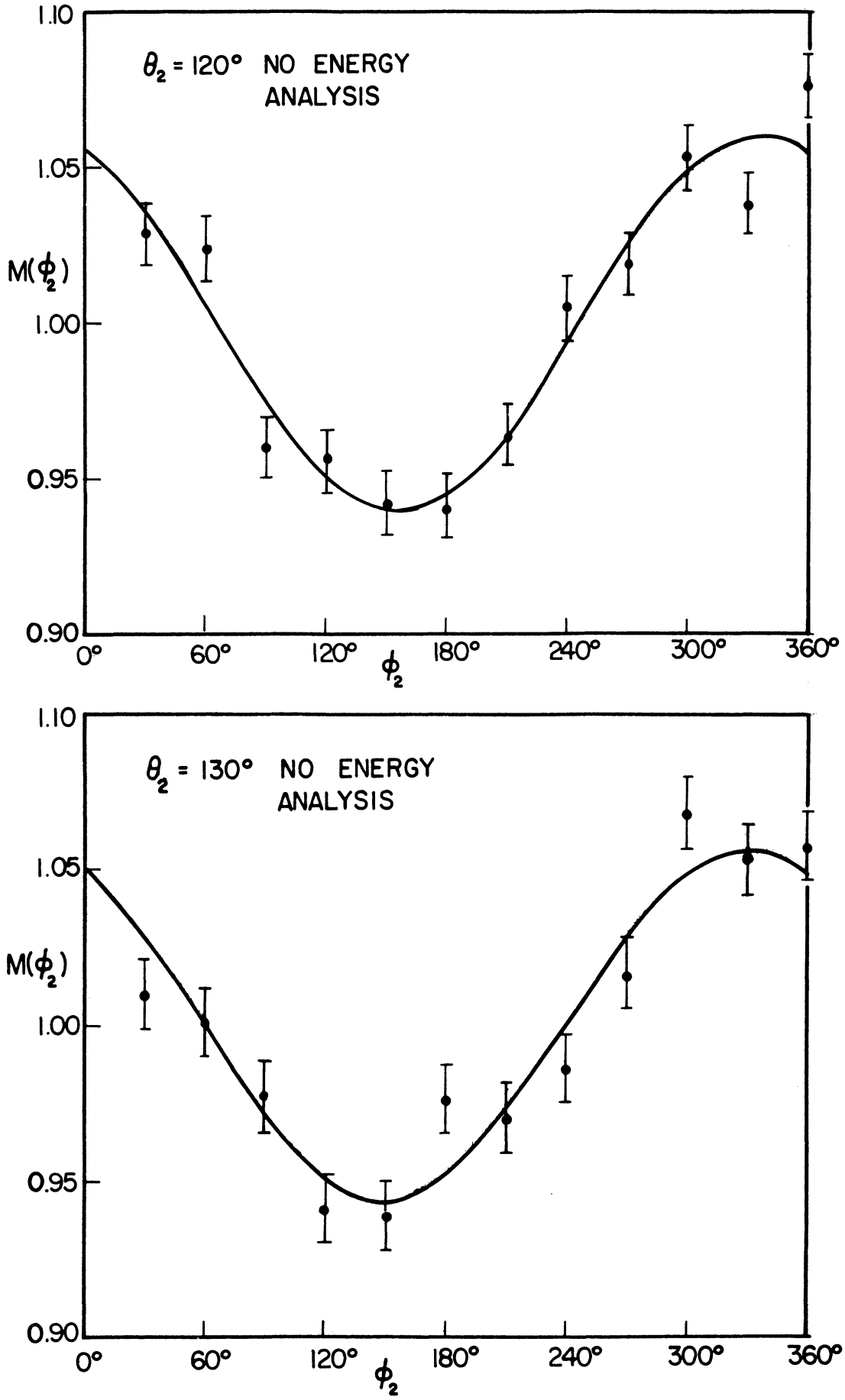

Figure 25. Mott Asymmetry - No Energy Analysis (θ_2 = 120°, 130°)

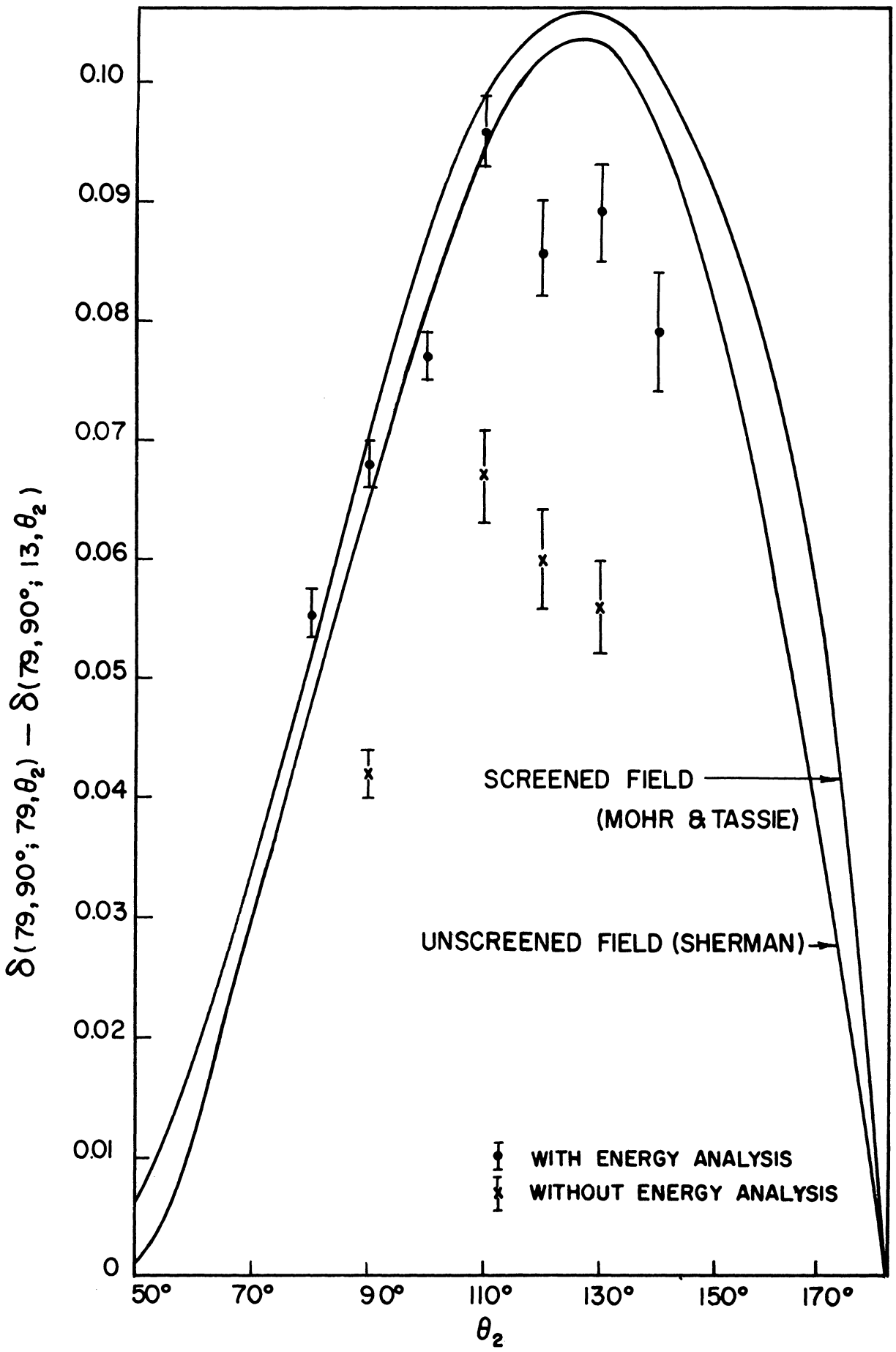

Figure 26. Measured Mott Asymmetry Factors

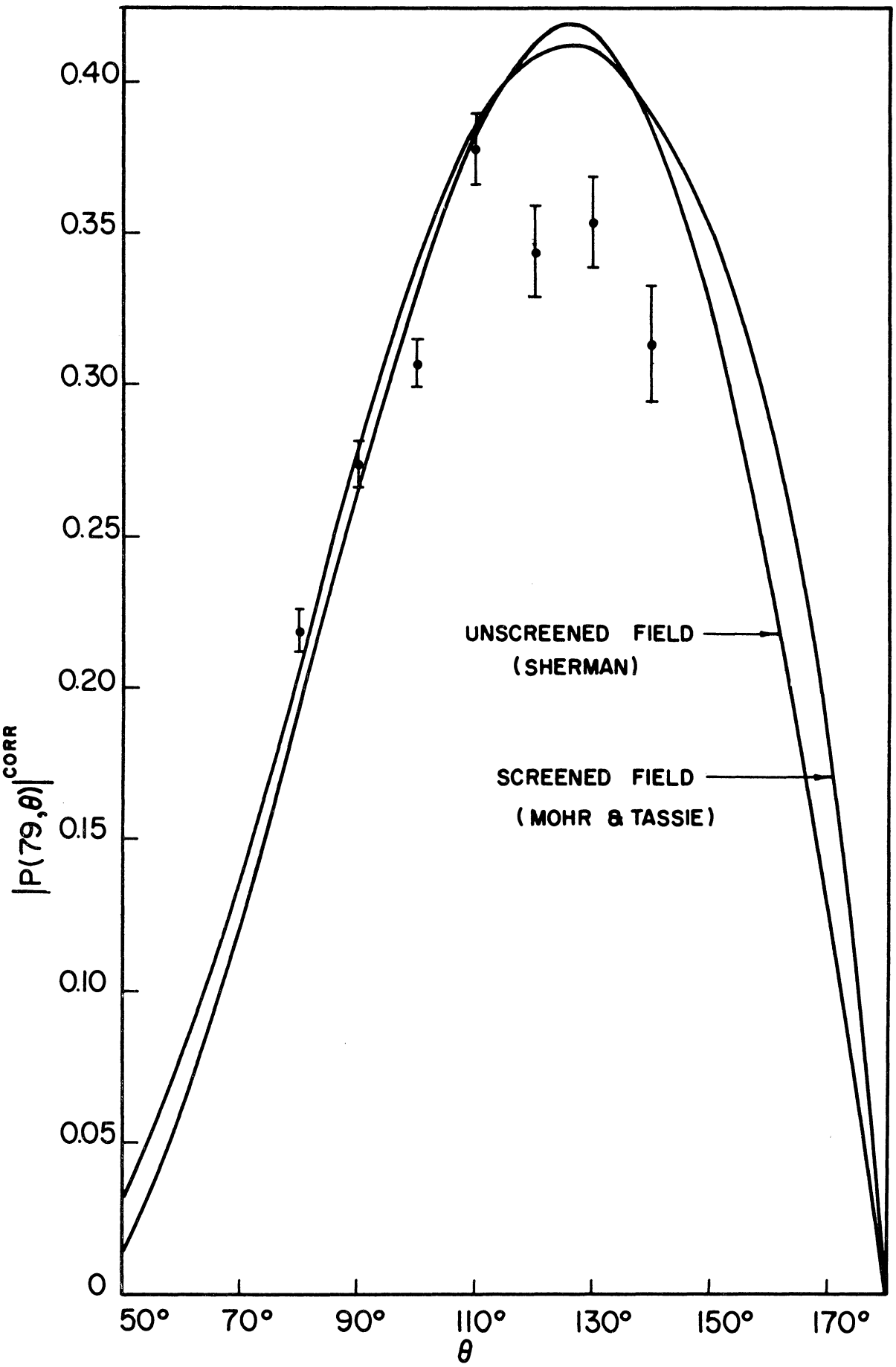

Figure 27. Measured Mott Polarizations

Discussion of Results

Two features of the data presented in Figure 26 are outstanding. First, there is good agreement between the asymmetry amplitudes measured with the electrostatic energy analyser and the theoretically predicted ones, especially for the middle range of scattering angles. Secondly, there is a large difference between the asymmetry amplitudes measured with and without the electrostatic energy analyser. These will be discussed in the above order.

The asymmetry amplitudes measured with the energy analyser at second scattering angles of 90°, 100°, and 110° agree quite well with either theoretical curve. The experimental points are not sufficiently accurate to decide between the curve for the pure Coulomb field and the one for the screened Coulomb field. As was pointed out in Chapter II the difference between these two curves may well be due more to calculational error in the screened Coulomb field curve than to the effect of the atomic electron cloud. Thus experimental agreement with either remains a possibility. The experimental value at 80° however is sufficiently above (17%) the unscreened field curve that a screening effect is indicated. For second scattering angles of 120°, 130°, and 140° the experimental asymmetry amplitudes fall about 20% below the two theoretical curves. The most likely cause of the discrepancy at these angles is plural scattering. A discussion of this and other sources of error will be given in the following section.

When no energy analysis of the doubly scattered beam is employed, four systematic effects are observed in the azimuthal asymmetry. First, the asymmetry amplitudes are smaller than those measured using energy

analysis. Second, the reduction in the asymmetry amplitude ($\sim$ 33%) is roughly independent of the second scattering angle. Third, the values of the phase angle α (see Table II) are larger than those measured using energy analysis. Fourth, the increase in the phase angle is roughly constant (independent of the second scattering angle) and equal to 26°.

Qualitatively, these effects may be explained by considering the effect of the magnetic focusing field on the energy distribution of the first scattered beam. This energy distribution arises from the ripple ($\pm$ 2%) on the 121 kev accelerating voltage and from the ionization losses in the polarizer target. The latter causes the straggling that is so characteristic of electrons. (Energy losses from bremstrahlung at this energy are negligible compared to ionization losses.) The spins of the electrons in the low energy tail of the energy profile, which are assumed to have roughly the same polarization as the electrons in the elastic peak, will precess more, because of their slower speed through the magnetic field, than the electrons in the elastic peak of the profile. This lack of coherence in the precession of the spins of the electrons in the beam as a whole causes a depolarization of the type discussed and calculated in Chapter II. A reduction in the asymmetry amplitude results. If the energy analyser accepts just the electrons in the elastic peak and the plain Geiger counter accepts the entire energy distribution, it is seen that this mechanism causes an increase in the precession angle of the polarization vector of the beam accepted by the plain Geiger counter as compared with the polarization vector of the beam accepted by the counter attached to the energy analyser. This increase in precession angle of the polarization vector causes the same increase in

the phase angle α of the azimuthal asymmetry. Since this precession angle depends only on the energy distribution of the first scattered beam and upon the magnetic field, it would be the same for the azimuthal asymmetries measured at different angles of second scattering. Also, since the shape of the energy profile is independent of scattering angle (to the extent that the same target thickness is traversed for all angles) the parts of the energy profile seen by the two types of counters are the same for all scattering angles. Thus, the reduction in the asymmetry amplitude would be expected to be independent of angle of second scattering. The four systematic differences in the measurements of the azimuthal asymmetry with and without the use of energy analysis are thus qualitatively explained in terms of the effect of the focusing magnetic field on the energy profile of the first scattered beam.

A quantitative explanation of these effects is more difficult. Through the years several investigators[47,48,49,50] have studied the energy profile of electrons that have lost energy by ionization collisions in passing through thin foils. These theories predict for the gold foils of this experiment a most probable energy loss of the order of a 150 ev for electrons of 121 kev incident energy. The predicted energy profile has a full width at half maximum of about 250 ev . Also, they predict that the probability of a loss in excess of ten times the most probable loss is only a few percent. Since the energy analyser has a resolution of about 8% and the beam has a width of about 4 kev due to ripple on the accelerating voltage, the straggling would seem to represent a very small effect on the observed energy profile. To account for a change in the phase angle α of 26° in conjunction with a reduction of the asymmetry

amplitude by 33% requires a tail on the profile of the order of 40 kev in length, containing something of the order of 33% of the electrons present in the whole profile, and having a polarization of the order of that of the elastic peak. None of these theories predict a tail on the distribution of anywhere near this size. However it is not at all clear that these theories apply at all far out on the tail of the distribution. Their agreement with experiment may be especially poor when the incident energy of the electrons is as close to the binding energy of the inner electrons of the atoms as 121 kev is to the 80 kev binding energy of the K electrons in gold. It would seem at least that these theories do not rule out the possibility of a sufficient number of electrons in the tail of the profile to account for the effect described above.

The question of the presence of a sufficient number of electrons far out on the tail unfortunately cannot be resolved experimentally with the present analyser. This is because there are indications that many of the electrons counted for deflection plate voltages far off the elastic peak are actually electrons present in the elastic peak which have been bent into the deflection plates and scattered off them into the counter.

Discussion of Errors

There are many possible sources of error in the present experiment. However, for the measurements made with the plain Geiger counter (no energy analysis) only three sources of error -- depolarization caused by the action of the magnetic field on the energy distribution, statistical fluxuations in the counting rates, and plural scattering -- are significant. The first of these has already been discussed extensively in the

last section and it appears that it is the cause of the large differences in the asymmetries measured with and without the energy analyser. The latter two of these sources of error are also the only major sources of error for the measurements made with the energy analyser. These will be discussed next.

Statistical fluxuations in the number of electrons counted arise from the randomness in time with which the electrons arrive at the counters. This source of error is unavoidable. If the number of counts is large, the probability of a deviation from the average number of counts recorded in a given time interval has the form of a Gaussian distribution. A convenient measure of the width of the Gaussian curve is the so-called standard deviation which is the root-mean-square deviation. The standard deviation is given by the square root of the average number of counts. The precise meaning of the standard deviation is that a measurement has a 68.3% probability of falling in an interval of twice the standard deviation centered about the peak of the Gaussian distribution. If a single measurement of the number of counts is made, it may be assumed to be close enough to the average so that the square root of this number may be used as the standard deviation. Following this procedure a standard deviation of the statistical error was given to each of the four numbers of counts given on the left side of (5.2). The propagation of these errors into the experimental values of the asymmetry amplitude, the phase angle α, and the polarization function were calculated. These errors are given in Table II and shown in Figures 26 and 27. They are of the order of 5%.

The discrepancy between the measured asymmetry amplitudes and the theoretical predictions at the larger scattering angles is believed

due to the inclusion of plurally scattered electrons in the counting rates. This effect increases at back angles in the present experimental arrangement since the angle between the target plane and the path of the scattered electron becomes less for larger scattering angles. This is because the plane of the target was set to bisect the supplement to the scattering angle. As was discussed in Chapter II, Ryu[17] has calculated roughly the effect of plural scattering at 90° scattering for a foil oriented at 45° to both the incident and scattered beams. He finds the plurally scattered electrons constitute 2% of the electrons counted on the transmission side of the foil. It is plausible that for a scattering angle of 140° and a target angle of 160° that 20% of the counting rate on the transmission side of the foil could be plurally scattered electrons. This would account for the discrepancy between the experimental points and theory at the back angles.

Multiple scattering occuring between the large angle scattering in the polarizer target and the large angle scattering in the analyser can cause a depolarization. The calculation of this effect by Rose and Bethe[19] was discussed in Chapter II. Using their figures and an effective target thickness of 9×10^{-6}cm sec $\frac{\theta}{2}$, where θ is the scattering angle, a reduction of the azimuthal asymmetry ranging from 1% to 2.3% results for the range of scattering angles from 80° to 140°. Since these errors are smaller than the statistical errors quoted their effect is probably not perceptible in the present experiment.

Figures 14 and 15 in Chapter IV show that variations within the regulation ranges of the current supplies of the solenoid field, the vertical

correction field, and the horizontal correction field do not change the ratio of the observed counting rates any significant amount. When the plain Geiger counter (no energy analysis) is used variations in the accelerating voltage cause no appreciable change in this ratio. However, when the energy analyser is used variations in either the accelerating voltage or the deflection plate voltage within their regulation ranges can cause changes in this ratio up to 3%. However, the fine fit of the experimental points to a cosine curve considering just the errors of statistical origin indicate that drifts causing changes in the ratio greater than 1% were a rare occurence. Since the apparatus was allowed to warm up for 24 hours before any run was made, no systematic drifts would be expected. Any small drifts occurring would then be random and their effect on a measurement of the Mott asymmetry would be small.

As was pointed out earlier in this chapter variations in the beam intensity can cause variations in the counting losses of the Geiger counters and thus introduce an error. A typical counting rate in this experiment was 15,000 counts per minute which corresponds to an average of one count every 4000 μsec. Since the Geiger counters had a dead time of about 80 μsec, a counting loss of about 2% results. This loss introduces no error provided it remains constant. During a run a typical variation in counting rate observed was about 25%. This could cause a change in the counting losses by .5%. However, the variation in the counting losses in each of the two counting rates in the denominator of the ratio given on the left side of (5.2) tend to divide out the variation in the counting losses in the counting rate in the numerator which was measured at the same time. The change in this ratio due to

the variation in counting losses caused by a 25% variation is beam intensity is in the worst cases only .5%. Since this maximum counting loss error is about ten times smaller than the statistical error and since it is somewhat random, it is a negligible contribution to the total error.

Several other possible sources of error have been discussed previously. In Chapter IV an extensive discussion of the finite aperture asymmetry showed that its effect was to systematically decrease the observed Mott asymmetry. However, the amount that the asymmetry factor was reduced was only .1% for the parameters of this experiment. Also, as was discussed in Chapter IV, the neglect of subtracting off background from the observed counting rates introduced some error. However, with the geometry used in this experiment background was at the cosmic ray level ($\sim$ 10 per minute). At the large counting rate ($\sim$ 10,000 per minute) used in this experiment neglect of backgrounnd introduced an error of at most .1%.

It is concluded that for the measurements using the energy analyser only two sources of error are significant: statistical errors in the numbers of counts recorded and a systematic error, due to plural scattering, which becomes larger for the larger scattering angles studied. For the measurements employing no energy analysis a significant error, in addition to the two mentioned above, is introduced by the depolarization caused by the interaction between the focusing magnetic field and the energy distribution.

Conclusions

The Mott asymmetry has been observed for 121 kev electrons scattered from thin gold targets at scattering angles of 90° at the polarizer and from 80° to 140° at the analyser using the energy analyser. Good agreement between the measured asymmetry factors and the theoretical predictions for an unscreened Coulomb field was obtained for angles between 90° and 110°. The discrepancy between observed and predicted values from 120° to 140° is believed due to plural scattering. The measurement at 80° is enough higher than the unscreened field prediction to indicate, though perhaps not prove, the existence of screening effects on the asymmetry amplitude at this angle. For all measurements of the asymmetry amplitude the cosine dependence on the azimuthal angle was observed.

It is believed that the success of the present experiment in comparison to previous attempts at observation of the Mott asymmetry in this energy region can be attributed in the most part to the following techniques: 1) the observation of the entire azimuthal dependence of the double scattering cross section rather than just at the points of expected maximum and minimum asymmetry, 2) the careful design and testing of the slit system and analyser assembly, 3) the great improvement in the ratio of scattered electron counting rate to the background counting rate through the use of a magnetic lens between the two scatterings, and 4) the use of energy selection after double scattering. On the basis of the present data it cannot be concluded that energy selection is necessary in a double scattering experiment in which no magnetic lens between the two scatterings is used. Such a conclusion does, however, remain a possibility.

Suggestions for Further Experimental Study

The shortcomings of the present experiment offer the best starting points for further study. Thus it is felt that the most important extension of the present experiment would be the study of the energy profile of the doubly scattered beam with a high resolution energy analyser and the dependence of the measured Mott asymmetry on the portion of the profile used. It would be advantageous if the construction of this analyser were such as to allow measurements at more extreme angles of scattering. Another study of considerable importance would be that of measuring the Mott asymmetry factor as a function of target plane angle so that the effect of plural scattering could be evaluated experimentally. A further improvement on the present experiment would be the use of an element of lower atomic number than aluminum in the analyser for the evaluation of the spurious instrumental asymmetry. Better still would be the adjustment of the experimental parameters so as to permit the use of aluminum targets at both the polarizer and analyser for this purpose. This would permit the comparison of the data with a single asymmetry factor rather a difference of two asymmetry factors as was done in Figure 26. If the above effects were well taken care of, it would then be worthwhile to obtain better statistics in the measurement of the asymmetry factor. An assessment of the screening correction to the Mott asymmetry factor could then be made. Extension of the measurements to other energies and target elements would then be in order.

When the technique of measurement of the Mott asymmetry is well understood, Mott scattering can then be used as an accurately calibrated detector of transverse polarization This can be of great use in studying

the polarization of β - rays. This yields information on the β - decay interaction and the conservation laws it obeys. Of course, since β - rays from an unoriented source possess only a longitudinal polarization, the polarization vector must be first rotated — either by a first large angle scattering or electric deflection plates — before undergoing Mott scattering.

APPENDIX

TABLES OF EXPERIMENTAL RESULTS

Part A: Runs Employing Energy Analysis

	$\theta_2 = 80°$		$\theta_2 = 80°$		$\theta_2 = 90°$	
ϕ_2	$C_{au\text{-}au}$ (M = 40,000)	$C_{au\text{-}al}$ (M = 100,000)	$C_{au\text{-}au}$ (M = 40,000)	$C_{au\text{-}al}$ (M = 100,000)	$C_{au\text{-}au}$ (M = 40,000)	$C_{au\text{-}al}$ (M = 100,000)
0°	47,202	56,399	46,606	58,461	34,964	34,179
30°	47,473	57,385	45,770	59,533	36,199	35,976
60°	47,463	58,237	45,166	60,938	35,544	36,808
90°	46,532	58,996	44,390	60,910	34,690	36,788
120°	46,433	58,727	43,859	59,626	34,027	36,695
150°	45,499	56,663	43,481	60,214	34,041	35,848
180°	45,763	56,945	44,375	60,505	34,556	35,497
210°	46,708	56,123	45,836	59,677	35,048	34,763
240°	47,134	56,409	46,881	59,675	35,376	33,734
270°	47,706	55,214	46,456	59,374	36,013	32,492
300°	48,478	55,051	48,444	58,367	35,772	32,517
330°	47,534	55,497	47,563	58,149	36,016	33,340

	$\theta_2 = 90°$		$\theta_2 = 90°$		$\theta_2 = 90°$	
ϕ_2	$C_{au\text{-}au}$ (M = 40,000)	$C_{au\text{-}al}$ (M = 100,000)	$C_{au\text{-}au}$ (M = 40,000)	$C_{au\text{-}al}$ (M = 100,000)	$C_{au\text{-}au}$ (M = 40,000)	$C_{au\text{-}al}$ (M = 100,000)
0°	34,709	34,095	33,836	33,482	36,678	35,568
30°	34,731	35,838	34,327	35,259	36,661	36,715
60°	34,396	36,705	34,233	35,521	36,461	37,673
90°	33,105	35,807	32,846	35,175	35,408	38,151
120°	31,866	34,797	31,801	34,357	34,892	37,389
150°	31,543	34,683	31,489	34,293	35,276	37,408
180°	32,466	34,269	32,399	33,959	35,413	36,674
210°	33,166	33,994	32,266	33,512	35,327	36,136
240°	33,375	33,463	32,941	33,271	36,333	35,023
270°	33,472	33,067	33,504	32,703	36,693	34,456
300°	33,684	32,584	33,854	32,619	37,184	34,793
330°	34,309	32,970	33,909	32,531	37,299	34,955

	θ_2 = 100°		θ_2 = 100°		θ_2 = 100°	
ϕ_2	$C_{au\text{-}au}$ (M = 40,000)	$C_{au\text{-}al}$ (M = 100,000)	$C_{au\text{-}au}$ (M = 40,000)	$C_{au\text{-}al}$ (M = 100,000)	$C_{au\text{-}au}$ (M = 40,000)	$C_{au\text{-}al}$ (M = 100,000)
240°	28,057	24,900	27,733	26,230	27,162	26,727
270°	28,477	24,859	29,125	26,372	28,163	27,377
300°	28,717	24,586	29,111	25,482	29,180	26,512
330°	28,966	24,438	28,660	26,239	29,161	26,547
0°	28,947	25,303	28,863	26,035	27,545	25,911
30°	28,301	25,662	28,405	26,645	26,795	26,220
60°	27,943	26,058	28,207	27,293	26,269	26,863
90°	26,913	26,349	26,993	27,284	25,588	26,664
120°	26,738	26,016	26,254	27,537	24,630	26,571
150°	26,877	26,019	25,903	26,690	24,231	26,508
180°	26,993	25,453	26,634	26,426	24,740	26,771
210°	27,145	25,170	27,133	26,285	25,551	26,175

	$\theta_2 = 110°$		$\theta_2 = 110°$		$\theta_2 = 120°$	
ϕ_2	$C_{au\text{-}au}$ (M = 40,000)	$C_{au\text{-}al}$ (M = 100,000)	$C_{au\text{-}au}$ (M = 40,000)	$C_{au\text{-}al}$ (M = 100,000)	$C_{au\text{-}au}$ (M = 40,000)	$C_{au\text{-}al}$ (M = 100,000)
0°	23,819	18,802	23,327	19,012	20,483	14,182
30°	23,379	19,159	23,683	19,407	20,372	14,942
60°	22,949	19,628	22,682	19,619	20,094	14,983
90°	22,269	19,784	22,250	21,095	19,637	15,296
120°	21,821	20,002	21,727	20,318	18,716	15,254
150°	21,766	19,404	21,881	20,088	18,535	15,065
180°	22,398	19,538	22,054	20,076	18,942	14,831
210°	22,746	19,205	23,005	19,247	19,476	14,448
240°	23,883	18,951	23,512	18,896	19,880	14,795
270°	24,453	19,023	24,452	19,066	20,872	14,220
300°	24,784	18,566	24,642	18,618	21,120	14,153
330°	24,621	18,299	24,121	18,792	20,760	13,908

	$\theta_2 = 120°$		$\theta_2 = 130°$		$\theta_2 = 130°$	
ϕ_2	$C_{au\text{-}au}$ (M = 40,000)	$C_{au\text{-}al}$ (M = 100,000)	$C_{au\text{-}au}$ (M = 40,000)	$C_{au\text{-}al}$ (M = 100,000)	$C_{au\text{-}au}$ (M = 40,000)	$C_{au\text{-}al}$ (M = 100,000)
0°	20,148	14,214	17,061	10,801	16,980	11,080
30°	20,297	14,565	16,698	11,124	16,582	11,321
60°	19,126	14,817	16,991	11,486	16,398	11,530
90°	18,526	14,783	16,671	11,438	15,984	11,444
120°	18,329	14,913	16,031	11,386	15,710	11,381
150°	18,322	14,697	15,795	11,085	15,193	11,717
180°	18,594	14,869	16,597	11,059	15,651	11,430
210°	18,985	14,652	16,680	11,028	16,397	11,229
240°	19,894	14,591	17,485	10,628	16,971	10,993
270°	20,016	14,348	17,866	10,705	17,361	10,865
300°	20,135	14,129	18,024	10,580	17,357	10,834
330°	20,197	14,167	17,763	10,515	17,090	10,793

	$\theta_2 = 140°$		$\theta_2 = 140°$	
ϕ_2	$C_{au\text{-}au}$ (M = 40,000)	$C_{au\text{-}al}$ (M = 100,000)	$C_{au\text{-}au}$ (M = 40,000)	$C_{au\text{-}al}$ (M = 100,000)
0°	14,224	6,865	13,904	7,299
30°	13,827	7,060	13,701	7,567
60°	14,107	6,990	14,193	7,502
90°	13,196	7,128	13,377	7,471
120°	13,113	7,158	12,992	7,700
150°	13,579	7,159	13,112	7,706
180°	13,464	7,150	13,394	7,501
210°	13,619	6,955	13,852	7,320
240°	13,998	6,814	14,296	7,242
270°	14,195	6,535	13,978	7,124
300°	14,112	6,486	14,238	6,839
330°	13,934	6,540	14,255	7,144

Part B: Runs Not Employing Energy Analysis

	$\theta_2 = 90°$		$\theta_2 = 90°$		$\theta_2 = 90°$	
ϕ_2	$C_{au\text{-}au}$ (M = 40,000)	$C_{au\text{-}al}$ (M = 100,000)	$C_{au\text{-}au}$ (M = 40,000)	$C_{au\text{-}al}$ (M = 100,000)	$C_{au\text{-}au}$ (M = 40,000)	$C_{au\text{-}al}$ (M = 100,000)
0°	48,876	53,720	48,934	54,074	48,730	53,707
30°	47,626	54,503	49,093	54,393	48,419	54,430
60°	47,974	54,580	48,063	55,562	47,731	55,859
90°	46,318	54,352	47,179	54,867	47,438	55,449
120°	46,170	54,323	46,128	55,019	46,715	54,750
150°	45,796	54,475	45,870	55,350	46,137	55,311
180°	46,661	55,250	46,914	56,341	47,460	56,233
210°	47,193	55,326	48,551	56,325	47,626	56,115
240°	47,632	52,990	48,946	55,161	48,465	55,754
270°	48,552	54,242	49,264	55,582	49,369	55,329
300°	48,618	54,246	49,497	54,411	49,559	55,876
330°	48,640	52,499	49,796	53,118	48,816	54,051

	$\theta_2 = 110°$		$\theta_2 = 120°$		$\theta_2 = 130°$	
ϕ_2	$C_{au\text{-}au}$ (M = 40,000)	$C_{au\text{-}al}$ (M = 100,000)	$C_{au\text{-}au}$ (M = 40,000)	$C_{au\text{-}al}$ (M = 100,000)	$C_{au\text{-}au}$ (M = 40,000)	$C_{au\text{-}al}$ (M = 100,000)
0°	33,148	30,757	29,698	27,086	24,809	22,411
30°	32,620	31,868	29,365	28,015	24,670	23,311
60°	33,046	33,174	29,292	28,090	25,350	24,186
90°	32,020	32,708	27,937	28,577	24,755	24,191
120°	31,415	32,662	27,308	28,047	23,461	23,815
150°	30,617	33,134	26,624	27,742	23,745	24,161
180°	31,416	32,919	27,343	28,501	24,695	24,171
210°	31,915	33,437	27,857	28,358	24,711	24,310
240°	32,867	33,170	28,315	27,650	24,868	24,104
270°	33,448	33,046	29,604	28,510	25,740	24,184
300°	33,852	32,744	29,794	27,763	26,521	23,725
330°	33,646	30,639	29,439	27,820	24,912	23,219

BIBLIOGRAPHY

1. Mott, N. F., Proc. Roy. Soc., A 124, 425 (1929); A 135, 429 (1932).

2. Louisell, W. H., Thesis, University of Michigan, 1953, (unpublished).

3. Louisell, W. H., Pidd, R. W., and Crane, H. R., Phys. Rev., 94, 7, (1954).

4. Mott, N. F. and Massey, H. S. W., The Theory of Atomic Collisions, Oxford University Press, London, (1949) p. 70.

5. Pauli, W., Handbuch der Physik, J. Springer, Berlin (1933), Vol. 24, Part 1, p. 242.

6. Cox, R. T., McIlwraith, C. G., and Kurrelmeyer, B., Proc. Nat'l Acad. Sci., 14, 544 (1928).

7. Chase, C. T., Phys. Rev., 34, 1069 (1929); 36, 1060 (1930).

8. Rupp, E., Phys. Zeits., 33, 158 (1932); 33, 937 (1932).

9. Rupp, E., Zeits. f. Physik, 79, 642 (1932); 88, 242 (1934); 90, 166 (1934).

10. Langstroth, G. O., Proc. Roy. Soc. (London), A 136, 558 (1932).

11. Dymond, E. G., Proc. Roy. Soc. (London), A 136, 638 (1932); A 145, 657 (1934).

12. Thomson, G. P., Phil. Mag., 17, 1058 (1934).

13. Richter, H., Ann. Physik, 28, 533 (1937).

14. Kikuchi, K., Proc. Phys.-Math. Soc. Japan, 21, 524 (1939); 22, 805 (1940).

15. Chase, C. T. and Cox, R. T., Phys. Rev., 58, 243 (1940).

16. Goertzel, G. and Cox, R. T., Phys. Rev., 63, 37 (1943).

17. Ryu, N., J. Phys. Soc. Japan, 5, 423 (1950).

18. Ryu, N., Hashimoto, K., and Nonaka, I., J. Phys. Soc. Japan, 8, 575 (1953).

19. Rose, M. E. and Bethe, H. A., Phys. Rev., 55, 277 (1939).

20. Rose, M. E., Phys. Rev., 57, 280 (1940).

21. Tolhoek, H. A., Rev. Mod. Phys., 28, 277 (1956).

22. Shull, C. G., Chase, C. T., and Myers, F. E., Phys. Rev., 63, 29 (1943).

23. Trounson, E. and Simpson, J. A., Phys. Rev., 63, 55 (1943).

24. Shinohara, K. and Ryu, N., J. Phys. Soc. Japan, 5, 119 (1950).

25. Ryu, N., J. Phys. Soc. Japan, 7, 125 (1952); 7, 130 (1952); 8, 804 (1953).

26. Pettus, W. G., Phys. Rev., 109, 1458 (1958).

27. Crane, H. R., private communication.

28. Tolhoek, H. A. and DeGroot, S. R., Physica, 17, 17 (1951).

29. Mendlowitz, H., Thesis, University of Michigan, 1954, (unpublished).

30. Mendlowitz, H. and Case, K. M., Phys. Rev., 97, 33 (1955).

31. Case, K. M., Phys. Rev., 106, 173 (1957).

32. Bethe, H. A. and Morrison, P., Elementary Nuclear Theory, Wiley (1956), Chapter XVII.

33. Tolhoek, H. A.,and DeGroot, S. R., Physica, 17, 1 (1951).

34. Bartlett, J. H. and Watson, R. E., Proc. Am. Acad. Arts Sci., 74, 53 (1940).

35. Sherman, N., Phys. Rev., 103, 1601 (1956).

36. Sherman, N., private communication.

37. Sauter, F., Ann. Physik, 18, 61 (1933).

38. Bartlett, Jr., J. H. and Welton, T. A., Phys. Rev., 59, 281 (1941).

39. Massey, H. S. W. and Mohr, C. B. O., Proc. Roy. Soc., A 177, 341 (1941).

40. Mohr, C. B. O., Proc. Roy. Soc., A 182, 189 (1943).

41. Mohr, C. B. O. and Tassie, L. J., Proc. Phys. Soc. (London), 67, 711 (1954).

42. See for example, Spangenberg, K. R., Vacuum Tubes, McGraw-Hill, (1948), Chapter 14.

43. Mendlowitz, H. and Case, K. M., Phys. Rev., 100, 1551 (1955).

44. Mohr, C. B. O and Tassie, L. J., Austal. J. Phys., 7, 217 (1954).

45. Williams, E. J., Proc. Roy. Soc., A 169, 531 (1938).

46. Whittaker, E. T. and Robinson, G., The Calculus of Observations, Blackie and Son, Ltd. (1944), Chapter X, p. 267.

47. Williams, E. J., Proc. Roy. Soc., A 125, 420 (1929).

48. Landau, L., J. Phys. U.S.S.R., 8, 201 (1944).

49. Blunck, O. and Leisegang, S., Z. Physik, 128, 500 (1950).

50. Blunck, O. and Westphal, K., Z. Physik, 130, 641 (1951).